21 Interactions in Macromolecular Complexes Used as Nonviral Vectors for Gene Delivery

Rudolf Podgornik, D. Harries, J. DeRouchey, H. H. Strey, and V. A. Parsegian

CONTENTS

21.1 INTRODUCTION

Designed by nature for information, valued by molecular biologists for manipulation, DNA is also a favorite molecule of physical chemists and physicists [1]. Its mechanical properties [2], interactions with other molecules [3], and modes of packing [4] present tractable but challenging problems whose answers have in vivo and in vitro consequences. In the context of DNA transfection and gene therapy [5], what has been learned through molecular mechanics, interaction and packing might teach us how to package DNA for more effective gene transfer. Among these modes of in vitro packaging are association with proteins, treatment with natural or synthetic cationic "condensing agents," and combination with synthetic positively charged lipids [6].

In vivo, DNA is tightly held, not at all like the dilute solution form often studied in vitro (see Figure 21.1). This tight assembly necessarily incurs huge energetic costs of confinement, which create a tension under which DNA is expected to ravel or to unravel its message. Through direct measurement of forces between DNA molecules [7] and direct observation of its modes of packing [8], we might see not only how to use concomitant energies to design better DNA transfer systems but also to reason better about the sequences of events by which DNA is read in cells.

What binds these structures? To first approximation, for large, flexible biological macromolecules, the relevant interactions resemble those found among colloidal particles [9] where the size of the molecule (such as DNA molecules, lipid membranes, actin bundles) distinguishes it from simpler, smaller species (such as small solutes or salt ions). On the colloidal scale of tens of nanometers ($1\,\text{nm} = 10^{-9}\,\text{m}$), only the interactions between macromolecules are evaluated explicitly, while the small molecular species only "dress" the large molecules and drive the interactions between them.

The electrical charge patterns of multivalent ions, such as Mn^{2+}, Co^{3+}, or spermine^{4+}, with cation binding to negative DNA create attractive electrostatic and solvation forces that move DNA double helices to finite separations despite the steric knock of thermal Brownian motion of the DNA [10]. Solvation patterns about the cation-dressed structures create solvation forces: DNA–DNA repulsion because of water clinging to the surface and attraction from the release of the solvent [11]. Positively charged histones spool DNA into carefully distributed skeins, which are arrayed for systematic unraveling and reading [12]. Viral capsids encase DNA, stuffed against its own DNA–DNA electrostatic and solvation repulsion, to keep it under pressure for release upon infection [13]. In artificial preparations, the glue of positively charged and neutral lipids can lump negative DNA into ordered structures that can move through lipids and through water solutions [14].

Changes in the suspending medium can modulate intermolecular forces. One example is the change in van der Waals charge-fluctuation forces (see below) between lipid bilayers when small sugars modifying the dielectric dispersion properties of water are added to the solution [15]. More dramatic, the addition of salt to water can substantially reduce electrostatic interactions between charged molecules such as DNA or other charged macromolecules bathed by an aqueous solution [16]. These changes can modify the behavior of macromolecules quantitatively or induce qualitatively new features into their repertoire, the most notable among these being the precipitation of DNA by addition of organic polycations to the solution [10]. AQ1

Similar observations can be made about the small molecules essential to practically every aspect of interaction between macromolecules. Through the dielectric constant or

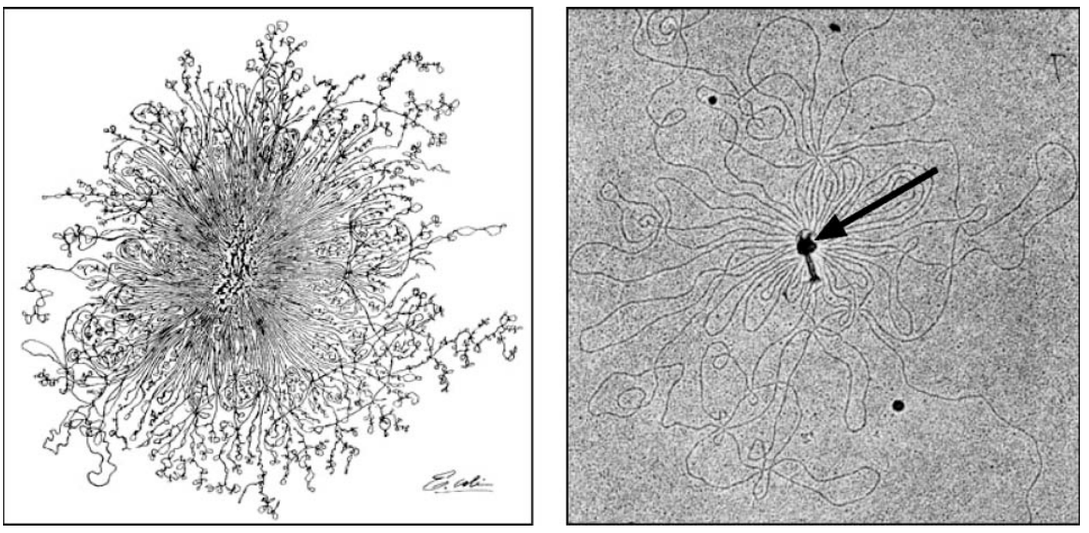

FIGURE 21.1 In vivo DNA is highly compacted. The figure shows *Esherichia coli* DNA and *T2* bacteriophage DNA after osmotic shock in distilled water has allowed them to expand from their much more compact in vivo configurations. (*E. coli* picture courtesy of Ruth Kavenoff, Bluegenes Inc., Los Angeles (1994); T2 picture from Kleinschmidt et al. *Biophys. Biochim. Acta* 1962, 61, 252. With permission.)

dielectric permittivity, it enters electrostatic interactions, through pH it enters charging equilibria, and through its fundamental molecular geometry, it enters the hydrogen bond network topology around simple solutes. This is, of course, the network of water molecule [17]. In what follows, we will limit ourselves to only three basic properties of macromolecules—charge, polarity (solubility), and conformational flexibility—that appear to govern the plethora of forces encountered in biological milieus. It is no surprise that highly ordered biological structures, such as the quasicrystalline spooling of DNA in viral heads or the multilamellar stacking of lipid membranes in visual receptor cells (Figure 21.2), can, in fact, be explained by the properties of a very small number of fundamental forces acting between macromolecules. Detailed experimental as well as theoretical investigations have identified hydration, electrostatic, van der Waals or dispersion, conformational fluctuation, and polyelectrolyte bridging forces as the most fundamental interactions governing the fate of biological macromolecules.

Our intent here is to sketch the measurements of these operative forces and to dwell upon concepts that rationalize them. It is from these concepts, with their insight into what controls organizing forces, that we expect people to learn to manipulate and to package DNA in more rewarding ways.

21.2 MOLECULAR FORCES

21.2.1 Origin and Measurement of Molecular Forces

We divide these forces into two broad categories, both of which can be either attractive or repulsive. First, there are interactions that are connected with fields emanating from sources within or on the macromolecules themselves [16]; for example, electrostatic fields pointing from the fixed charge distributions on macromolecules into the surrounding space and fields of connectivity of hydrogen bond networks extending from the macromolecular surfaces into the bulk solution that are seen in hydration interactions. Second, there are the forces due to fluctuations that originate either in thermal Brownian motion or quantum jitter [15]. Consequent interactions include the van der Waals or dispersion forces that originate from thermal as well as quantum mechanical fluctuations of electromagnetic fields in the space between and within the interacting molecules and conformation–fluctuation forces from thermal gyrations of the macromolecule when thermal agitation pushes against the elastic energy resistance of the molecule and confinement imposed by neighboring macromolecules [16].

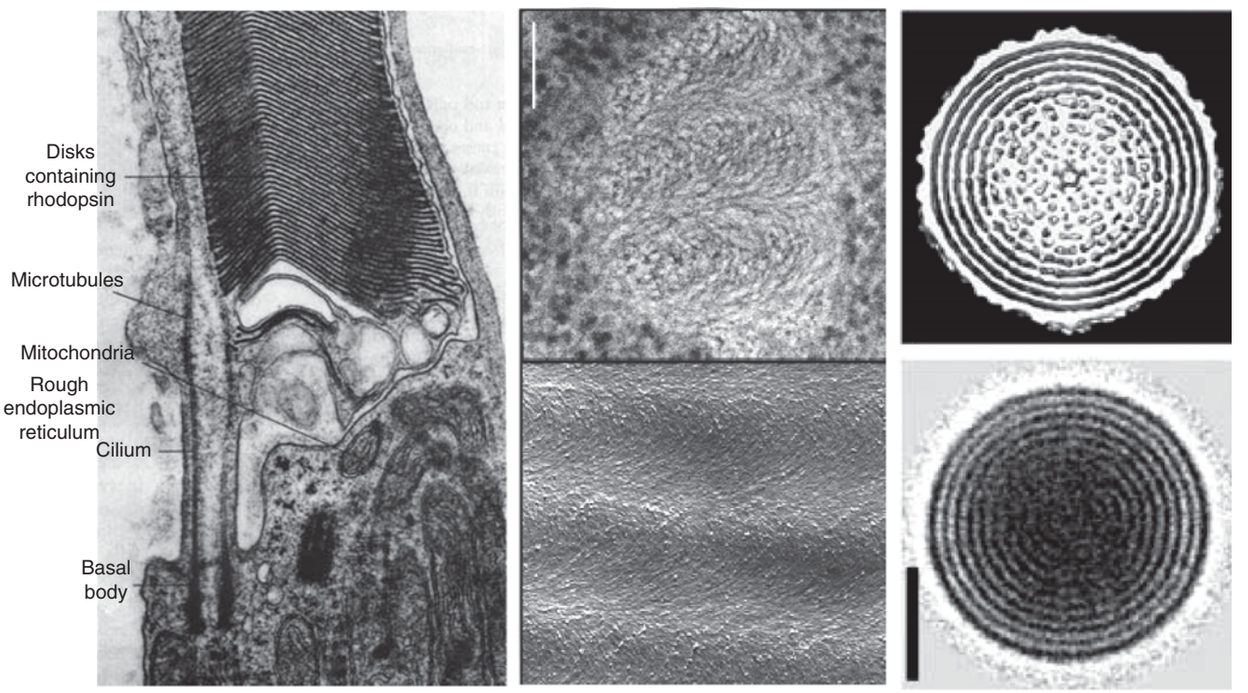

FIGURE 21.2 Highly ordered assemblies, ubiquitous among biological structures, can be explained through the properties of a very small number of fundamental forces acting between macromolecules. On the –left-hand side, electron micrograph of a part of a human eye rod cell showing multilamellar bilayer aggregate. (From Kessel, R.G. and Kardon, R.H., *Tissues and Organs*,W.H. Freeman and Co., San Francisco, CA, 1979.) In the middle, electron micrograph of an in vivo cholesteric phase of a wild type *E. coli* DNA. (Adapted from Frankiel Krispin, D. et al., *EMBO J.*, 2001, 20, 1184.) For comparison, we show the same type of structure for DNA in vitro below. (Adapted from Leforestier, A. and Livolant, F., *Biophys. J.*, 1993, 65, 56.) On the right-hand side, cryo-micrographs and computer-processed images of T7 phage heads showing ordered DNA spooling within the viral heads. (From Cerritelli, M.E., Cheng, N., Rosenberg, A.H., McPherson, C.E., Booy, F.P., and Steven, A.C., *Cell*, 1997, 91, 271. With permission.)

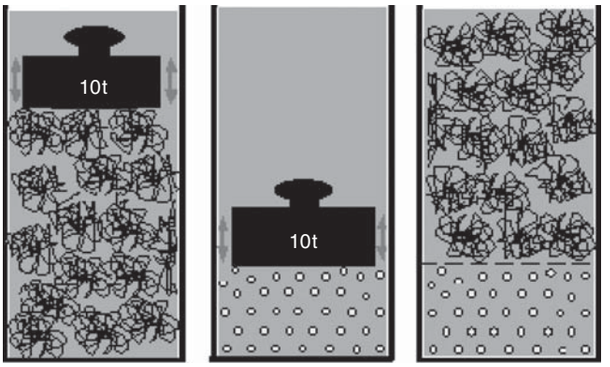

FIGURE 21.3 Osmotic pressure in macromolecular arrays. Dissolved polymers such as PEG exert an osmotic pressure on the part of the solution from which they are excluded (shown schematically by the weight). Instead of exerting osmotic pressure directly on the macromolecular subphase such as DNA or lipid arrays (small circles), one can equilibrate it with a solution of PEG at a set concentration and the PEG itself will exert osmotic stress on the macromolecular subphase. Osmotic weighing of polymers one against the other (the one with the known, set osmotic pressure against the unknown one) is the essence of the osmotic stress technique of measuring interactions in macromolecular solutions.

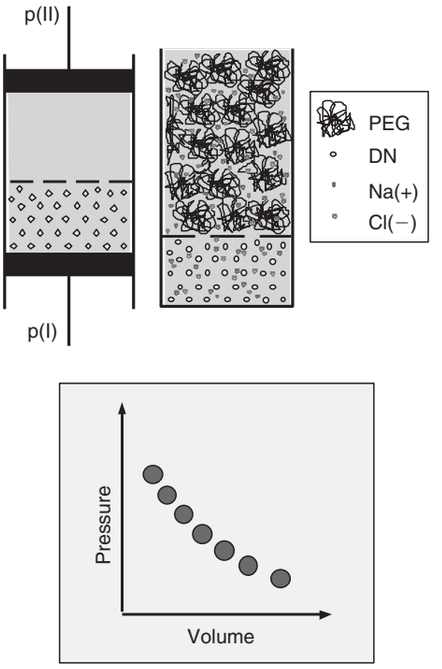

FIGURE 21.4 (See color insert following page xxx.) Osmotic stress method. (From Parsegian, V.A., Rand, R.P., Fuller, N.L., and Rau, D.C., *Methods Enzymol*., 1986, 127, 400.) DNA liquid crystals are equilibrated against solutions of a neutral polymer (such as PEG or PVP, depicted as disordered coils). These solutions are of known osmotic pressure, pH, temperature, and ionic composition. (From Rau, D.C., Lee, B.K., and Parsegian, V.A., *Proc. Natl Acad. Sci. USA*, 1984, 81, 2621.) Equilibration of DNA under the osmotic stress of external polymer solution is effectively the same as exerting mechanical pressure on the DNA subphase with a piston that passes water and small solutes but not DNA. After equilibration under this known stress, DNA separation is measured either by X-ray scattering, if the DNA subphase is sufficiently ordered, or by densitometry. (From Strey, H.H., Parsegian, V.A., and Podgornik, R., *Phys. Rev. Lett.,* 1997, 78, 895.) DNA density and osmotic stress thus determined immediately provide an equation of state (osmotic pressure as a function of the density of the DNA subphase) to be codified in analytic form over an entire phase diagram.

There are many ways to detect interactions between macromolecules. In this chapter, we consider only macromolecules interacting in ordered arrays that are particularly relevant for investigations of the packing and energetics of DNA–lipid complexes.

A fundamental concept in macromolecular arrays is that of osmotic pressure (Figure 21.3). It is equal to the pressure needed to hold a macromolecular array together against the forces acting between its constituent macromolecules. It can be applied either mechanically across a semipermeable membrane or via the osmotic stress of a high molecular weight (e.g. polyethylene glycol (PEG), polyvinyl pyrrolidone (PVP), dextran) polymer solution. At chemical equilibrium, the osmotic pressure of one solution (macromolecular array) balances that of the other (the bathing polymer solution). The chemical equilibrium can be maintained either via a semipermeable membrane or simply because the bathing polymer solution phase separates from the macromolecular array, as is many times the case with PEGs, PVP, and dextran. This osmotic balancing of different molecular solutions is the basis of the "osmotic stress method" to measure the equation of state of macromolecular arrays [18].

The equation of state of a macromolecular solution is defined as the dependence of its osmotic pressure on the density of the array (see Figure 21.4). By equilibrating the macromolecular array versus a solution of high molecular weight polymer with a known osmotic pressure, one can set the osmotic pressure in the macromolecular array itself [18]. If in addition, one measures the concurrent density of the macromolecular array, either via X-ray scattering or direct densitometry, one gets the dependence of the osmotic pressure of the array on its density, i.e., its equation of state. This is the essence of the osmotic stress method.

21.2.1.1 Hydration Forces

The hydration force is connected with a very simple observation that it takes increasing amounts of work to remove water from between electrically neutral lipids in multilamellar arrays or from between ordered arrays of polymers at large polymer concentrations [18]. Direct measurements of this work show that it increases exponentially with the diminishing separation between colloid surfaces with a decay length that depends as much on the bulk properties of the solvent as on the detailed characteristics of the interacting surfaces. There is nevertheless some profound universality in the interactions between macromolecular surfaces at close distances (see Figure 21.5)—whether they are charged, zwitterionic, or uncharged—that strongly suggest that water is essential to maintaining the stability of biological matter at high densities.

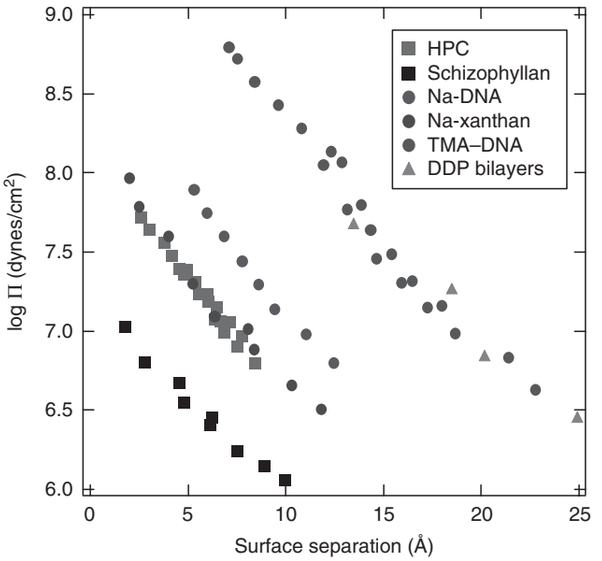

FIGURE 21.5 (See color insert following page xxx.) Interactions between biological macromolecules show striking universality at close surface-to-surface separations (or equivalently at very large densities). Hydroxypropyl cellulose, schizophyllan, different DNA salts, xanthan, and DDP bilayers at small intermolecular separations (given in terms of the separation between effective molecular surfaces of the interacting molecules) all show a strong repulsive interactions decaying with about the same characteristic decay length. The log-linear plot is thus more or less a straight line (composite data, courtesy D.C. Rau).

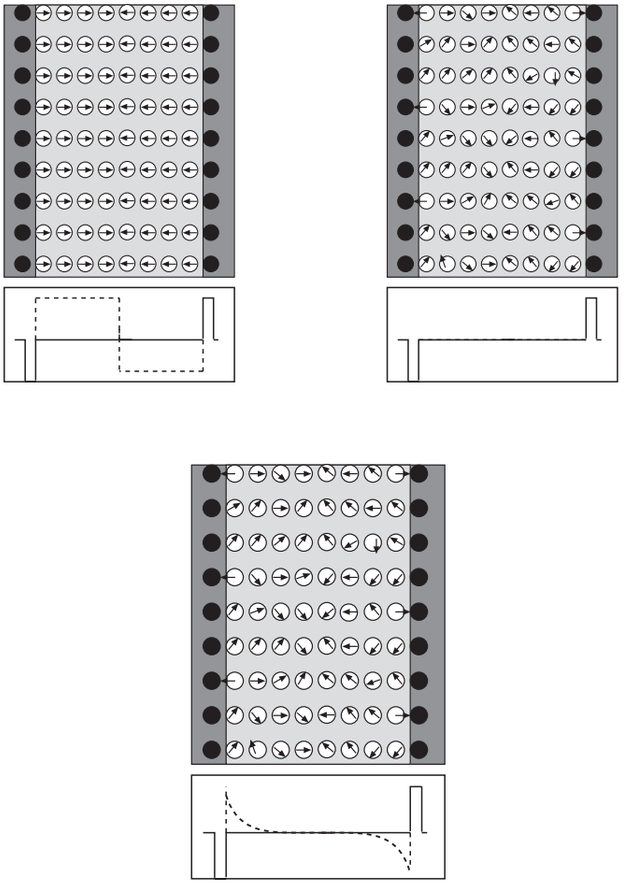

FIGURE 21.6 The hydration force. Marãelja, S. and Radiç, N., *Chem. Phys. Lett.,* 1976, 42, 129, introduced an order parameter P that would capture the local condition, or local ordering, of solvent molecules between the surfaces. We represent it as an arrow (that has magnitude and direction) on each water molecule that is trapped between the two apposing surfaces and is being acted upon by the surface fields, depicted schematically with a bold line below each of the three drawings. Minimizing the energy corresponding to a spatial profile of P leads to a configuration where P points (for example) away from both surfaces and there is thus mismatch at the midplane (the dotted line below the leftmost drawing). The entropy on the other hand would favor completely disordered configurations with no net value of P (the dotted line below the rightmost drawing). The free energy strikes a compromise between the two extrema, leading to a smooth profile of P, varying continuously as one goes from one surface to the other (the dotted line below the bottom drawing). As the two surfaces approach the nonmonotonic profile of the order parameter P, it leads to repulsive forces between them.

Hydration forces can be understood in different terms with no consensus yet on mechanism [11]. Marãelja and Radiç [19] first proposed the idea that colloid surfaces perturb the vicinal water and that the exponential decay of the hydration force is due to the weakening of the perturbation of the solvent as a function of the distance between the interacting surfaces (Figure 21.6). They introduced an order parameter $P(z)$ as a function of the transverse coordinate z, between the surfaces located at $z = D/2$ and $z = -D/2$, that would capture the local condition or local ordering of solvent molecules between the surfaces. The detailed physical nature of this order parameter is left unspecified, but since the theory builds on general principles of symmetry and perturbation expansions, molecular details are not needed. All one needs to know about P is that within the bulk water $P = 0$ and close to a macromolecular surface P remains nonzero. As a mnemonic, one can envision P as an arrow associated with each water molecule. In bulk water, the arrows point in all directions with equal probability. Close to a bounding macromolecular surface, they point preferentially toward or away from the surface (Figure 21.6) depending on the surface-orienting fields.

If we envisage solvent molecules between two perturbing surfaces, we can decompose the total free energy F of their configuration into its energy W and entropy S parts via the well-known thermodynamic definition $F = W - TS$, where T is the absolute temperature. Energetically, it would be most favorable for the surface-induced order to persist away from the surfaces, but that would create conflict between the apposing surfaces (see Figure 21.3). Entropy fights any type of ordering and wants to eliminate all orderly configurations between the two surfaces, creating a homogeneous state of molecular disorder characterized by $P = 0$. Energy and entropy compromise to create a nonuniform profile of the order parameter between the surfaces; surface-induced order propagates but progressively decreases away from the surfaces.

From the free energy, we can derive the repulsive hydration osmotic pressure p acting between the surfaces because, by definition, it is proportional to the derivative of the free energy with respect to the separation D. Osmotic pressure between two apposed lipid surfaces has been measured extensively for different lipids [20] and has been found to have the form $p = p_0 \exp(-D/\lambda)$. This is consistent with the previous theoretically derived form of the hydration free energy if one assumes that $p_0 \sim P^2(z = D/2)$. The corresponding interaction free energy per unit surface area of the interacting surfaces, $F(D)$, would thus behave as $F(D) \sim p_0\lambda \exp(-D/\lambda)$. From these experiments, one can deduce the magnitude of the prefactor p_0, which determines the absolute magnitude of the hydration repulsion for a great variety of lipids and lipid mixtures within an interval 10^{12} to 10^{10} dynes/cm^2 or equivalently in the hundreds of atmospheres. AQ3

As already noted, in this simple theoretical approach, the hydration decay length depends only on the bulk properties of the solvent and not on the properties of the surface. In order to generalize this simplification, Kornyshev and Leikin [21] formulated a variant of the hydration force theory also to take into account explicitly the nature of surface ordering. They derived a modified hydration decay length that clearly shows how surface order couples with the bare hydration decay length. Without going too deeply into this theory, we note that if the interacting surfaces have two-dimensional ordering patterns characterized by a wave vector $Q = 2\lambda$, where λ is the characteristic scale of the spatial variations of these patterns, then the effective hydration force decay length would be $\lambda_{KL} = 1/2\lambda$. Inserting numbers for the case of DNA, where the "surface" structure has a characteristic scale of 1–2 Å, we realize that the hydration decay length in this case would be almost entirely determined by the surface structure and not the bulk solvent properties. Given the experimentally determined variety of forces between phospholipids [20], it is indeed quite possible that even in the simplest cases, the measured decay lengths are not those of the water solvent itself but instead also include the surface properties in the characteristic scale of the surface ordering.

The other important facet of this theory is that it predicts that in certain circumstances, the hydration forces can become attractive [11]. This is particularly important in the case of interacting DNA molecules where this hydration attraction connected with condensing agents can hold DNAs into an ordered array even though the van der Waals forces themselves would be unable to accomplish [22]. This attraction is always an outcome of nonhomogeneous surface ordering and arises in situations where apposing surfaces have complementary checkerboard like order [11]. Unfortunately, in this situation, many mechanisms can contribute to attractions; it is difficult to argue for one strongest contribution.

21.2.1.2 Electrostatic Forces

Electrostatic forces between charged colloid bodies are among the key components of the force equilibria in (bio)colloid systems [23]. At larger separations, they are the only forces that can counteract van der Waals attractions and thus stabilize colloid assembly. The crucial role of the electrostatic interactions in (bio)colloid systems is well documented and explored following the seminal realization of Bernal and Fankuchen [24] that electrostatic interaction is the stabilizing force in tobacco mosaic virus (TMV) arrays.

Though the salient features of electrostatic interactions of fixed charges in a sea of mobile countercharges and salt ions are intuitively straightforward to understand, they are difficult to evaluate. These difficulties are clearly displayed by the early ambiguities in the sign of electrostatic interactions between two equally charged bodies that was first claimed to be attractive (Levine), then repulsive (Verwey-Overbeek), and finally realized that it is usually repulsive except if the counterions or the salt ions are of higher valency [25].

In this section, we introduce the electrostatic interaction on an intuitive footing (see Figure 21.7). Assume we have two equally charged bodies with counterions in between. Clearly the minimum of electrostatic energy W_E [28], which for the electrostatic field configuration at the spatial position $\mathbf{r}$, $\mathbf{E}(\mathbf{r})$, is proportional to the integral of $\mathbf{E}^2(\mathbf{r})$ over the whole space where one has nonzero electrostatic field, would correspond to the adsorption of counterions to the charges, leading to their complete neutralization. The equilibrium electrostatic field would be thus entirely concentrated right next to the surface. However, at a finite temperatures, it is not the electrostatic energy but rather the free energy [26], $F = W_E - TS$, containing also the entropy S of the counterion distribution, that should be minimized. The entropy of the mobile particles with the local density $\rho_i(r)$ (we assume there is more than one species of mobile particles, for example, counterions and salt ions, tracked through the index i) is taken as an ideal gas entropy [26], which is proportional to the volume integral of $\sum_i[\rho_i(r)\ln(\rho_i(r)/\rho_0) - \rho_i(r) - \rho_{i0}]$, where ρ_{i0} is the density of the mobile charges in a reservoir that is in chemical equilibrium with the confined system under investigation. Entropy by itself would clearly lead to a uniform distribution of counterions between the charged bodies, $\rho_i(r) = \rho_{i0}$, while together with the electrostatic energy, it obviously leads to a nonmonotonic profile of the mobile charge distribution between the surfaces, minimizing the total free energy of the mobile ions.

The above discussion, though being far from rigorous, contains all the important theoretical underpinnings known under the title of "Poisson-Boltzmann theory" [27]. In order to arrive at the central equation corresponding to the core of this theory, one simply has to formally minimize the free energy $F = W_E - TS$, just as in the case of structural interactions, together with the basic electrostatic equation [28] (the Poisson equation) that connects the sources of the electrostatic field with the charge densities of different ionic species. The standard procedure now is to minimize the free energy, take into account the Poisson equation, and what follows is the well-known Poisson-Boltzmann equation, the solution of which gives the nonuniform profile of the mobile charges between the surfaces with fixed charges. This equation can be solved explicitly for some particularly simple geometries [27]. For two charged planar surfaces, the solution gives a screened

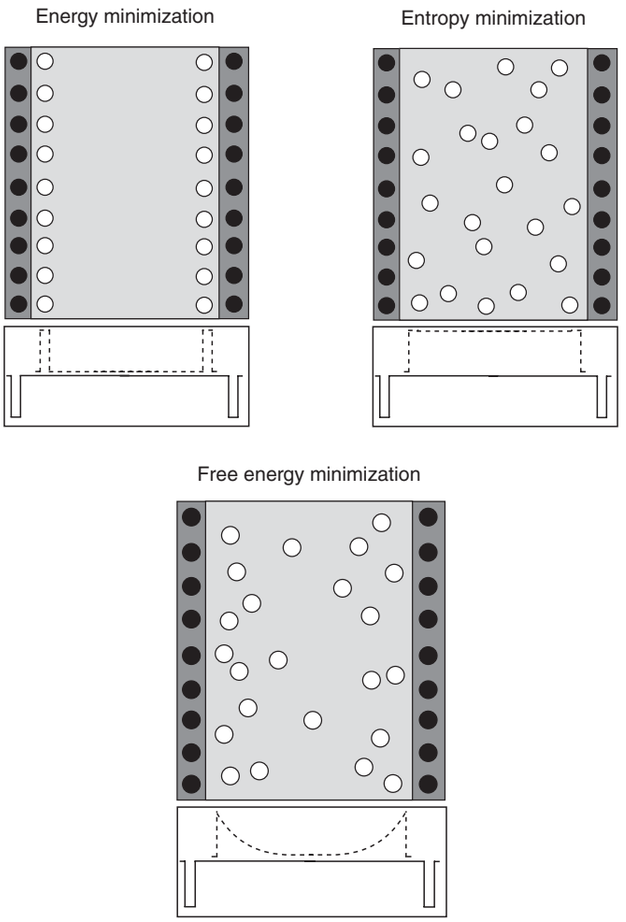

FIGURE 21.7 Pictorial exposition of the main ideas behind the Poisson-Boltzmann theory of electrostatic interactions between (bio)colloidal surfaces. Electrostatic energy by itself would favor adsorption of counterions (white circles) to the oppositely charged surfaces (black circles). The equilibrium profile of the counterions in this case is presented by the dotted line below the leftmost drawing. Entropy, on the contrary, favors a completely disordered configuration, i.e., a uniform distribution of counterions between the surfaces, presented by the dotted line below the rightmost drawing. The free energy works a compromise between the two principles leading to a nonmonotonic profile of the counterion density (From Verwey, E.J.W. and Overbeek, J.T.G., *Theory of the Stability of Lyophobic Colloids*, Elsevier, New York, 1948), varying smoothly in the intersurface region. As the two surfaces are brought close, the overlapping counterion distributions originating at the fixed charge at the surfaces (the bold line below each of the drawings) create repulsive forces between them.

electrostatic potential that decays exponentially away from the walls. It is thus smallest in the middle of the region between the surfaces and largest at the surfaces. The spatial variation of the electrostatic interaction is just as in the case of structural interactions described with a characteristic decay length, termed the Debye length in this case, which for uni–uni valent salts assumes the value of λ_D *E* 3 Å/$\sqrt{I}$, where *I* is the ionic strength of the salt in moles per liter. A 0.1 M solution of uni–uni valent salt, such as NaCl, would thus have the characteristic decay length of about 9.5 Å. Beyond this separation, the charged bodies do not feel each other any more. By adding or removing salt from the bathing solution, we are thus able to regulate the range of electrostatic interactions.

The exponential decay of the electrostatic field away from the charged surfaces with a characteristic length independent (to the lowest order) of the surface charge is one of the most important results of the Poisson-Boltzmann theory.

Obviously as the surfaces come closer together, their decaying electrostatic potentials begin to interpenetrate [25]. The consequence of this interpenetration is a repulsive force between the surfaces that again decays exponentially with the intersurface separation and a characteristic length again equal to the Debye length. For two planar surfaces at a separation *D*, bearing sufficiently small charges, characterized by the surface charge density σ, so that the ensuing electrostatic potential is never larger than k_BT/e, where k_B is the Boltzmann's constant and *e* is the elementary electron charge, one can derive the expression $F(D) \sim \sigma^2\lambda \exp(-D/\lambda_D)$ [27] for the interaction free energy per unit surface area $F(D)$. The typical magnitude of the electrostatic interaction in different systems of course depends on the magnitude of the surface charge. It would not be unusual in lipids to have surface charge densities in the range of one elementary charge per 50 to 100 Å^2 surface area [29]. For this range of surface charge densities, the constant prefactor in the expression for the osmotic pressure would be of the order 0.4–1.2 × 10^7 N/m.

The same type of analysis would apply also to two charged cylindrical bodies, e.g. two molecules of DNA, interacting across an electrolyte solution. What one evaluates in this case is the interaction free energy per unit length of the cylinders [30], $g(R)$, where *R* is the separation between the cylinders, which can be obtained in the approximate form $g(R) = \mu^2 \exp(-R/\lambda_D)$. It is actually possible to get also an explicit form [30] of the interaction energy between two cylinders even if they are skewed by an angle θ between them. In this case, the relevant quantity is the interaction free energy itself (if θ is nonzero, then the interaction energy does not scale with the length of the molecules) that can be obtained in a closed form as $F(R,\theta) \sim \mu^2\lambda_D R^{1/2} \exp(-R/\lambda_D)/\sin\theta$.

The predictions for the forces between charged colloid bodies have been reasonably well borne out for electrolyte solutions of uni–uni valent salts [31]. In that case, there is near quantitative agreement between theory and experiment. However, for higher valency salts, the Poisson-Boltzmann theory does not only give the wrong numerical values for the strength of the electrostatic interactions, but also misses their sign. In higher valency salts, the correlations among mobile charges between charged colloid bodies due to thermal fluctuations in their mean concentration lead effectively to attractive interactions [32] that are in many respects similar to van der Waals forces that we analyze next.

21.2.1.3 van der Waals Forces

Van der Waals charge fluctuation forces are special in the sense that they are a consequence of thermodynamic as well as

quantum mechanical fluctuations of the electromagnetic fields [15]. They exist even if the average charge, dipole moment, or higher multipole moments on the colloid bodies are zero. This is in stark contrast to electrostatic forces that require a net charge or a net polarization to drive the interaction. This also signifies that van der Waals forces are much more general and ubiquitous than any other force between colloid bodies [9].

There are many different approaches to van der Waals forces [15,33,34]. For small molecules interacting at a relatively large distance, one can distinguish different contributions to the van der Waals force, stemming from thermally averaged dipole–dipole potentials (the Keesom interaction), dipole-induced dipole interactions (the Debye interaction), and induced dipole–induced dipole interactions (the London interaction) [35]. They are all attractive and their respective interaction energy decays as the sixth power of the separation between the interacting molecules. The magnitude of the interaction energy depends on the electromagnetic absorption (dispersion) spectrum of interacting bodies, hence also the term dispersion forces.

For large colloidal bodies composed of many molecules, the calculation of the total van der Waals interactions is not trivial [15,34], even if we know the interactions between individual molecules composing the bodies. Hamaker assumed that one can simply add the interactions between composing molecules in a pairwise manner. It turned out that this was a very crude and simplistic approach to van der Waals forces in colloidal systems, as it does not take into account the highly nonlinear nature of the van der Waals interactions in condensed media. Molecules in a condensed body interact among themselves, thus changing their properties, hence their dispersion spectrum, which in turn modifies the van der Waals forces between them.

Lifshitz, following work of Casimir [9,15,34], realized how to circumvent this difficulty and formulated the theory of van der Waals forces in a way that already includes all these nonlinearities. The main assumption of this theory is that the presence of dielectric discontinuities, as in colloid surfaces, modifies the spectrum of electromagnetic field modes between these surfaces (see Figure 21.8). As the separation between colloid bodies varies, so do the eigenmode frequencies of the electromagnetic field between and within the colloid bodies. It is possible to deduce the change in the free energy of the electromagnetic modes due to the changes in the separation between colloid bodies coupled to their dispersion spectral characteristics [36].

Based on the work of Lifshitz, it is now clear that the van der Waals interaction energy is just the change of the free energy of field harmonic oscillators at a particular eigenmode frequency ω as a function of the separation between the interacting bodies D and temperature T, $\omega = \omega(D,T)$. With this equivalence in mind, it is quite straightforward to calculate the van der Waals interaction free energy between two planar surfaces at a separation D and temperature T; the dielectric permittivity between the two surfaces, ε, and within the surfaces, ε', must both be known as a function of the frequency ω of the electromagnetic field [36]. This is a consequence of the fact that in general, the dielectric media comprising the

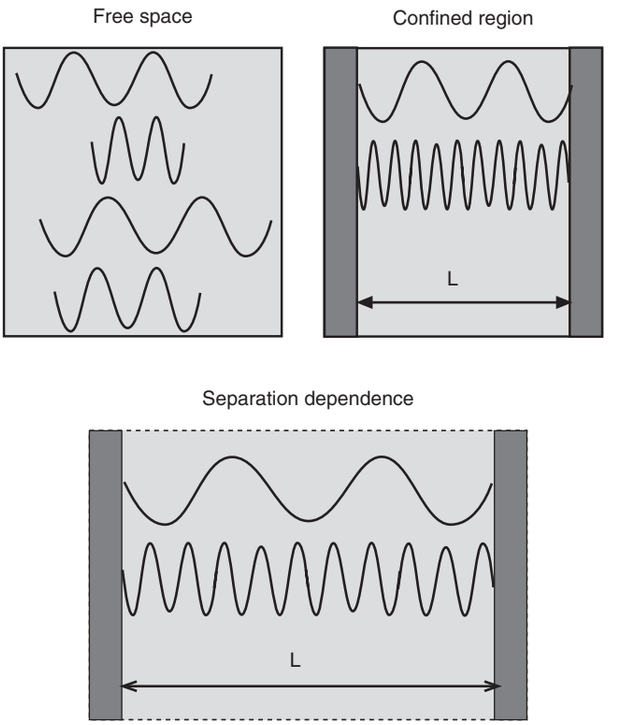

FIGURE 21.8 Pictorial introduction to the theory of Lifshitz-van der Waals forces between colloid bodies. Empty space is alive with electromagnetic (EM) field modes that are excited by thermal as well as quantum mechanical fluctuations. Their frequency is unconstrained and follows the black body radiation law. Between dielectric bodies only those EM modes survive that can fit into a confined geometry. As the width of the space between the bodies varies, so do the allowed EM mode frequencies. Every mode can be treated as a separate harmonic oscillator, each contributing to the free energy of the system. Since this free energy depends on the frequency of the modes that in turn depend on the separation between the bodies, the total free energy of the EM modes depends on the separation between the bodies. This is an intuitive description of the Lifshitz-van der Waals force. (From Mahanty, J. and Ninham, B.W., *Dispersion Forces*, Academic Press, London, 1976.)

surfaces as well as the space between them are dispersive, which means that their dielectric permittivities depend on the frequency of the electromagnetic field, i.e. $\varepsilon = \varepsilon(\omega)$. With this in mind, one can derive the interaction free energy per unit surface area of the interacting surfaces in the form $F(D) = A(D)12\pi D^2$, where the s.c. Hamaker coefficient A depends on AQ5 the difference between the dielectric permittivities of the interacting materials at different imaginary frequencies $\iota\xi$. It can, in general, be split into two terms: the first term in the Hamaker coefficient is due to thermodynamic fluctuations, such as Brownian rotations of the dipoles of the molecules composing the media or the averaged dipole-induced dipole forces and depends on the static ($\omega = 0$) dielectric response of the interacting media, while the second term is purely quantum mechanical in nature [15]. The imaginary argument of the dielectric constants is not that odd since $\varepsilon(\iota\xi)$ is an even function of ξ, which makes $\varepsilon(\iota\xi)$ also a purely real quantity [36].

In order to evaluate the magnitude of the van der Waals forces, one has to know the dielectric dispersion $\varepsilon(\omega)$, or more appropriately $\varepsilon(\iota\xi)$, of all the media involved. This is no simple task and can be accomplished only for very few materials [34]. Experiments seem to be a much more straightforward way to proceed. The values for the Hamaker coefficients of different materials interacting across water are between 0.3 and 2.0×10^{-20} J. Specifically for lipids, the Hamaker constants are quite close to theoretical expectations except for the phosphatidylethanolamines that show a much larger attractive interactions probably due to headgroup alignment [31]. Evidence from direct measurements of attractive contact energies as well as direct force measurements suggest that van der Waals forces are more than adequate to provide attraction between bilayers for them to form multilamellar systems [37].

For cylinders, the same type of argument applies except that due to the geometry, the calculations are a bit more tedious [38]. Here the relevant quantity is not the free energy per unit area but the interaction free energy per unit length of the two cylinders of radius a, $g(R)$, considered to be parallel at a separation R. The calculation [39] leads to the following form: $g(R) \sim Aa^4/R^5$ where the constant A again depends on the differences between dielectric permittivities, $\varepsilon_{\parallel}$ and $\varepsilon_{\perp}$, respectively, the parallel and the perpendicular components of the dielectric permittivity of the dielectric material of the cylinders, and ε_m, the dielectric permittivity of the bathing medium.

If however the two interacting cylinders are skewed at an angle θ, then the interaction free energy $G(R,\theta)$, this time not per length, is obtained [39] in the form $G(R) \sim (A + B\cos^2\theta)(a^4/R^4 \sin\theta)$. The constants A and B describe the dielectric mismatch between the cylinder and the bathing medium at different imaginary frequencies. The same correspondence between the thermodynamic and quantum mechanical parts of the interactions as for two parallel cylinders applies also to this case. Clearly the van der Waals force between two cylinders has a profound angular dependence that, in general, creates torques between the two interacting molecules.

Taking the numerical values of the dielectric permittivities for two interacting DNA molecules, one can calculate that the van der Waals forces are quite small, typically one to two orders of magnitude smaller than the electrostatic repulsions between them, and in general cannot hold the DNAs together in an ordered array. Other forces, leading to condensation phenomena in DNA [10], clearly have to be added to the total force balance in order to get a stable array. There is as yet still no consensus on the exact nature of these additional attractions. It seems that they are due to the fluctuations of counterions atmosphere close to the molecules.

21.2.1.4 DLVO Model

The popular Derjaguin-Landau-Verwey-Overbeek (DLVO) [9,25] model assumes that electrostatic double layer and van der Waals interactions govern colloid stability. Applied with a piety not anticipated by its founders, this model actually does surprisingly work rather well in many cases. Direct osmotic stress measurements of forces between lipid bilayers show that at separations less than ~10 Å, there are qualitative deviations from the DLVO thinking [40]. For micron-sized objects and for macromolecules at greater separations, electrostatic double-layer forces and sometimes van der Waals forces tell us what we need to know about interactions governing movement and packing.

21.2.1.5 Geometric Effects

Forces between macromolecular surfaces are most easily analyzed in plane-parallel geometry. Because most of the interacting colloid surfaces are not planar, one must either evaluate molecular interactions for each particular geometry or devise a way to connect the forces between planar surfaces with forces between surfaces of a more general shape. The Derjaguin approximation [9] assumes that interactions between curved bodies can be decomposed into interactions between small plane-parallel sections of the curved bodies (see Figure 21.9). The total interaction between curved bodies would be thus equal to a sum where each term corresponds to a partial interaction between quasiplane-parallel sections of the two bodies.

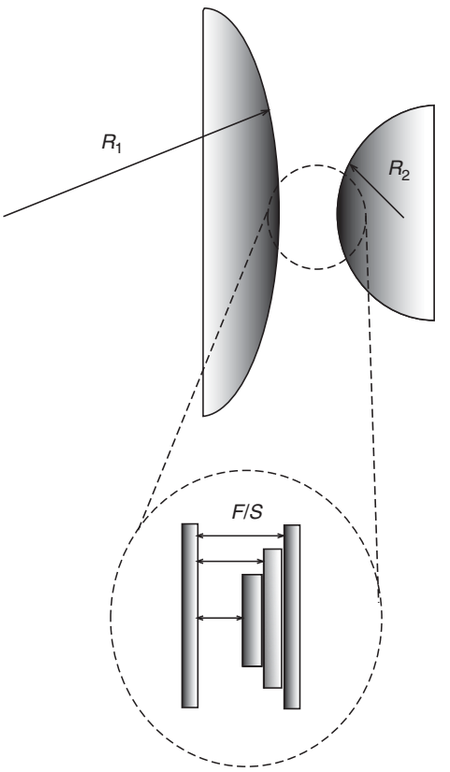

FIGURE 21.9 The Derjaguin approximation. Formulating forces between oppositely curved bodies (e.g., cylinders, spheres etc.) is very difficult. But it is often possible to use an approximate procedure. Two curved bodies (two spheres of unequal radii in this case) are approximated by a succession of planar sections, interactions between which can be calculated relatively easily. The total interaction between curved bodies is obtained through a summation over these planar sections.

This idea can be given a completely rigorous form and leads to a connection between the interaction free energy per unit area of two interacting planar surfaces, $F(D)$, and the force acting between two spheres at minimal separation D, $f(D)$, one with the mean radius of curvature R_1 and the other one with R_2. The formal equivalence can be written as follows: $f(D) = 2\pi(R_1R_2/(R_1 + R_2))F(D)$. A similar equation can also be obtained for two cylinders in the form, $f(D) = 2\pi(R_1R_2)^{1/2} F(D)$.

These approximate relations clearly make the problem of calculating interactions between bodies of general shape tractable. The only caveat here is that the radii of curvature should be much larger than the proximal separation between the two interacting bodies, effectively limiting the Derjaguin approximation to sufficiently small separations.

Using the Derjaguin formula or evaluating the interaction energy explicitly for those geometries for which it is not an insurmountable task, one can now obtain a whole range of DLVO expressions for different interaction geometries (see Figure 21.10). The salient features of all these expressions are that the total interaction free energy always has a primary minimum that can only be eliminated by strong short range hydration forces and a secondary minimum due to the compensation of screened electrostatic repulsion and van der Waals–Lifshitz attraction. The position of the secondary minimum depends as much on the parameters of the forces (Hamaker constant, fixed charges, and ionic strength) as well as on the interaction geometry. One can state generally that the range of interaction between the bodies of different shapes is inversely proportional to their radii of curvature.

Thus the longest-range forces are observed between planar bodies, and the shortest between small (point-like) bodies. What we have not indicated on Figure 21.7 is that the interaction energy between two cylindrical bodies, skewed at a general angle θ and not just for parallel or crossed configurations, can be obtained in an explicit form. It follows simply from these results that the configuration of two interacting rods with minimal interaction energy is the one corresponding to $\theta = \pi/2$, i.e. corresponding to crossed rods.

21.2.1.6 Fluctuation Forces

The term "fluctuation forces" is a bit misleading in this context because clearly van der Waals forces already are fluctuation forces. What we have in mind is thus a generalization of

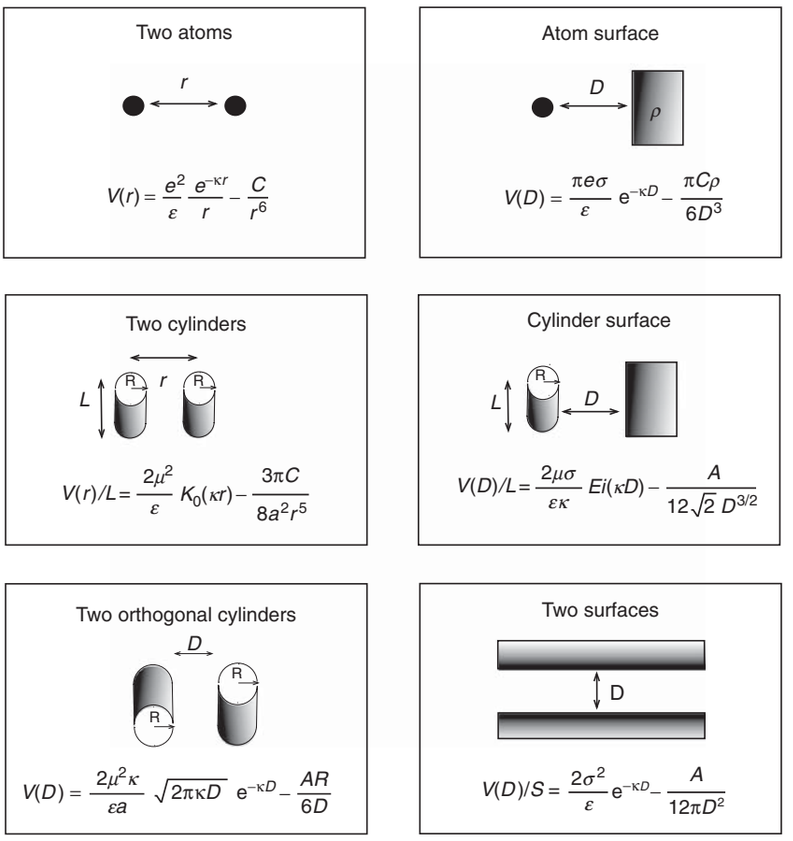

FIGURE 21.10 A representative set of DLVO interaction expressions for different geometries most commonly encountered in biological milieus: Two small particles, a particle and a wall, two parallel cylinders, a cylinder close to a wall, two skewed cylinders, and two walls. The DLVO interaction free energy is always composed of a repulsive electrostatic part (calculated from a linearized Poisson-Boltzmann theory) and an attractive van der Waals part. Charge: e, charge per unit length of a cylinder: μ, charge per unit surface area of a wall: σ, C are geometry-dependent constants, ε the dielectric constant, κ the inverse Debye length, and ρ the density of the wall material. The functions $K_0(x)$ (the Bessel function K_0) and $Ei(x)$ (the exponential integral function) both depend essentially exponentially on their respective argument.

the van der Waals forces to situations where the fluctuating quantities are not electromagnetic fields but other quantities subject to thermal fluctuations. No general observation as to the sign of these interactions can be made; they can be either repulsive or attractive and are as a rule of thumb comparable in magnitude to the van der Waals forces.

The most important and ubiquitous force in this category is the undulation or Helfrich force [41]. It has a very simple origin and operates among any type of deformable bodies as long as their curvature moduli are small enough (comparable to thermal energies). It was shown to be important for multilamellar lipid arrays [42] as well as in hexagonal polyelectrolyte arrays [43] (see Figure 21.11).

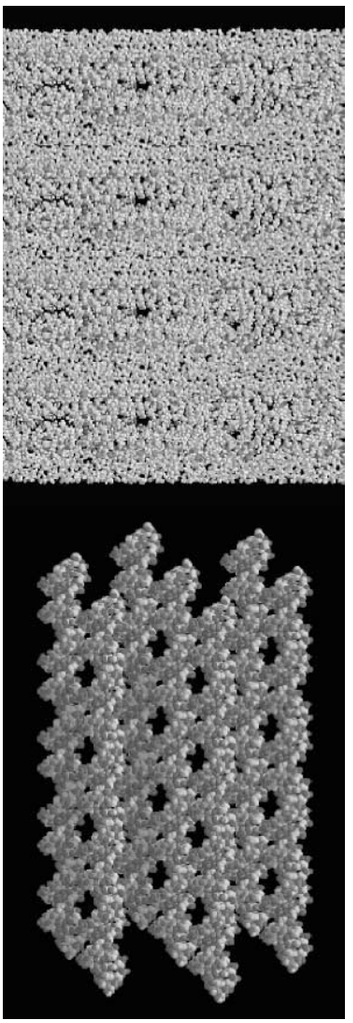

FIGURE 21.11 (See color insert following page xxx.) Thermally excited conformational fluctuations in a multilamellar membrane array (small molecules are waters and long chain molecules are phospholipids) or in a tightly packed polyelectrolyte chain array (the figure represents a hexagonally packed DNA array) leading to collisions between membranes or polyelectrolyte chains. These collisions contribute an additional repulsive contribution to the total osmotic pressure in the array, a repulsion that depends on the average spacing between the fluctuating objects.

The mechanism is simple. The shape of deformable bodies fluctuates because of thermal agitation (Brownian motion) [26]. If the bodies are close to each other, the conformational fluctuations of one will be constrained by the fluctuations of its neighbors. Thermal motion makes the bodies bump into each other, which creates spikes of repulsive force between them. The average of this force is smooth and decays continuously with the mean separation between the bodies.

One can estimate this steric interaction for multilamellar lipid systems and for condensed arrays of cylindrical polymers (Figure 21.11). The only quantity entering this calculation is the elastic energy of a single bilayer that can be written as the square of the average curvature of the surface, summed over the whole area of the surface, multiplied by the elastic modulus of the membrane, K_C. K_C is usually between 10 and 50 kBT [44] for different lipid membranes. If the instantaneous deviation of the membrane from its overall planar shape in the plane is now introduced as u, the presence of neighboring membranes introduces a constraint on the fluctuations of u that basically demands that the average of the square of u must be proportional to D^2, where D is the average separation between the membranes in a multilamellar stack. Thus we should have $u^2 \sim D^2$. The free energy associated with this constraint can now be derived in the form $F(D) \sim (k_BT)^2(K_CD^2)$, and is seen to decay in inverse proportion to the separation between bilayers squared [41].

It has thus obviously the same dependence on D as the van der Waals force. This is, however, not a general feature of undulation interactions as the next example clearly shows. Also we only indicated the general proportionality of the interaction energy. The calculation of the prefactors can be a difficult [45] especially because the elastic bodies usually do not interact with idealized hard repulsions but rather through soft potentials that have both attractive as well as repulsive regimes.

The same line of thought can now be applied to flexible polymers in a condensed array [43]. This system is a one-dimensional analog of the multilamellar membrane system. For polymers, the elastic energy can be written similarly to the membrane case as the square of the local curvature of the polymer, multiplied by the elastic modulus of the polymer, integrated over its whole length. The elastic modulus K_C is usually expressed through a persistence length $L_p = K_C/(kBT)$. The value of the persistence length tells us how long a polymer can be before the thermal motion forces it to fluctuate wildly. For DNA, this length is about 50 nm. It spans, however, the whole range of values between about 10 nm for hyaluronic acid, all the way to 3 mm for microtubules. Using now the same constraint for the average fluctuations of the polymer away from the straight axis, one derives the relationship for the free energy change due to this constraint, $F(D) \sim (k_BT)(L_p^{1/3}D^{2/3})$ [43].

Clearly the D dependence for this geometry is very much different from the one for van der Waals force, which would be D^{-5}. There is thus no general connection between the van der Waals force and the undulation fluctuation force. Here again one has to indicate that if the interaction potential between fluctuating bodies is described by a soft potential, with no discernible hard core, the fluctuation interaction can have a profoundly different dependence on the mean separation [43].

Apart from the undulation fluctuation force, there are other fluctuation forces. The most important among them appears to be the monopolar charge fluctuation force [46], recently investigated in the context of DNA condensation. It arises from transient charge fluctuations along the DNA molecule due to constant statistical redistributions of the counterion atmosphere.

The theory of charge fluctuation forces is quite intricate and mathematically demanding [47]. Let us just quote a rather interesting result: if two point charges interact via a "bare" potential $V_0(R)$, where R is the separation between them, then the effect of the thermal fluctuations in the number of counterions surrounding these charges would lead to an effective interaction of the form $V(R) \sim kBT(V_0(R))^2$. The fluctuation interaction in this case would thus be attractive and proportional to the square of the bare interaction.

This simple result already shows one of the salient features of the interaction potential for monopolar charge fluctuation forces, i.e., it is screened with half the Debye screening length (because of $V^2(R)$). If there is no screening, however, the monopolar charge fluctuation force becomes the strongest and longest ranged among all the fluctuation forces. It is however much less general than the related van der Waals force and at present, it is still not clear what the detailed conditions should be for its appearance, the main difficulty being the question whether charge fluctuations in the counterion atmosphere are constrained or not.

21.2.1.7 Attractive Electrostatic Forces: Strong Coupling and Polyelectrolyte Bridging

As we pointed out in the section on the electrostatic forces, the predictions of the Poisson-Boltzmann theory for interactions between charged macroions in electrolyte solutions of univalent salts conform well with osmotic stress experiments on ordered DNA arrays to the extent of a near quantitative agreement between theory and experiment [43]. The effective surface charge on DNA obtained from osmotic stress experiments is close, but nevertheless consistently somewhat smaller from the theoretical predictions based on the Manning counterion condensation theory. Theoretical arguments based on the more detailed analysis of the counterion condensation in the presence of salt [48] generally agree that the effective charge on DNA in an ionic solution should be smaller than the one based on the estimate of Manning condensation theory.

When the same analysis of the osmotic stress experiments is furthermore applied to salts containing at least one higher valency counterion, such as Mn^{2+}, $Co(NH_3)_6^{3+}$ or various polyamines, the theoretical predictions based on the Poisson-Boltzmann theory tend to lose agreement with experiment. Not only does the Poisson-Boltzmann theory give the wrong numerical values for the strength of the electrostatic interactions, but also and more importantly misses their sign since experiments point to the existence of electrostatic attractions [22]. This attraction is deduced from the shape of the osmotic pressure as a function of density of DNA, i.e. there are regions of DNA density where the corresponding osmotic pressure in a DNA array remains constant [49] (see left panel of Figure 21.12 for $Co(NH_3)_6^{3+}$concentrations of 12 and 6 mM).

This is quite similar to the pressure versus volume isotherms in the case of a liquid–gas transition [50] (see right panel of Figure 21.12). In that case due to attractive van der Waals interactions between gas molecules, the gaseous phase condenses into a liquid phase at a certain condensation pressure that depends on the temperature. As we reduce the

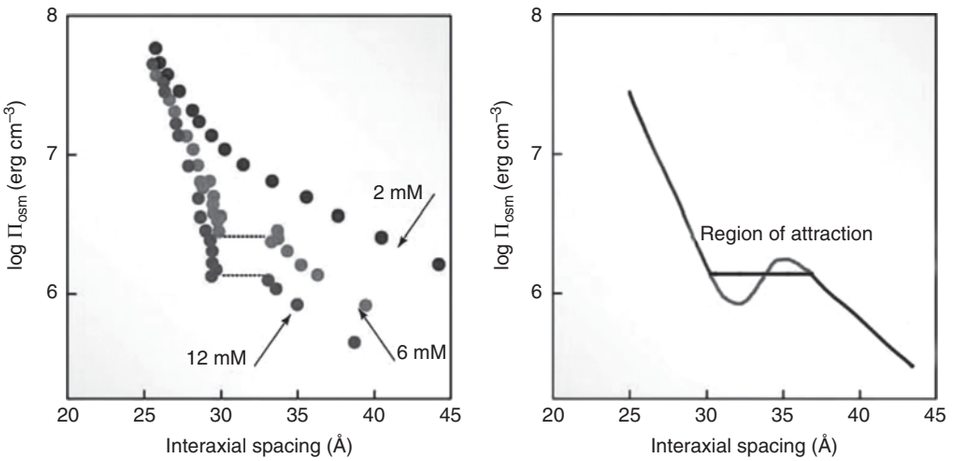

FIGURE 21.12 Left-hand side: Osmotic pressure as a function of DNA concentration in a DNA array with monovalent salt (0.25 M NaCl) with added trivalent counterion CoHex ($Co(NH_3)_6^{3+}$) at concentration from 0 to 20 mM. Above a sufficiently large value of CoHex concentration (17 mM), DNA spontaneously precipitates. For smaller values of CoHex concentration, e.g., 6 mM, the osmotic pressure dependence on the interaxial spacing shows a horizontal transition line between two regimes of repulsive forces. Right-hand side: A schematic explanation of the 6 mM CoHex concentration line. The dependence of the osmotic pressure on the interaxial spacing is in fact nonmonotonic due to the presence of attractive interactions in the region depicted in red. Because of the condition of stability, just as in the case of the van der Waals isotherm, the regions of attraction can only be traversed via a horizontal transition line.

volume in the region of liquid–gas coexistence, more of the gas condenses into liquid, while the applied force required to keep the gas in place is unchanged. As a result, the part of the isotherm between the start and the end of the condensation process is flat (see right panel of Figure 21.12). In the DNA case, the role of inverse temperature is played (roughly) by the concentration of the polyvalent counterion. For sufficiently large concentration, for example, of $Co(NH_3)_6^{3+}$, the DNA array spontaneously precipitates or condenses into an ordered high density phase. One thus concludes that the polyvalent counterion should confer some kind of attractive interactions between nominally equally charged DNA molecules. What is so special about multivalent counterions, such as Mn^{2+}, $Co(NH_3)_6^{3+}$, or various polyamines, that leads to a complete breakdown of the simple Poisson-Boltzmann framework?

In order to understand this anomaly, we should first relinquish a seemingly obvious explanation—that we are dealing with the effects of DNA–DNA van der Waals interactions as is the case in condensation of gases (see above). These forces are much too small to account for the strong attractions seen with polyvalent counterions [34]. So how are we to rationalize the polyvalent counterion-mediated DNA attractions?

When dealing with small univalent counterions in the Poisson-Boltzmann framework, we actually assume that they can be described collectively, via their number or charge density, without acknowledging that we have individual charges (see, for example, the chapter by Andelman in Ref. [27]). This approach is usually referred to as the mean-field approach in statistical thermodynamics and is used in a plethora of contexts. It works only if the concentration of the counterions or salt ions, in general, is high enough. Poisson-Boltzmann theory is, in fact, a mean-field theory. When we go to polyvalent counterions of valency Z, and for the sake of the argument, assume that $Z \gg 1$, we have fewer counterions to satisfy the overall electroneutrality of the system. In an extreme case, we would be dealing with just a few of them as represented schematically in Figure 21.13. In this case, the mean-field description would break down miserably. Why? Because there is no proper "mean-field" to speak of. We have to deal with each of the counterions individually. This demands a completely different approach that has to be set apart and formulated in a completely different language than the popular Poisson-Boltzmann (mean-field) theory. This alternative approach has been formulated by various people and goes under the strong-coupling approach [51] or the strong-correlation approach [52].

Let us try to describe this alternative approach without invoking the heavy analytical machinery on which it relies. For instance, assume that we have only one giant polyvalent counterion between two fixed charges of opposite sign (see right panel of Figure 21.13). The charge of this giant counterion would have to be large indeed in order to neutralize the two surfaces with fixed charge of opposite sign, but this is the assumption. The overall force between the fixed charges is composed of direct repulsion between the fixed charges, since they are assumed to be equally charged plus the attraction between the left fixed charge and the counterion (remember, they bear charges of opposite sign), assumed to be in the middle of the space between the fixed charges and the attraction between the right fixed charge and the counterion (again remember, they bear charges of opposite sign). Summing together all these contribution, we get an overall attraction. Thus in this case, like-charged surfaces do not repel as goes the common wisdom, in fact they attract. This intuitive argument can be made exact within the strong-coupling approximation that supersedes the Poisson-Boltzmann description in the case of polyvalent counterions. The strong coupling approach can be formulated also in an alternative form of the s.c. correlated Coulomb fluid theory [52], but is always reduced to the assumption that polyvalent counterions interact with the fixed charges individually and not collectively as in the Poisson-Boltzmann framework. The attraction usually outweighs repulsion only at small separation between the surfaces bearing fixed charges, and as the separation increases the idealization invoked above becomes increasingly less realistic, we move smoothly from the strong-coupling attraction to the standard Poisson-Boltzmann repulsion.

An alternative interpretation of the same effect [22] would be that the polyvalent counterion adsorbs onto the charged surface and thus changes its hydration pattern by interacting much more strongly with the water molecules in its vicinity than with the fixed charges on the surface. This modulation of the hydration pattern on both of the apposed surfaces could also induce structural attractions, qualitatively similar to the strong coupling electrostatic interactions. Both effects are short-ranged and are thus difficult to disentangle. Strong counterion specificity in the magnitude of attractive

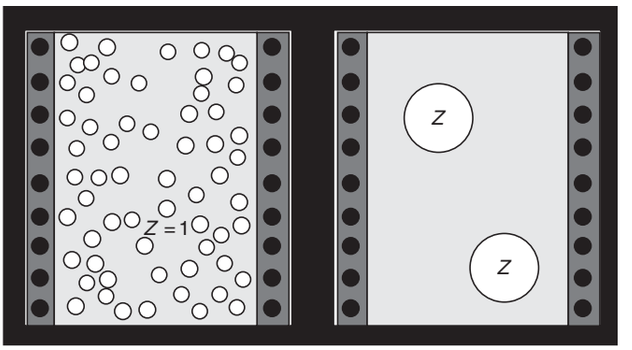

FIGURE 21.13 Monovalent counterions (small white circles) assumed to be positive between two oppositely charged surfaces (small black circles) vs. polyvalent positive counterions (large white circles) in the same geometry. In the idealized case when the valency (Z) of the counterion is assumed to be very large ($Z \gg 1$), we can treat just a single counterion (of the two depicted in the right panel) in the space between the two surfaces bearing fixed charges. Direct electrostatic interactions between negatively charged surfaces are repulsive, but the interactions between the (single) counterion and the surfaces are attractive since the counterion bears a charge opposite in sign to those on the surfaces. The sum of the two is also net attractive. This is the physical origin of the correlation attraction in polyvalent counterion systems such as DNA with trivalent $Co(NH_3)_6^{3+}$counterion.

interactions shows that at least a part of it has an origin in counterion properties other than its valency.

Until now, when invoking polyvalent counterions what we had in mind were relatively small charged particles without any inherent structure. We now move forward. By increasing the valency of the counterions, thus adding more and more charge to them, ions do not only grow in size but in fact usually become more and more polymer-like. Their inherent chemical structure becomes increasingly chain-like. In fact, we refer to them as polyelectrolytes [53], which in this context means long, usually positively charged polymer chains. Typical examples include polyamines, such as spermine, and polypeptides such as poly-L-lysine and poly-L-arginine. Mixing these long flexible polycations with DNA in an ionic solution leads again to ordered DNA arrays that allow the application of the osmotic stress technique, resulting in equation of state, i.e. osmotic pressure as a function of the DNA density, just as in the case of simple salts [54]. Strong attractions between DNA molecules have been measured also in solutions containing such polycations. In this case, however, it would be difficult to invoke the previous argument based on the strong-coupling picture, since the charged polymer chains have very extended configurations that do not allow us to use gedanken experiments based on point charge models as we did before, where the total interaction was composed of direct repulsion between the fixed charges plus the attraction between the fixed charges and the counterion. So what would be an appropriate conceptual picture to explain attractions between surfaces with fixed negative charges mediated by these long polycations?

We again give a simple description of what is going on without going into complicated mathematical details [55]. Imagine the situation of two cylindrical macroions with fixed negative charge together with a polycation chain and possibly simple salt and counterions (as depicted in Figure 21.14). Because the polyelectrolyte chain is oppositely charged from the macroions, it would like to neutralize them due to electrostatic attraction. In the case of sufficiently long polycations, the flexible chain can wrap around both macroions with fixed charges, creating a polyelectrolyte bridge between them (see the schematic representation on the left panel of Figure 21.14). This bridge is trying to pull the two fixed charges together by an entropic elastic force due to a tendency to maximize the possible number of polymer conformations, thus creating an attractive force between them. However, in this case, there is no strong-coupling or correlation effect. The chain draws the two macroions together simply because of its connectivity [56]. The total force in this case is composed of the direct electrostatic repulsion between the macroions with partially neutralized charges and the elastic term corresponding to the part of the polyelectrolyte chain between the macroions. Note the difference however. In the strong coupling viewpoint, the attraction is still electrostatic in origin, stemming from the sharing of the simple polyvalent counterion between the two fixed charges. In the case of polyelectrolyte bridging on the other hand, the attraction is only distantly electrostatic in origin, stemming more directly from the elasticity, connectivity, and conformational flexibility of the polycation chain. Similar to the situation with simple, not polymeric, counterions, the polyelectrolyte bridging attraction is also usually short-ranged except in arrays of macromolecules where it can be also long(er) ranged [57].

Both mechanisms, strong coupling attraction as well as polyelectrolyte bridging, have a profound effect on the balance of forces in DNA arrays as well as for conformations of a single DNA in a very dilute solution. In the former case, they have been observed directly in the DNA–polycation complexes analyzed by the osmotic stress technique that we will describe in more detail later [54], whereas in the latter case, they are responsible for the phenomenon of DNA condensation that we will not deal with specifically in this chapter.

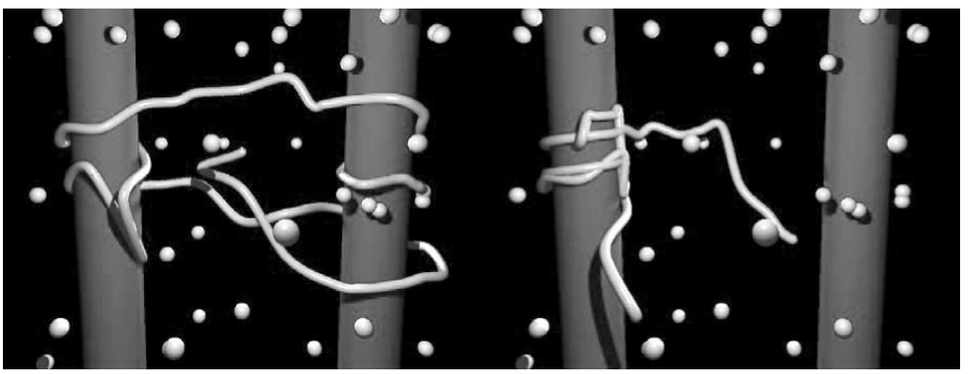

FIGURE 21.14 A schematic presentation of two cylindrical macroions with fixed (negative) charges (blue cylinders) with a polycation chain (green wire) and explicit salt- and counterions (small yellow spheres) in between. The polycation chain tends to neutralize the fixed charges and thus wraps around both cylindrical macroions in a bridging configuration. Left-hand side: For small enough separation between the counterions, the polycation can bridge the space between them resulting in attractive bridging interactions. Right-hand side: For larger separations, the polycation cannot bridge the space between macroions and the bridging attraction is not present. This polycation-mediated bridging attraction is usually of short range but much stronger than the van der Waals interaction.

21.2.1.8 Lessons

Molecular forces apparently convey a variety that is surprising considering the fact that they are all to some extent or another just a variant of electrostatic interactions. Quantum and thermal fluctuations apparently modify the underlying electrostatics, leading to qualitatively novel and unexpected features. Electrostatic interactions mediated by polyvalent counterions show a quite surprising feature of being actually attractive even between nominally equally charged macroions such as two DNA molecules. These attractions can be due to either complicated correlation or hydration effects, or polyelectrolyte bridging attractions if the counterions have long flexible charged chains. The menagerie of forces obtained in this way is what one has to deal with and understand when trying to make them work for us.

21.3 DNA MESOPHASES

21.3.1 Polyelectrolyte Properties of DNA

We can define several levels of DNA organization similar to Ref. [1]. Its primary structure is the sequence of base pairs. Its secondary structure is the famous double helix that can exist in several conformations. In solution, the B-helical structure dominates [58]. The bases are perpendicular to the axis of the molecule and are 0.34 nm apart, and 10 of them make one turn of the helix. These parameters can vary for DNA in solution where up to 10.5 base pairs can make a whole turn of the double helix [59]. In the A structure, the bases are tilted with respect to the direction of the helix and this arrangement yields an internal hole, wider diameter, and closer packing (see Figure 21.15). Other conformations, such as the left-handed Z form, are rare. In solution, DNA's tertiary structure includes the many bent and twisted conformations in three dimensions.

DNA lengths can reach macroscopic dimensions. For instance, the human genome is coded in approximately 3 billion base pairs with a collective linear stretch on the order of a meter. Obviously, this molecule must undergo extensive compaction in order to fit in the cell nucleus. In natural environments, DNA is packaged by basic proteins, which form chromatin structures to keep DNA organized. In the test tube, DNA can be packaged into very tight and dense structures as well, primarily by various "condensing" agents. Their addition typically induces a random coil to globule transition. At large concentrations, DNA molecules, like lipids, form ordered liquid crystalline phases [10] that have been studied extensively at different solution conditions [8].

In vitro, at concentrations above a critical value [60], polyelectrolyte DNA self-organizes in highly ordered mesophases [8]. In this respect, it is a lyotropic liquid crystal. But contrary to the case of lipid mesophases, where the shape of constituent molecules plays a determining role, the organization of DNA in condensed phases is primarily a consequence of its relatively large stiffness [8]. The orientational ordering of DNA at high concentrations is promoted mostly by the interplay between entropically favored disorder or misalignment and the consequent price in terms of the high interaction

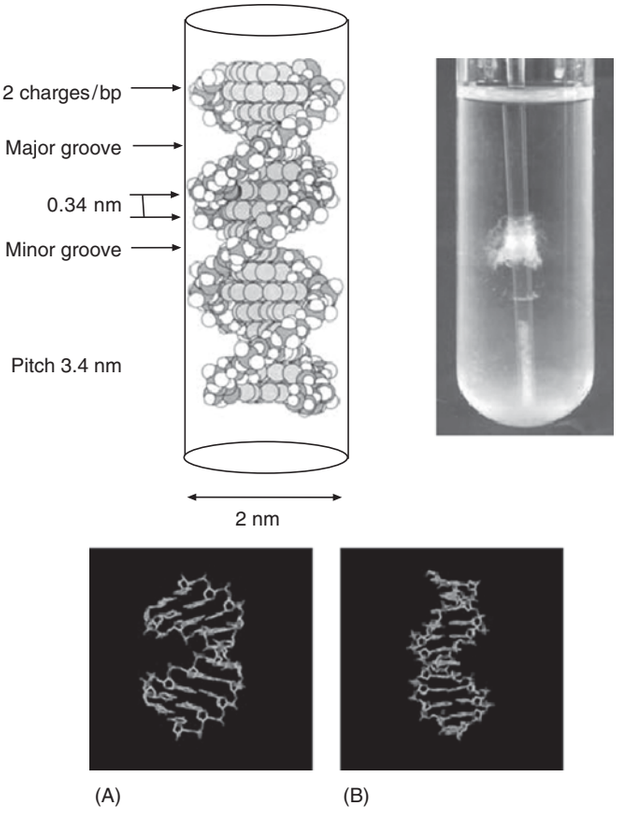

Polymer	Solvent	Persistence length (nm)
Microtubule	Water	3,000,000
F-actin	Water	15,000
Schizophyllan	Water	200
Xanthan	0.1 M NaCl	120
DNA	0.2 M NaCl	50
Hyaluronic acid	0.2 M NaCl	7

FIGURE 21.15 Structural parameters of a DNA molecule. The two relevant configurations of the DNA backbone: A-DNA, common at small hydrations or high DNA densities, and B-DNA common in solution at large hydrations and lower DNA densities. The test tube holds ethanol-precipitated DNA in solution. Its milky color is due to the light scattering by thermal conformational fluctuations in the hexatic phase (see main text). Box: Typical persistence lengths for different (bio)polymer chains in nanometers. DNA persistence length was first inferred from light scattering experiments in 1953 by Peterlin (From Peterlin, A., *Nature*, 1953, 171, 259).

energy. The mechanism of orientational ordering is thus the same as in standard short nematogens [61], with the main difference arising from the extended length of the polymeric chains. The discussion that follows will concentrate mostly on very long, on the order of 1000 persistence lengths, microns long, DNA molecules.

21.3.2 Flexibility of DNA Molecules in Solution

In isotropic solutions, DNA can be in one of the several forms. For linear DNA, individual molecules are effectively straight

over the span of a persistence length that can be defined also as the exponential decay length for the loss of angular correlation between two positions along the molecule, while for longer lengths they form a worm-like random coil. The persistence length of DNA is about 50 nm [1]. The persistence length has been determined by measuring the diffusion coefficient of different-length DNA molecules using dynamic light scattering and by enzymatic cyclization reactions [62]. It depends only weakly on the base-pair sequence and ionic strength.

DNA can also be circular as in the case of a plasmid. The closed form of a plasmid introduces an additional topological constraint on the conformation that is given by the linking number Lk [2]. The linking number gives the number of helical turns along a circular DNA molecule. Because plasmid DNA is closed, Lk has to be an integer number. By convention, Lk of a closed right-handed DNA helix is positive. The most frequent DNA conformation for plasmids in cells is negatively supercoiled. This means that for such plasmids, Lk is less than it would be for a torsionally relaxed DNA circle; negatively supercoiled DNA is underwound. This is a general phenomenon with important biological consequences. It seems that free energy of negative supercoiling catalyzes processes that depend on DNA untwisting such as DNA replication and transcription, which rely on DNA [63]. While the sequence of bases in exons determine the nature of proteins synthesized, it is possible that such structural features dictate the temporal and spatial evolution of DNA-encoded information.

21.3.3 Liquid Crystals

The fact that DNA is intrinsically stiff makes it form liquid crystals at high concentration [8]. Known for about 100 years, the simplest liquid crystals are formed by rodlike molecules. Solutions of rods exhibit a transition from an isotropic phase with no preferential orientation to a nematic phase, a fluid in which the axes of all molecules point on average in one direction (see Figure 21.11). The unit vector in which the molecules point is called the nematic director **n**. Nematic order is orientational order [61], in contrast to positional order that distinguishes between fluid and crystalline phases. Polymers with intrinsic stiffness can also form liquid crystals. This is because a long polymer with persistence length L_p acts much like a solution of individual rods that are all one persistence length long, thus the term "polymer nematics" [64].

If the molecules that comprise the liquid crystal are chiral, have a natural twist such as double helical DNA, then their orientational order tends to twist. This twist originates from the interaction between two molecules that are both of the same handedness. This chiral interaction is illustrated in Figure 21.16 for two helical or screw-like molecules. For steric reasons, two helices pack best when tilted with respect to each other. Instead of a nematic phase, chiral molecules form a cholesteric phase [61]. The cholesteric phase is a twisted nematic phase in which the nematic director twists continuously around the so-called cholesteric axis as shown in Figure 21.16. Using the same arguments as for plain polymers, chiral polymers form polymer cholesterics.

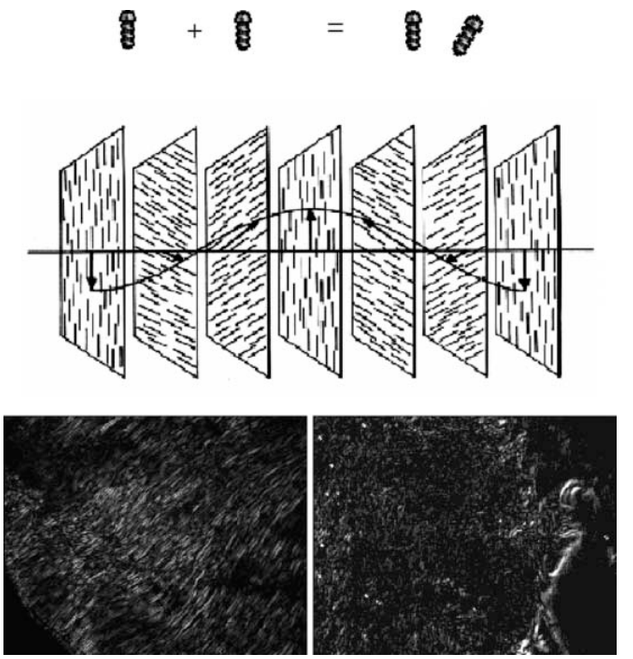

FIGURE 21.16 "Chiral" interaction for two helical or screw-like molecules. For steric reasons, two helices just as two screws (depicted on the figure) pack best when slightly tilted with respect to each other. Since DNA because of its double-stranded, helical nature, is a type of molecular screw, it too exhibits chiral interactions. Instead of a nematic phase depicted in Figure 21.11, characterized by the average constant direction of molecules, chiral molecules form a cholesteric phase. (From De Gennes, P.G. and Prost, J., *The Physics of Liquid Crystals*, 2nd ed., Oxford University Press, Oxford, 1993.) The cholesteric phase is a twisted nematic phase in which the nematic director twists continuously around a "cholesteric axis" depicted on the middle drawing. Under crossed polarizers (bottom), the DNA cholesteric phase creates a characteristic striated texture. For long DNA molecules, the striations appear disordered.

Both cholesteric and hexagonal liquid crystalline DNA phases were identified in the 1960s. This discovery was especially exciting because both phases were also found in biological systems. The hexagonal liquid crystalline phase can be seen in bacterial phages and the cholesteric phase can be seen in cell nuclei of dinoflagellates [8].

21.3.4 Measurements of Forces Between DNA Molecules

Liquid crystalline order lets us measure intermolecular forces directly. With the osmotic stress method, DNA liquid crystals are equilibrated against neutral polymer (such as PEG or PVP) solutions of known osmotic pressure, pH, temperature, and ionic composition [65]. Equilibration of DNA under osmotic stress of external polymer solution is effectively the same as exerting mechanical pressure on the DNA subphase with a piston (see Figure 21.4). In this respect, the osmotic stress technique is formally very much similar to the Boyle experiment

where one compresses a gas with mechanical pistons and measures the ensuing pressure. After equilibration under this known stress, DNA separation is measured either by X-ray scattering, if the DNA subphase is sufficiently ordered, or by straightforward densitometry [66]. Known DNA density and osmotic stress immediately provide an equation of state (osmotic pressure as a function of the density of the DNA subphase) to be codified in analytic form for the entire phase diagram. Then, with the local packing symmetry derived from X-ray scattering [7,65], and sometimes to correct for DNA motion [42], it is possible to extract the bare interaxial forces between molecules which can be compared with theoretical predictions as developed in Chapter 2. In vivo observation of DNA liquid crystals [67] shows that the amount of stress needed for compaction and liquid crystalline ordering is the same as for DNA in vitro.

21.3.5 Interactions Between DNA Molecules

Direct force measurements performed on DNA in univalent salt solutions reveal two types of purely repulsive interactions between DNA double helices [4]:

1. At interaxial separations less than ~3 nm (surface separation ~1 nm), an exponentially varying "hydration" repulsion is thought to originate from partially ordered water near the DNA surface.
2. At surface separations greater than 1 nm, measured interactions reveal electrostatic double layer repulsion presumably from negative phosphates along the DNA backbone.

Measurements give no evidence for a significant DNA–DNA attraction expected on theoretical grounds [68]. Though charge fluctuation forces must certainly occur, they appear to be negligible at least for liquid crystal formation in monovalent-ion solutions. At these larger separations, the double layer repulsion often couples with configurational fluctuations to create exponentially decaying forces whose decay length is significantly larger than the expected Debye screening length [42].

Bare short-range molecular interactions between DNA molecules appear to be insensitive to the amount of added salt. This has been taken as evidence that they are not electrostatic in origin, as attested also by similar interactions between completely uncharged polymers such as schizophyllan (Figure 21.5). The term "hydration force" associates these forces with perturbations of the water structure around the DNA surface [65]. Alternatively, short-range repulsion has been viewed as a consequence of the electrostatic force specific to high DNA density and counterion concentration [69].

21.3.6 High-Density DNA Mesophases

Ordering of DNA can be induced by two alternative mechanisms. First of all, attractive interactions between different DNA segments can be enhanced by adding multivalent counterions thought to promote either counterion-correlation forces [70] or electrostatic [71] and hydration attraction [22]. In these cases, DNA aggregates spontaneously. Alternatively, one can add neutral crowding polymers to the bathing solution that phase separate from DNA and exert osmotic stress on the DNA subphase [72]. In this case, the intersegment repulsions in DNA are simply counteracted by the large externally applied osmotic pressure. DNA is forced in this case to condense under externally imposed constraints. This latter case is formally (but only formally) analogous to a Boyle gas pressure experiment but with osmotic pressure playing the role of ordinary pressure. The main difference being that ordinary pressure is set mechanically while osmotic pressure has to be set through the chemical potential of water, which is in turn controlled by the amount of neutral crowding polymers (such as PEG, PVP, or dextran) in the bathing solution [66].

At very high DNA densities, where the osmotic pressure exceeds 160 atm, DNA can exist only in a (poly)crystalline state [73]. Nearest neighbors in such an array are all oriented in parallel and show correlated (nucleotide) base stacking between neighboring duplexes (see Figures 21.11 and 21.17). This means that there is a long-range correlation in the positions of the backbone phosphates between different DNA molecules in the crystal. The local symmetry of the lattice is monoclinic. Because of the high osmotic pressure, DNA is actually forced to be in an A conformation characterized by a somewhat larger outer diameter as well as a somewhat smaller pitch than in the canonical B conformation (see Figure 21.15), which persists at smaller densities. If the osmotic pressure of such a crystal is increased above 400 atm, the helix begins to crack and the sample loses structural homogeneity [73].

Lowering the osmotic pressure does not have a pronounced effect on the DNA crystal until it is down to ~160 atm. Then the crystal as a whole simultaneously expands while individual DNA molecules undergo an A to B conformational transition (see Figure 21.17) [73]. This phase transformation is thus first order, and besides being a conformational transition for single DNA, is connected also with the melting of the base stacking as well as positional order of the helices in the lattice. The ensuing low-density mesophase, where DNA is in the B conformation, is therefore characterized by short-range base stacking order, short-range 2D positional order, and long-range bond orientational order (see Figure 21.18) [74]. This order is connected with the spatial direction of the nearest neighbors [75]. It is for this reason that the phase has been termed a "line hexatic" phase. Hexatics usually occur only in 2D systems. They have crystalline bond orientational order but liquid-like positional order. There might be a hexatic to hexagonal columnar transition somewhere along the hexatic line though a direct experimental proof is lacking.

The difference between the two phases is that the hexagonal columnar phase has also a crystalline positional order and is thus a real 2D crystal (see Figure 21.18) [76]. It is the long-range bond orientational order that gives the line hexatic

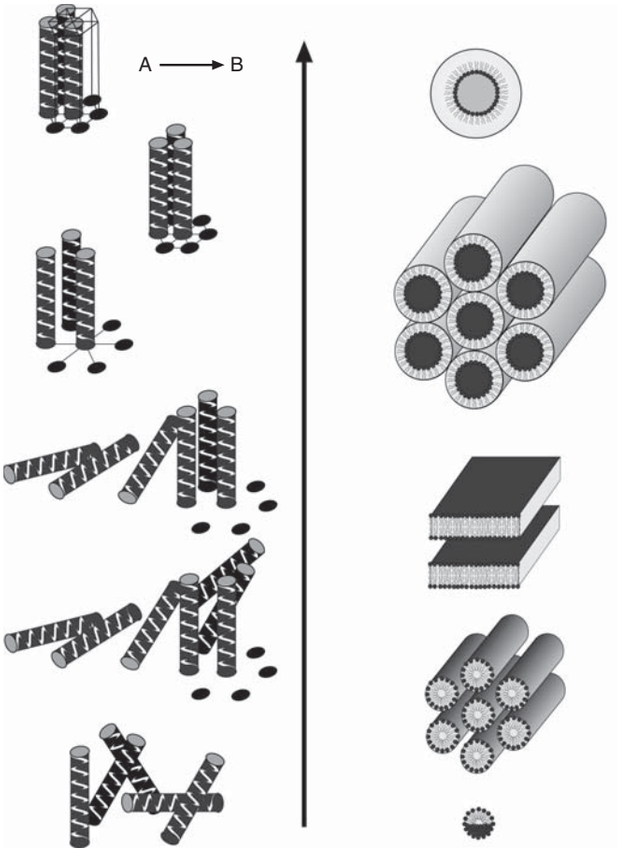

FIGURE 21.17 Schematic phase diagrams for DNA (left) and lipids (right). In both cases, the arrow indicates increasing density in both cases. DNA starts (bottom) as a completely disordered solution. It progresses through a sequence of "blue" phases characterized by cholesteric pitch in two perpendicular directions (From Leforestier, A. and Livolant, F., *Mol. Cryst. Liquid Cryst*., 1994, 17, 651) and then to a cholesteric phase with pitch in only one direction. At still larger densities, this second cholesteric phase is succeeded by a hexatic phase, characterized by short-range liquid-like positional order and long range crystal-like bond orientational (or hexatic order, indicated by lines). At highest densities, there is a crystalline phase, characterized by long-range positional order of the molecules and long-range base stacking order in the direction of the long axes of the molecules. Between the hexatic and the crystalline forms, there might exist a hexagonal columnar liquid-crystalline phase that is similar to a crystal, but with base stacking order only on short scales. The lipid phase diagram (From Small, D.M., *The Physical Chemistry of Lipids*: *From Alkanes to Phospholipids*, Plenum Press, New York, 1986) is a composite of results obtained for different lipids. It starts from a micellar solution and progresses through a phase of lipid tubes to a multilamellar phase of lipid bilayers. This is followed by an inverted hexagonal columnar phase of water cylinders and possibly goes to an inverted micellar phase. Most lipids show only a subset of these possibilities. Boundaries between the phases shown here might contain exotic cubic phases not included in this picture.

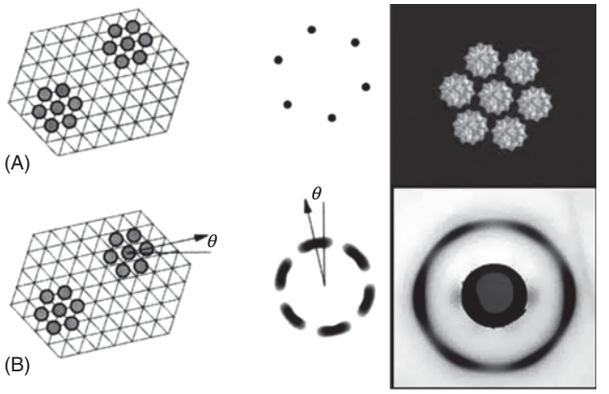

FIGURE 21.18 Bond orientational or hexatic order. With a real crystal, if one translates part of the crystal by a lattice vector, the new position of the atoms completely coincides with those already there. (Adapted from Chaikin, P.M. and Lubensky, T.C., *Principles of Condensed Matter Physics*, Cambridge University Press, Cambridge, MA, 1995.) In a hexatic phase, the directions to the nearest neighbors (bond orientations) coincide (after rotation by 60°), but the positions of the atoms do not coincide after displacement in one of the six directions. Consequently, a real crystal gives a series of very sharp Bragg peaks in X-ray scattering (upper half of box) whereas a hexatic gives hexagonally positioned broad spots. The pattern of X-ray scattering by high-density DNA samples gives a fingerprint of a hexatic phase. The densitogram of the scattering intensity (right half of figure) shows six pronounced peaks that can be Fourier decomposed with a marked sixth-order Fourier coefficient, another sign that that the scattering is due to long-range bond orientational order. (From Podgornik, R., Strey, H.H., Gawrisch, K., Rau, D.C., Rupprecht, A., and Parsegian, V.A., *Proc. Natl Acad. Sci. USA*, 1996, 93, 4261.)

phase some crystalline character [77]. The DNA duplexes are still packed in parallel, while the local symmetry perpendicular to the long axes of the molecules is changed to hexagonal. The directions of the nearest neighbors persist through macroscopic dimensions (on the order of mm) while their positions tend to become disordered already after several (typically 5 to 10) lattice spacings. This mesophase has a characteristic X-ray scattering fingerprint (see Figure 21.18). If the X-ray beam is directed parallel to the long axis of the molecules, it shows a hexagonally symmetric diffraction pattern of broad liquid-like peaks [78].

Typical lattice spacings in the line hexatic phase are between 25 and 35 Å (i.e. between 600 and 300 mg/mL of DNA) [74]. The free energy in this mesophase is mostly a consequence of the large hydration forces stemming from removal of water from the phosphates of the DNA backbone. Typically independent of the ionic strength of the bathing solution, these hydration forces [65] depend exponentially on the interhelical separation and decay with a decay length of about 3 Å [11] at these large densities. This value of the hydration decay length seems to indicate that it is determined solely by the bulk properties of the solvent, i.e. water.

It is interesting to note that the behavior of short-fragment DNA in this range of concentrations is different from the long DNA [76]. The short-fragment DNA, typically the nucleosomal DNA fragment of 146 bp, forms a two-dimensional hexagonal phase at interaxial spacing of ~30 Å, which progressively orders into a three-dimensional hexagonal phase on decrease of the interaxial spacing to ~23 Å [76].

At still larger concentrations, the short-fragment DNA forms a three-dimensional orthorhombic crystal, with a deformed hexagonal unit cell perpendicular to the *c*-axis. Concurrently to this symmetry transformation, the helical pitch of the condensed phase decreases continuously from 34.6 to 30.2 Å [76]. The reasons for this fundamental difference between the behaviors of long as opposed to short-fragment DNA are still not well understood.

When the osmotic pressure is lowered to about 10 atm (corresponding to interaxial spacing of about 35 Å or DNA density of about 300 mg/mL), the characteristic hexagonal X-ray diffraction fingerprint of the line hexatic mesophase disappears continuously. This disappearance suggests the presence of a continuous, second-order transition into a low-density cholesteric [74]. It is characterized by short-range (or effectively no) base stacking order, short-range positional order, short-range bond orientational order, but long-range cholesteric order, manifested in a continuing rotation of the long axis of the molecules in a preferred direction. In this sense, the cholesteric DNA mesophase would retain the symmetry of a one-dimensional crystal. X-ray diffraction pattern of the DNA in the cholesteric phase is isotropic and has the form of a ring. Crossed polarizers, however, reveal the existence of long-range cholesteric order just as in the case of short chiral molecules. The texture of small drops of DNA cholesteric phase (spherulites) under crossed polarizers (see Figure 21.19) reveals the intricacies of orientational packing of DNA where its local orientation is set by a compromise between interaction forces and macroscopic geometry of a spherulite. It is thus only at these low densities that the chiral character of the DNA finally makes an impact on the symmetry of the mesophase. It is not yet fully understood why the chiral order is effectively screened from the high-density DNA mesophases.

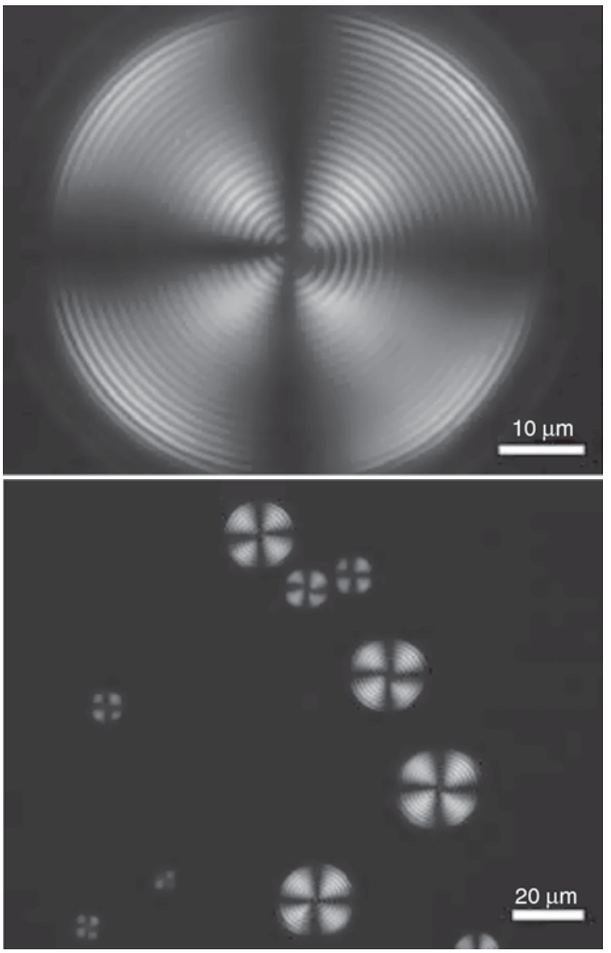

FIGURE 21.19 Texture of small drops of DNA cholesteric phase (spherulites) in a PEG solution under crossed polarizers. These patterns reveal the intricacies of DNA orientational packing when its local orientation is set by a compromise between interaction forces and the macroscopic geometry of a spherulite. The change from a bright to a dark stripe indicates that the orientation of the DNA molecule has changed by 90°.

At still smaller DNA densities, the predominance of the chiral interactions in the behavior of the system remains. Recent work on the behavior of low-density DNA mesophases indicates [79] that the cholesteric part of the phase diagram might end with a sequence of blue phases that would emerge as a consequence of the loosened packing constraints coupled to the chiral character of the DNA molecule. At DNA density of about 10 mg/mL, the cholesteric phase line would end with DNA reentering the isotropic liquid solution where it remains at all subsequent densities except perhaps at very small ionic strengths [80].

21.3.7 DNA Equation of State

The free energy of the DNA cholesteric mesophase appears to be dominated by the large elastic shape fluctuations of its constituent DNA molecules [81] that leave their imprint in the very broad X-ray diffraction peak [66]. Instead of showing the expected exponential decay characteristic of screened electrostatic interactions [82], where the decay length is equal to the Debye length, it shows a fluctuation-enhanced repulsion similar to the Helfrich force existing in the flexible smectic multilamellar arrays [41]. Fluctuations not only boost the magnitude of the existing screened electrostatic repulsion but also extend its range through a modified decay length equal to four times the Debye length. The factor-of-four enhancement in the range of the repulsive force is a consequence of the coupling between the bare electrostatic repulsions of exponential type and the thermally driven elastic shape fluctuations described through elastic curvature energy that is proportional to the square of the second derivative of the local helix position [42]. In the last instance, it is a consequence of the fact that DNAs in the array interact via an extended, soft-screened electrostatic potential and not through hard bumps as assumed in the simple derivation in Chapter 2.

The similarity of the free energy behavior of the smectic arrays with repulsive interactions of Helfrich type and the DNA arrays in the cholesteric phase, which can as well be understood in the framework of the Helfrich-type enhanced repulsion, satisfies a consistency test for our understanding of flexible supermolecular arrays.

21.4 LIPID MESOPHASES

21.4.1 Aggregation of Lipids in Aqueous Solutions

Single-molecule solutions of biological lipids exist only over a negligible range of concentrations; virtually all interesting lipid properties are those of aggregate mesophases such as bilayers and micelles. Lipid molecules cluster into ordered structures to maximize hydrophilic and minimize hydrophobic interactions [83,84]. These interactions include negative free energy contribution from the solvation of polar heads and van der Waals interactions of hydrocarbon chains, competing with positive contributions such as steric, hydration, and electrostatic repulsions between polar heads. The "hydrophobic effect," which causes segregation of polar and nonpolar groups, is said to be driven by the increase of the entropy of the surrounding medium.

Intrinsic to the identity of surfactant lipids is the tension between water-soluble polar groups and lipid-soluble hydrocarbon chains. There is no surprise then that the amount of water available to an amphiphile is a parameter pertinent to its modes of packing and to its ability to incorporate foreign bodies.

These interactions therefore force lipid molecules to self-assemble into different ordered microscopic structures, such as bilayers, micelles (spherical, ellipsoidal, rodlike, or disklike), which can, especially at higher concentrations, pack into macroscopically ordered phases such as lamellar, hexagonal, inverted hexagonal, and cubic. The morphology of these macroscopic phases changes with the balance between attractive van der Waals and ion correlation forces versus electrostatic, steric, hydration, and undulation repulsion [85].

21.4.2 Lipid Bilayer

The workhorse of all lipid aggregates is the bilayer (see Figure 21.20) [84]. This sandwich of two monolayers, with nonpolar hydrocarbon chains tucked in toward each other and polar groups facing water solution, is only about 20 to 30 Å thick. Yet it has the physical resilience and the electrical resistance to form the "plasma" membrane that divides "in" from "out" in all biological cells. Its mechanical properties have been measured in terms of bending and stretching moduli. These strengths together with measured interactions between bilayers in multilamellar stacks have taught us to think quantitatively about the ways in which bilayers are formed and maintain their remarkable stability.

With some lipids, such as double-chain phospholipids, when there is the need to encompass voluminous hydrocarbon components compared with the size of polar groups, the small surface-to-volume ratio of spheres, ellipsoids, or even cylinders cannot suffice even at extreme dilution. Bilayers in this case are the aggregate form of choice. These may occur as single "unilamellar" vesicles, as onion-like multilayer vesicles, or multilamellar phases of indefinite extent. In vivo, bilayer-forming phospholipids create the flexible but tightly sealed plasma–membrane matrix that defines the inside from the outside of a cell. In vitro, multilayers are often chosen as a matrix of choice for the incorporation of polymers. Specifically, there are tight associations between positively charged lipids that merge with negatively charged DNA in a variety of forms (see below). AQ1

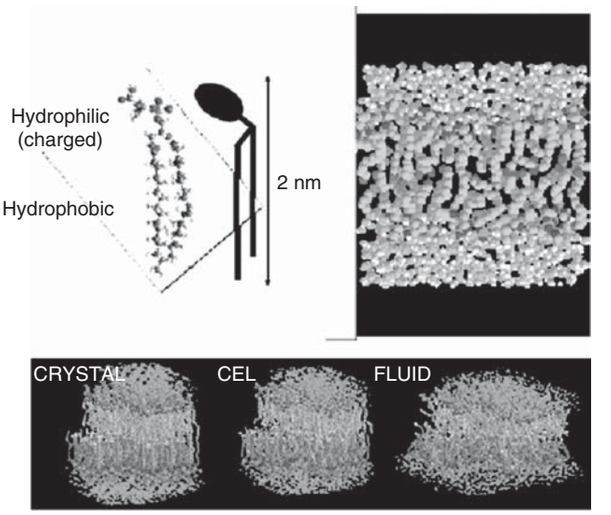

Lipid	Bending regidity (10^{-19}J)	Area compression (mN/m)
DMPC	1.15	145
SOPC	0.9	200
EggPC	0.4–2	
Plasma membrane	0.2–2	700
Red blood cell	0.13–0.3	450

FIGURE 21.20 (See color insert following page xxx.) The lipid bilayer. A lipid molecule has a hydrophilic and a hydrophobic part (here shown is the phosphatidylserine molecule that has a charged headgroup). At high enough densities, lipid molecules assemble into a lipid bilayer. Together with membrane proteins as its most important component, the lipid bilayer is the underlying structural component of biological membranes. The degree of order of the lipids in a bilayer depends drastically on temperature and goes through a sequence of phases (see main text): Crystalline, gel, and fluid, as depicted in the middle drawing. The box at the bottom gives sample values of bilayer bending rigidity and area compressibility for some biologically relevant lipids and one well-studied cell membrane.

The organization of lipid molecules in the bilayer itself can vary [84]. At low enough temperatures or dry enough conditions, the lipid tails are frozen in an all-*trans* conformation that minimizes the energy of molecular bonds in the alkyl tails of the lipids. Also the positions of the lipid heads along the surface of the bilayer are frozen in 2D positional order, making the overall conformation of the lipids in the bilayer crystal (L_C). The chains can either be oriented perpendicular to the bilayer surface (L_β and $L_{\beta'}$) or be tilted (crystalline phase L_C or ripple phase P_β). Such a crystalline bilayer cannot exist by itself but assembles with others to make a real 3D crystal.

Upon heating, various rearrangements in the 2D crystalline bilayers occur, first the positional order of the headgroups melts leading to a loss of 2D order ($L_{\beta'}$) and tilt (L_β) and then

at the gel–liquid crystal phase transition, the untilted or rippled (P_β phase) bilayer changes into a bilayer membrane with disordered polar heads in two dimensions and conformationally frozen hydrocarbon chains, allowing them to spin around the long axes of the molecules, the so-called L_α phase. At still higher temperatures, the thermal disorder finally destroys also the ordered configuration of the alkyl chains, leading to a fluidlike bilayer phase. The fluid bilayer phase creates the fundamental matrix that according to the fluid mosaic model [83] contains different ingredients of biological membranes, e.g. membrane proteins, channels etc.

Not only bilayers in multilamellar arrays but also liposome bilayers can also undergo such phase transitions; electron microscopy has revealed fluid phase, rippled and crystalline phase in which spherical liposomes transform into polyhedra due to very high values of bending elasticity of crystallized bilayers [86].

The fluid-phase of the lipid bilayer is highly flexible. This flexibility makes it prone to pronounced thermal fluctuations resulting in large excursions away from a planar shape. This flexibility of the bilayer is essential for understanding the range of equilibrium shapes that can arise in closed bilayer (vesicles) systems [87]. Also, just as in the case of flexible DNA, it eventually leads to configurational entropic interactions between bilayers that have been crammed together [41]. Bilayers and linear polyelectrolytes thus share a substantial amount of fundamentally similar physics that allows us to analyze their behavior in the same framework.

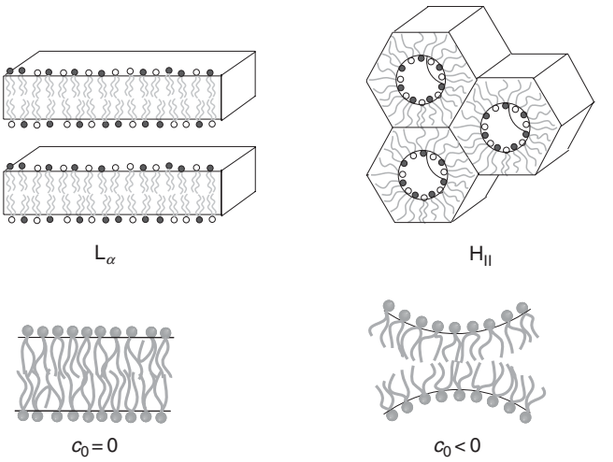

FIGURE 21.21 Different lipids are strained to different degrees when forced into lamellar packing. Relaxation of this strain contributes to the conditions for lamellar-to-inverted hexagonal phase transitions that depend on temperature, hydration, and salt concentration (for charged lipids).

21.4.3 Lipid Polymorphism

Low-temperature phases [88] are normally lamellar with frozen hydrocarbon chains tilted (crystalline phase L_C or ripple phase P_β) or nontilted (L_β and $L_{\beta'}$ form 3D, 2D, or 1D crystalline or gel phases) with respect to the plane of the lipid bilayers. Terminology from thermotropic liquid crystals phenomenology [61] can be used efficiently in this context: these phases are smectic, and SmA describes 2D fluid with no tilt while a variety of SmC phases with various indices encompass tilted phases with various degrees of 2D order. Upon melting, liquid crystalline phases with 1D (lamellar L_α), 2D (hexagonal II), or 3D (cubic) positional order can form.

The most frequently formed phases are micellar, lamellar, and hexagonal (Figure 21.17). Normal hexagonal phase consists of long cylindrical micelles ordered in a hexagonal array, while in the inverse hexagonal II (H_{II}) phase, water channels of inverse micelles are packed hexagonally with lipid tails filling the interstices. In excess water, such arrays are coated by a lipid monolayer. The morphology of these phases can be maintained upon their (mechanical) dispersal into colloidal dispersions. Despite the requirement that energy has to be used to generate dispersed mesophases, relatively stable colloidal dispersions of particles with lamellar, hexagonal, or cubic symmetry can be formed.

Many phospholipids found in lamellar cell membranes after extraction, purification, and resuspension prefer an inverted hexagonal geometry (Figure 21.21) [88]. Under excess-water conditions, different lipids assume different most-favored spontaneous radii for the water cylinder of this inverted phase [89]. An immediate implication is that different lipids are strained to different degrees when forced into lamellar packing. There are lamellar-inverted hexagonal phase transitions that occur with varied temperature, hydration, and salt concentration (for charged lipids) that form in order to alleviate this strain (see Figure 21.21).

In the presence of an immiscible organic phase, emulsion droplets can assemble [90]. In regions of phase diagram, which are rich in water, oil-in-water emulsions and microemulsions ($c > 0$) can be formed, while in oil-rich regions, these spherical particles have negative curvature and are therefore water-in-oil emulsions. The intermediate phase between the two is a bicontinuous emulsion that has zero average curvature and an anomalously low value of the surface tension (usually brought about the use of different cosurfactants) between the two immiscible components. Only microemulsions can form spontaneously (analogously to micelle formation) while for the formation of a homogeneous emulsion, some energy has to be dissipated into the system.

The detailed structure of these phases as well as the size and shape of colloidal particles are probably dominated by

- the average molecular geometry of lipid molecules,
- their aqueous solubility and effective charge,
- weaker interactions such as intra- and intermolecular hydrogen bonds, and
- stereoisomerism as well as interactions within the medium.

All depend on the temperature, lipid concentration, and electrostatic and van der Waals interactions with the solvent and solutes. With charged lipids, counterions, especially anions,

may also be important. Ionotropic transitions have been observed with negatively charged phospholipids in the presence of metal ions leading to aggregation and fusion [91]. In cationic amphiphiles, it was shown that simple exchange of counterions can induce micelle–vesicle transition. Lipid polymorphism is very rich and even single-component lipid systems can form a variety of other phases, including ribbon-like phases, coexisting regions and various stacks of micelles of different shapes.

21.4.4 Forces in Multilamellar Bilayer Arrays

Except for differences in dimensionality, forces between bilayers are remarkably similar to those between DNA. At very great separations between lamellae, the sheet-like structures flex and "crumple" because of (thermal) Brownian motion [41]. Just as an isolated flexible linear polymer can escape from its one linear dimension into the three dimensions of the volume in which it is bathed, so can two-dimensional flexible sheets. In the most dilute solution, biological phospholipids typically form huge floppy closed vesicles; these vesicles enjoy flexibility while satisfying the need to keep all greasy nonpolar chains comfortably covered by polar groups rather than exposed at open edges. For this reason, in very dilute solution, the interactions between phospholipid bilayers are usually space wars of collision and volume occupation. This steric competition is always seen for neutral lipids; it is not always true for charged lipids [85].

Especially in the absence of any added salt, planar surfaces emit far-ranging electrostatic fields [27] that couple to thermally excited elastic excursions to create very long-range repulsion [44,92]. As with DNA, this repulsion is a mixture of direct electrostatic forces and soft collisions mediated by electrostatic forces rather than by actual bilayer contact. In some cases, electrostatic repulsion is strong enough to snuff out bilayer bending when bilayers form ordered arrays with periodicities as high as hundreds of angstroms [93].

Almost always bilayers align into well-formed stacks when their concentration approaches ~50 to 60 wt.% and their separation is brought down to a few tens of angstroms. In this region, charged layers are quite orderly with little lamellar undulation. In fact, bilayers of many neutral phospholipids often spontaneously fall out of dilute suspension to form arrays with bilayer separations between 20 and 30 Å. These spontaneous spacings are thought to reflect a balance between van der Waals attraction and undulation-enhanced hydration repulsion [85]. One way to test for the presence of van der Waals forces has been to add solutes such as ethylene glycol, glucose, or sucrose to the bathing solutions. It is possible then to correlate the changes in spacing with changes in van der Waals forces due to the changes in dielectric susceptibility as described above [94]. More convincing, there have been direct measurements of the work to pull apart bilayers that sit at spontaneously assumed spacings. This work of separation is of the magnitude expected for van der Waals attraction [95].

Similar to DNA, multilayers of charged or neutral lipids, subjected to strong osmotic stress, reveal exponential variation in osmotic pressure versus bilayer separation [85]. Typically at separations between dry "contact" and 20 Å, exponential decay lengths are 2–3 Å in distilled water or in salt solution, whether phospholipids are charged or neutral. Lipid bilayer repulsion in this range is thought to be due to the work of polar group dehydration sometimes enhanced by lamellar collisions from thermal agitation [96]. Normalized per area of interacting surface, the strength of hydration force acting in lamellar lipid arrays and DNA arrays is directly comparable.

Given excess water, neutral lipids usually find the above-mentioned separation of 20 to 30 Å at which this hydration repulsion is balanced by van der Waals attraction. Charged lipids, unless placed in solutions of high salt concentration, swell to take up indefinitely high amounts of water. Stiff charged bilayers repel with exponentially varying electrostatic double layer interactions, but most charged bilayers undulate at separations where direct electrostatic repulsion has weakened. In that case, similar to what has been described for DNA, electrostatic repulsion is enhanced by thermal undulations [97].

21.4.5 Equation of State of Lipid Mesophases

Lipid polymorphism shows much less universality than DNA. This is of course expected since lipid molecules come in many different varieties [84] with strong idiosyncrasies in terms of the detailed nature of their phase diagrams. One thus cannot achieve the same degree of generality and universality in the description of lipid phase diagram and consequent equations of state as was the case for DNA.

Nevertheless, recent extremely careful and detailed work on PCs by Nagle and his group [98] points strongly to the conclusion that at least in the lamellar part of the phase diagram of neutral lipids, the main features of the DNA and lipid membrane assembly physics indeed is the same [96]. This statement however demands qualification. The physics is the same provided one first disregards the dimensionality of the aggregates—one dimensional in the case of DNA and two dimensional in the case of lipid membranes—and takes into account the fact that while van der Waals forces in DNA arrays are negligible, they are essential in lipid membrane force equilibria. One of the reasons for this state of affairs is the large difference, unlike in the case of DNA, between the static dielectric constant of hydrophobic bilayer interior, composed of alkyl lipid tails, and the aqueous solution bathing the aggregate.

We have already pointed out that in the case of DNA arrays, quantitative agreement between theory, based on hydration and electrostatic forces augmented by thermal undulation forces, and experiment has been obtained and extensively tested [7,42]. The work on neutral lipids [96] claims that the same level of quantitative accuracy can also be achieved in lipid membrane assemblies if one takes into account hydration and van der Waals forces again augmented by thermal undulations. Of course, the nature of the fluctuations in the two systems is different and is set by the

dimensionality of the fluctuating aggregates: one- versus two-dimensional.

The case of lipids adds an additional twist to the quantitative link between theory and experiments. DNA in the line hexatic as well as cholesteric phases (where reliable data for the equation of state exist) is essentially fluid as far as positional order is concerned and thus has unbounded positional fluctuations. Lipid membranes in the smectic multilamellar phase on the other hand are quite different in this respect. They are not really fluid as far as positional order is concerned but show something called quasilong range (QLR) order, meaning that they are in certain respects somewhere between a crystal and a fluid [61,78]. The quasilong-range positional order makes itself recognizable through the shape of the X-ray diffraction peaks in the form of persistent (Caille) tails [78].

In a crystal, one would ideally expect infinitely sharp peaks with Gaussian broadening only because of finite accuracy of the experimental setup. Lipid multilamellar phases, however, show peaks with very broad, non-Gaussian, and extended tails that are one of the consequences of QLR positional order. The thickness of these peaks for different orders of X-ray reflections varies in a characteristic way with the order of the reflection [78]. It is this property that allows us to measure not only the average spacing between the molecules but also the amount of fluctuation around this average spacing. Luckily the theory predicts this property also and without any free parameters (all of them being already determined from the equation of state), the comparison between predicted and measured magnitude in positional fluctuations of membranes in a multilamellar assembly is more than satisfactory [96].

In summing up, the level of understanding of the equation of state reached for DNA and neutral lipid membrane arrays is pleasing.

21.5 DNA–LIPID INTERACTIONS

Mixed in solution with cationic lipids (CL), DNA spontaneously forms CL–DNA aggregates of submicron size. These DNA–lipid aggregates, sometimes called "lipoplexes," [99] are routinely used for cell transfection in vitro. More important, they are used primarily as potential gene delivery vehicles for in vivo gene therapy (for recent reviews, see Refs. [100–105] and references therein). Under appropriate conditions, these aggregates reveal complex underlying thermodynamic phase behavior. There is a practical paradox here. We use stable equilibrium structures to reveal the forces that cause aggregation and assembly; we use this knowledge of forces to create the unstable preparations likely to be most efficient in transfection.

Lipoplexes for transfection were first proposed by Felgner and coworkers [106,107]. The guiding idea was to overcome the electrostatic repulsion between cell membranes (containing negatively charged lipids) and negative DNA by complexing DNA with positively charged CL. Preliminary experimental data showed that at least some lipoplexes deliver DNA through direct fusion with the cell membrane [108,109]. More often however, lipoplex internalization probably proceeds through endocytosis after initial interaction with the cell's membrane.

Prior to the attempts to utilize lipoplexes for transfection, studies of DNA aggregated with multivalent cations and coated with negatively charged liposomes were also explored as possible vectors. It was hoped that CL–DNA complexes would no longer require an additional complexing agent, and that also, the transfection efficiency would be higher. The complex's lipid coating could protect the tightly packed DNA cargo during its passage to the target cells. In recent years, this strategy has been slightly modified to complex DNA and anionic (or even neutral) membranes in ordered lamellar phases that should have lower cytotoxicity than the alternative CLs. An unresolved problem of this approach is the inefficient association between the ALs and DNA molecules, which is attributed to their like-charge electrostatic repulsion [110–114].

While not confronted with the immunological response, risked by the alternative viral vector strategy, the use of lipoplexes in gene therapy is still hampered by toxicity of the CL and low in vivo transfection efficiency despite the in vitro efficiency of some CL formulations. This discrepancy can be attributed to the multistage and multibarrier process the complexes must endure before transfection is achieved. These steps typically include passage in the serum, interaction with target and other cells, internalization, complex disintegration in the cytoplasm, transport of DNA into the nucleus, and ultimately expression.

In the search for increasingly more potent gene delivery vectors, the intimate relationship between the lipoplex's phase structure (or morphology) and its transfection efficiency probably serves as the greatest motivation for their study. How is transfection affected by lipoplex morphology? How may this structure be controlled? Experiment and theory of the past decade shed some light on such fundamental questions. They may give perspective for future strategies to design CL-based nonviral vectors.

To this end, we present here our current understanding of the structure and phase behavior of CL–DNA complexes. We review the relation of structure to transfection efficiency, and more specifically, to the way the complex formation overcomes one barrier to DNA release into the cytoplasm.

21.5.1 Structure of CL–DNA Complexes

In general, the structures of CL–DNA composite phases can be viewed as morphological hybrids of familiar pure-lipid and pure-DNA phases. A first example is the lamellar-like structure initially proposed by Lasic et al. [115,116]. The first comprehensive and unambiguous evidence for this structure came from a series of studies by Rädler et al. [117–121]. From high-resolution synchrotron X-ray diffraction and optical microscopy, they reported the existence of novel lamellar CL–DNA phase morphologies. In particular, one complex structure was shown to consist of lamellar multilayer. In this case,

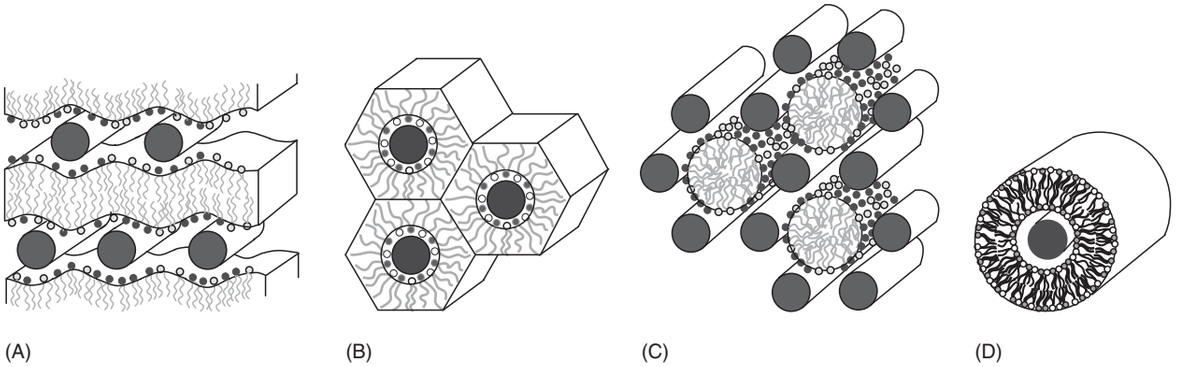

FIGURE 21.22 Schematic illustration of some possible structures of DNA–mixed lipid (cationic/nonionic) complexes. (A) The sandwich-like (L_α^c) lamellar complex composed of parallel DNA molecules intercalated between lipid bilayers. (B) The honeycomb-like (H_{II}^c) hexagonal complex, composed of a hexagonally packed bundle of monolayer-coated DNA strands. (C) Two interpenetrating hexagonal lattices, one of DNA, the other of micelles. (D) Spaghetti-like complex, composed of bilayer-coated DNA. (From May, S., Harries, D., and Ben-Shaul, A., *Biophys. J.*, 2000, 79, 1747. With permission.)

smectic-like stacks of mixed bilayers, each composed of a mixture of CL (e.g. dioleoyltrimethylammonium propane (DOTAP)) and neutral "helper" lipid (e.g. dioleoylphosphatidylcholin (DOPC)), with monolayers of DNA strands intercalated within the intervening water gaps (see Figure 21.22A) like a multilipid bilayer L_α phase [122]. Helper lipids (HLs) are often added for their fusogenic properties. Dioleoylphosphatidylethanol amine (DOPE), for example, is conjectured to promote transfection. In addition, because pure (synthetically derived) CLs often tend to form micelles in solution, HLs facilitate the formation of membranes.

In this L_α^c complex geometry, the DNA strands within each gallery are parallel to each other, exhibiting a well-defined repeat distance *d*. While *d* depends on the CL/DNA and CL/HL concentration ratios, the spacing between two apposed lipid monolayers is nearly constant at ~26 Å corresponding to the diameter of double stranded B-DNA, ca. 20 Å, surrounded by a thin hydration shell. This L_α^c lamellar ("sandwich") complex is stabilized by the electrostatic attraction between the negatively charged DNA and the CL bilayer. Because of strong electrostatic repulsion between the charged bilayers (particularly at low salt conditions), the lamellar lipid phase is unstable without DNA.

Quite different equilibrium ordered phase morphologies were found to occur from other choices of neutral HL. In the case of DOPE, or lecithin, for example, inverted hexagonal ("honeycomb" or H_{II}^c) organization of the lipid, with stretches of double-stranded DNA laying in the aqueous solution regions, were found to form (see Figure 21.22B) [106,118,123]. The H_{II}^c structure may be regarded as the inverse-hexagonal (H_{II}) lipid phase, with DNA strands wrapped within its water tubes. Here too, the diameter of the water tubes is only slightly larger than the diameter of the DNA "rods." The presence of DNA is crucial for stabilizing the hexagonal structure. Without it, strong electrostatic repulsion will generally drive the lipids to organize themselves into planar bilayers. In fact, the most abundant aggregate structure of pure CL and HL mixtures, from which hexagonal complexes are subsequently formed, is single-bilayer liposomes.

Other CL–DNA phases have also been observed. One of the earliest studies probing the structure of lipoplexes showed some evidence for a hexagonal arrangement of rodlike micelles intercalated between hexagonally packed DNA (Figure 21.22C) [124,125]. More recently, such structures have been unambiguously characterized in complexes composed of lipids that possess large, typically polyvalently charged headgroups [126]. There is also evidence that some lipid mixtures promote the formation of cubic phases that are also able to transfect [127].

The number of possibilities is even larger if one also considers metastable intermediates. The "spaghetti" structure (see Figure 21.22D), observed using freeze-fracture electron microscopy, has been predicted by theory to probably be one such metastable morphology [128,129]. In this structure, each (possibly supercoiled) DNA strand is coated by a cylindrical bilayer of the CL/HL lipid mixture [130,131]. Early proposed models of the CL–DNA complexes suggested a "beads on a string" type complex, in which the DNA is wrapped around or in between lipid vesicles (and even spherical micelles). While this may not turn out to be an equilibrium structure, such aggregates are sometimes found and may also serve as unstable intermediates [132–134]. Other structures, such as the bilamellar invaginated liposomes (BIV) made of DOTAP-Chol, have been proposed and demonstrated to be efficient vectors [108,135]. These structures resemble to some degree the L_α^c phase. However, formed from extruded liposomes, the BIVs are most probably metastable.

What factors determine which of these phases (or possibly several coexisting structures) actually form in solution? To what degree can we control and predict them? Control can first be achieved through the choice of type of CL and HL, and the ratio between the two used in forming liposomes. This in turn will determine such basic properties as the lipid bilayer's bending rigidity, spontaneous curvature, and surface

charge density of the water–lipid aggregate interface. An additional experimentally controllable parameter is the ratio between the lipid and DNA content in solution. We show that both these parameters have significant effects on the phases that are formed.

21.5.2 Counterion Release

From the start, it was realized that the expected condensation of DNA with oppositely charged lipids could be used to package and send DNA to transfect targeted cells. The expectation that the DNA and lipids would aggregate was intuitively based on the notion that oppositely charged bodies attract. Early experiments confirmed the aggregation of DNA and lipids. However, the mechanism by which CL and DNA were found to associate—previously termed in the context of macromolecular association "counterion release" [136]—is more intricate than the "opposites attract" mechanism that may be naively expected.

Prior to association, DNA and lipids are bathed in the aqueous solutions containing their respective counterions, so that the solutions are overall electrostatically neutral. The counterions are attracted to the oppositely charged macromolecules, thus gaining electrostatic energy. Here, in addition to DNA, we shall also refer to the preformed CL liposomes as a "macromolecules" since they typically retain their integrity in solution, even upon association with other charged macromolecules. The counterions are therefore confined to the vicinity of the oppositely charged macromolecules at the compromise of greater translational entropy in solution.

Upon association, the two oppositely charged macromolecules condense to form CL–DNA complexes (see Figure 21.23). Many (possibly all) previously confined counterions can now be expelled into the bulk solution from the lipoplex interior, thus gaining translational entropy. While the translational entropy of the paired macromolecules is reduced by (typically) only a few k_BTs, due to loss of conformational and translational entropy, many released counterions can now favorably contribute to a gain in entropy, each by a comparable amount. For this reason, it is sometimes stated that the DNA–lipid condensation is "entropically driven." The electrostatic energy can also contribute somewhat to stabilizing the lipoplexes. However, it has been well argued, both experimentally and theoretically, that the cardinal contribution to the association free energy of CL–DNA complexes is the entropy gain associated with counterion release [137–139].

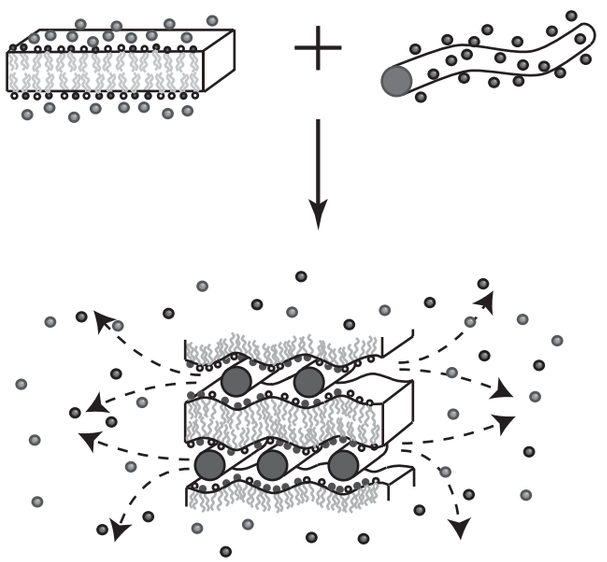

FIGURE 21.23 Schematic illustration of the condensation of DNA and lipid bilayers (liposomes) into CL–DNA complexes. In the process, the previously confined counterions are released into the bathing solution, thereby gaining translational entropy.

Further support was given by counting released ions using conductivity measurements of the supernatant. It was possible to determine that a maximal number of counterions were released when the number of "fixed" charges on the DNA and lipid were exactly equal.

Calorimetric measurements confirm this finding and furthermore reveal that the association could in fact be endothermic so that it is only favorable for entropic reasons [140,141]. The special point at which the number of positive and negative fixed charges is equal has been termed the "isoelectric point." At this point, the (charging) free energy of the complex is minimal: the fixed charges of opposite signs fully compensate each other, thus allowing essentially *all* the counterions to be released into solution. Note, that by "counterions," we do not refer here to added salt ions. Ions of added salt will span the entire solution including the lipoplex interior. Thus, the salt content changes the thermodynamic phase behavior and the value of the adsorption free energy, mainly because a high ambient salt concentration lowers the entropic gain associated with releasing a counterion.

Theoretical predictions and estimates from calorimetry show that for a salt solution of concentration $n^0 = 4\,\text{mM}$, and a 1:1 CL/HL mole ratio, the gain in free energy upon adsorption at the isoelectric point is a bemusingly large ~$7.5\,k_BT$ per fixed charge pair (DNA and CL) [138–141]. This value translates to over $2000\,k_BT$ when considering the energy per persistence length of DNA (about 50 nm), carrying approximately 300 charges.

21.5.3 Lamellar DNA–Lipid Complexes and Overcharging

Many degrees of freedom with competing contributions are expected to ultimately determine the free energy minimum for equilibrium DNA/membrane structures. Typically these include (but are not limited to) electrostatic energy, elastic bending, solvation, van der Waals, ion mixing, and lipid mixing. Therefore, considering the lipoplex phase behavior, we begin, for simplicity, by discussing systems where only L_α^c complexes are found. This can be expected when the lipid membranes are rather rigid, such as in the case of mixtures of DOTAP/DOPC [100,118] or DMPC/DC-Chol [142]. The main structural parameter for the L_α^c phase is the DNA–DNA distance, reflecting the DNA packing density within the complex. A series of X-ray measurements by Rädler et al. revealed AQ6

how the DNA–DNA spacings d vary with the ratio ρ of the number of lipid charges to the total number of charges on DNA. The measurements were repeated for each of several different lipid compositions defined by the ratio of charged to overall number of lipids, ϕ. It was found that for a lipid mixture of a given composition ϕ, the spacings are constant throughout the low ρ range where the complex coexists with excess DNA. In the high ρ range, where the complex coexists with excess lipid, the spacings are also nearly constant. In between these limits, there exists a "single-phase" region, where all the DNA and lipids participate in forming lipoplexes. This region is generally found to include the isoelectric point where, by definition, $\rho = 1$ (see Figure 21.24).

Several theoretical studies have been proposed to account for this phase behavior [137,143,144]. It was found that it is possible to account for most of the experimental observations within the scope of the nonlinear Poisson-Boltzmann (PB) equation [144]. In this theoretical model, elastic deformations of the DNA and lipid bilayers were neglected, treating them as rigid macromolecules. On the other hand, the lipid's lateral (in plane) mobility in the membrane layer was explicitly taken into account. This turns out to be an important degree of freedom in mixed fluid bilayers, enabling the system to greatly enhance the free energy gain upon complexation, with respect to the case where no lipid mobility is allowed. This adds to the stability of the L_α^c complex. Generally, it was found that lipid mobility favors optimal (local) charge matching of the apposed DNA and lipid membrane. This is the state in which a maximal number of mobile counterions are expelled from the interaction zone, implying a maximal gain in free energy upon complex formation [145]. However, the tendency for charge matching (hence migration of lipid to and from the region of proximity) is opposed by an unfavorable local lipid demixing entropy loss. This entropic penalty will somewhat suppress the membrane's tendency to polarize in the vicinity of the DNA molecule. The extent to which the membrane will polarize is determined by the intricate balance between the electrostatic and lipid mixing entropy contributions to the free energy of the complex. The contribution of lipid demixing to the stabilization of the complex is most pronounced when the membrane's average composition is far from that of the DNA, namely for low ϕ. Here, the system can gain most out of the polarization so as to come close to local charge matching.

The tendency of charged lipids to segregate in the vicinity of adsorbed rigid macromolecules has gained some experimental support from nuclear magnetic resonance (NMR) studies [146] although many systems may display a more complex behavior. Molecular dynamic simulations of L_α^c complexes, for a lipid mixture of DMTAP and DMPC, showed evidence for a favorable pairing of DMPC and DMTAP lipid molecules through the (partial) negative charge on DOPC and an interaction of the (remaining) positive charge of the zwiterionic DOPC with the DNA. In contrast to the model discussed above, this implies a nonideal lipid demixing: these lipid molecules preferentially move in pairs [147]. This may be anticipated since it is well known that lipids do not generally mix ideally even in free (unassociated) membranes [148]. Furthermore, there is evidence that to some extent neutral lipids also interact directly with DNA [149].

Figure 21.25 shows the experimental results and theoretical calculations for the dependence of d on ρ for several values of ϕ. For a specific value of ϕ (say $\phi = 0.5$), the three-phase

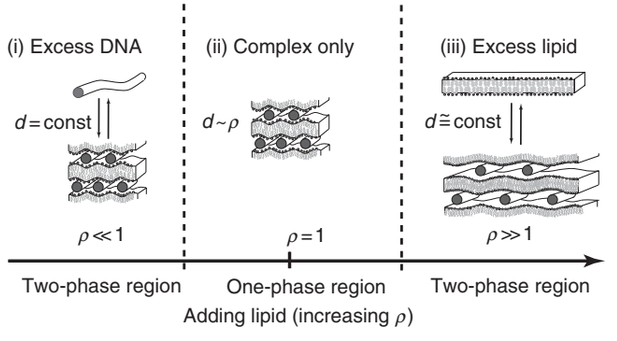

FIGURE 21.24 Schematic illustration of the phase evolution of the L_α^c complexes, for a constant lipid composition (cationic to nonionic lipid ratio). As lipid is added (ρ increases), the system evolves from a two-phase (complex and excess DNA) region through a one-phase (complex only) region, and finally to a two-phase (complex and excess lipid) region. The isoelectric point is generally contained within the one-phase region.

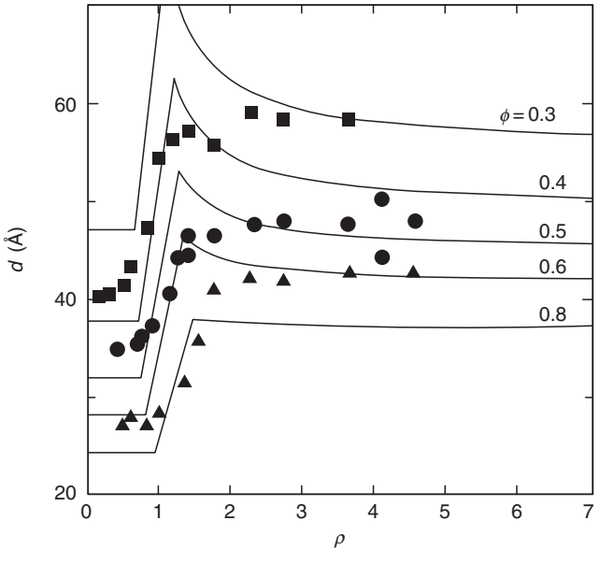

FIGURE 21.25 DNA–DNA spacing as a function of ρ in a series of theoretical and experimental results. The theoretical results correspond to (top to bottom) $\phi = 0.3$, 0.4, 0.5, 0.6, 0.8; all results are presented for a screening length of 50 Å (corresponding to ca. 4 nm of bathing salt solution). The experimental results correspond to $\phi = 0.3$ (squares), 0.5 (circles), 0.7 (triangles), and were performed with no added salt. (Theoretical results adapted from Harries, D., May, S., Gelbart, W.M., and Ben-Shaul, A., *Biophys. J.,* 1998, 75, 159 and Harries, D., PhD dissertation, The Hebrew University, Jerusalem, Israel, 2001; experimental results adapted from Rädler, J.O., Koltover, I., Salditt, T. et al., *Science*, 1997, 275, 810.)

regimes can clearly be seen. As ρ increases, d changes from ≈ 35 Å (in the excess DNA regime, $\rho \ll 1$) to ≈ 47 Å (in the excess lipid regime, $\rho \gg 1$). Both theory and experiment show that for a wide range of lipid composition, ϕ, there exists a one-phase, complex-only region at ρ values somewhat larger and smaller than the isoelectric point. This implies that complexes may become either negatively or positively "overcharged" so that the total number of fixed positive and negative charges is not equal. Hence, the complex accommodates either an excess number of lipids or else an excess amount of DNA. The complex's free energy is thus not at its minimum, which occurs at isoelectricity ($\rho = 1$). The interplay between possible phases to minimize the total system's free energy dictates that the complex moves away from its minimal free energy. The alternative would be to expel the excess lipid ($\rho > 1$) or excess DNA ($\rho < 1$) into solution. The charge densities on these "free" unneutralized macromolecules would be very large, rendering this scenario highly unfavorable. Using a simple model based on this overcharging phenomenon, it was possible to account for the considerable extent of this one-phase region [144]. Within this model, only the uncompensated charges on apposed (DNA–DNA or bilayer–bilayer) surfaces of a L_α^c unit cell ("box") were considered in estimating the complex's free energy. Figure 21.25 also shows that as the membrane becomes enriched in CL (ϕ increases) the DNA–DNA distance is systematically reduced, reflecting the fact that smaller amounts of lipid membrane are needed to achieve isoelectricity.

Salt has a significant effect on the phase behavior. In general, added salt causes a significant decrease in d, presumably due to a screening of the repulsive DNA–DNA interaction. This effect is most pronounced when divalent salts are added in increasing amounts. A sharp decrease in the d value is observed for a certain salt molar concentration, resulting in very highly condensed DNA in each gallery [89,130]. Another interesting observation is that the identity of the CL's counterion used changes the (endothermic) association enthalpy considerably, particularly in the excess DNA region [140]. This probably reflects the nonelectrostatic interaction energies of different ions with membranes, which may influence the thermotropic behavior of the lipid membranes [150,151].

21.5.4 DNA Adsorption on Lipid Membranes

Further insight into the in-plane DNA ordering in L_α^c complexes has been gained through the atomic force microscopy (AFM) study by Fang and Yang [152,153] of DNA adsorption on supported lipid bilayers. In these experiments, DNA was first adsorbed on dipalmitoyldimethylammoniumylpropane (DPDAP) or distearoyl-DAP (DSDAP) CL bilayers, assumed to be in the gel phase. After equilibration and saturation of the surface, the DNA bulk solution was removed, and the surface was put in contact with solution of various concentrations of NaCl. After further equilibration, the salt solution was removed and the surface imaged by AFM. Plasmid and linear DNA similarly treated showed similar results.

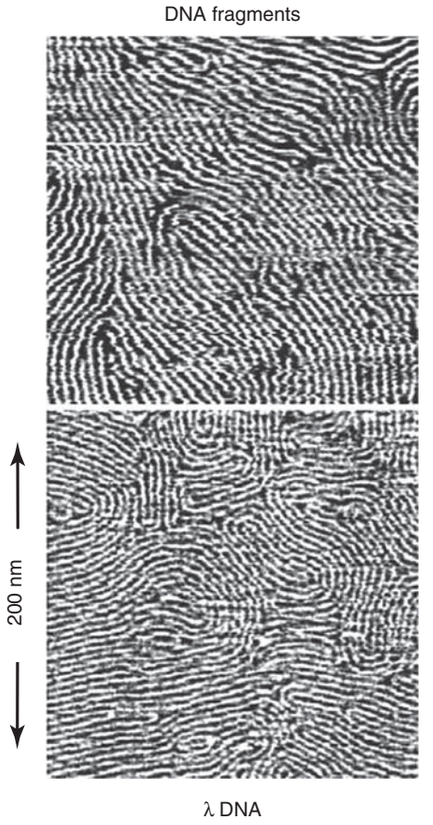

FIGURE 21.26 Atomic force microscopy images of DNA from different sources (see figure for details) condensed on DPDAP bilayers at room temperature in 20 mM NaCl. Striking fingerprint-like order is apparent, with a domain size of the order of the persistence length (ca. 50 nm) (courtesy of J. Yang).

Striking, fingerprint-like images of DNA adsorbed on the surface were revealed (Figure 21.26). The typical domain size for the aligned, smectic-like order is usually several hundred angstroms, reflecting the DNA's intrinsic persistence length. These structures are expected to be like those found in L_α^c complexes: the domain size, inferred from X-ray scattering is quite similar [119,120]. Furthermore, it was found that the surfaces are often overcharged when DNA is adsorbed, i.e. the number of DNA fixed charges exceeds the number of lipid charges. This can be anticipated on the basis of theoretical studies of a similar problem: adsorption of charged globular proteins (yet another macroion) on oppositely charged membranes [154]. In both cases the driving force for adsorption is similar to that driving lipoplex formation, namely counterion release. In L_α^c complex formation, much of the DNA can interact with the two sandwiching bilayers. In contrast, topology dictates that adsorbates on a single lipid bilayer will always possess a part proximal and a part distal to the interaction zone. If both parts are charged, as is the case with DNA, complete counterion release cannot be achieved since the distal part does not interact significantly with the underlying bilayer. Therefore, although charges on the lipid membrane are fully

cancelled by charges on adsorbed DNA macroions, still the portion of DNA away from the contact zone imparts a net surface charge, i.e., overcharging of the DNA-covered membrane.

Yet another interesting feature is the dependence of the DNA–DNA distance on salt concentration. As the NaCl concentration was varied between 20 and 1000 mM, this distance grew from around 45 Å to almost 60 Å. At first this may seem baffling: adding salt should be expected to decrease the DNA–DNA electrostatic repulsion, and hence lower the distance between neighboring interacting strands. This is indeed the general trend that has been observed in L_α^c complexes [117,144]. However, because the DNA was primarily allowed to saturate the surface, and only subsequently treated with the salt solution (which was later also washed away), adsorption here was not at equilibrium. In fact, when faced with a neat salt solution, the adsorbed DNA can only detach and will not generally readsorb onto the surface. It is therefore hard to give full theoretical reasoning for the trend.

Theoretical explanations have previously been offered to account for this salt-dependent behavior based on a balance between membrane-mediated effective attraction (that may be the result of the DNA perturbation of the lipid bilayer) and electrostatic repulsion between DNA strands [155]. The predicted DNA–DNA spacing as a function of screening length is nonmonotonic: increasing first for low screening lengths and decreasing for high values. An alternative to this approach is related to the free energy gain upon adsorption and how it changes with the addition of salt. In the presence of added salt, the adsorption free energy can be expected to be lower since the gain in entropy upon release of counterions becomes very small when releasing an ion from an adsorbed layer into a bathing solution with a comparable concentration. Assuming that unbinding would occur when the free energy gain per persistence length is $\approx k_B T$, we can estimate from a simple model that the thickness of the confined layer is $l_{\text{eff}} \approx 5$ Å, rather close to the screening length in solution (3–4 Å) [138–141]. Thus, the lower binding free energy may cause some of the DNA strands to dissociate from the lipid surface once the system is exposed to salt. Allowing DNA to rearrange on the surface would then lead to an increase in the average DNA–DNA distance.

When multivalent salt is used, a crowding of DNA molecules is first observed as salt is added (in accordance with the observations in the L^c complexes), and then starts to grow for higher concentrations [100,156]. This may be a manifestation of the two competing forces as salt is added: lessened repulsion between strands vs. weakened adsorption energy.

21.5.5 From Lamellar to Hexagonal Complexes

So far, we have discussed the L_α^c lipoplexes formed from lipid membranes that are rigid (bending rigidity much greater than $k_B T$) and tend to a planar geometry. Other lipoplex structures may ensue when the lipids possess a spontaneous curvature which is nonplanar, or when the membranes are soft enough to be deformed under the influence of the apposed macroion. The lipid membrane thus responds to the presence of DNA by deforming elastically and by locally changing its composition ϕ.

Membrane elasticity may be varied substantially either by changing the lipid CL/HL composition, changing the lipid species, or by adding other agents, such as alcohols, to the membrane [157,158]. In contrast, double-stranded DNA generally remains rather stiff, with a typical persistence length of ≈ 500 Å. Hence, the lipoplex geometries are restricted to structures in which DNA remains linear on these large length scales. Usually, it is the interplay between the elastic (spontaneous curvature and bending rigidity) and electrostatic (charge density) properties of the membrane that will determine the optimum lipoplex geometry at equilibrium.

Often, the membrane elasticity and electrostatic contribution to the free energy display opposing tendencies. For example, the hexagonal H_{II}^c complex is electrostatically favored due to the cylindrical wrapping of the DNA by the lipid monolayer. This allows better contact between the two macromolecular charged surfaces. However, the highly curved lipid geometry may incur substantial elastic (curvature deformation) energy. The price to pay will be lower when the lipid (monolayer's) spontaneous curvature matches closely the DNA intrinsic (negative) curvature or when it has low bending rigidity. Under such conditions, the H_{II}^c complex may become more stable than the L_α^c phase. Usually, a neutral HL is used for adjusting the spontaneous curvature to the required negative curvature, since pure CLs typically tend to form uncurved or positively curved aggregates. Use of more HL in the mixed membranes may, on one hand, lower the elastic penalty, while, on the other hand, lower the monolayer's charge density, compromising the electrostatic energy gain upon association.

These qualitative notions were elegantly demonstrated by experiments in which the elastic properties of the lipid monolayers were controlled by changing the nature of the lipid mixture. The spontaneous curvature of the lipid bilayer was modified by changing the identity of HL. It was found that when using a mixture of DOTAP/DOPE, H_{II}^c was the preferred structure, while DOTAP/DOPC mixtures promoted the formation of the L_α^c phase. This is consistent with the fact that pure DOPE forms the inverted hexagonal phase, H_{II}, due to its high negative spontaneous curvature [159–161], while DOPC self-assembles into planar bilayer. In addition, by adding hexanol to the DOTAP/DOPC–DNA lipid mixture, the bending rigidity could be diminished by about one order of magnitude [157,158]. This induced a clear first-order $L_\alpha^c \rightarrow H_{II}^c$ phase transition [118].

Additional complexity can be expected when accounting for the coexistence of more than one phase in solution. A theoretical study of the phase equilibrium took into account the bare lipid phases L_α and H_{II}, the naked DNA and the complex L_α^c and H_{II}^c phases [162]. The phase diagram of the system was evaluated by minimization of the total free energy, which included electrostatic, elastic, and lipid demixing contributions. Several systems of different compositions were considered. Figure 21.27 shows the predicted phase coexistence corresponding to the simplest case already discussed of rigid

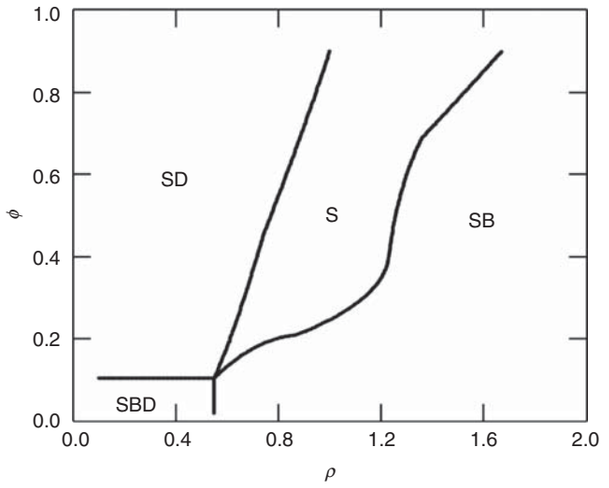

FIGURE 21.27 Phase diagram of a lipid–DNA mixture for lipids, which self-assemble into rigid planar membranes. The phase diagram was calculated for membranes characterized by a bending rigidity in the range of $4 < \kappa < \infty\ k_BT$ and a spontaneous curvature of $c = 0\ Å^{-1}$ for both helper and cationic lipids. The symbols S, B, and D denote, respectively, the L_α^c, L_α, and uncomplexed (naked) DNA phases. (From May, S., Harries, D., and Ben-Shaul, A., *Biophys. J.* 2000, 79, 1747. Reprinted by permission from Biophysical Society.)

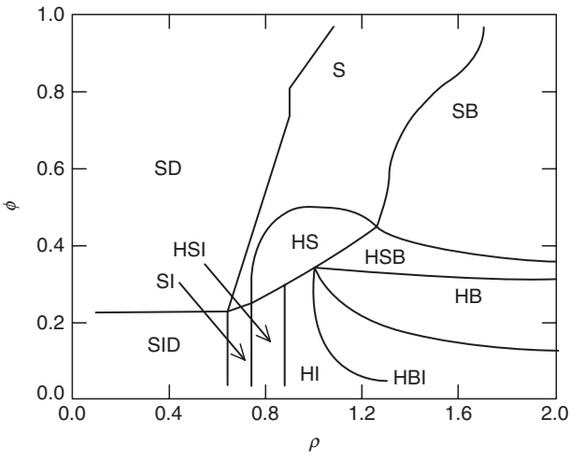

FIGURE 21.28 Phase diagram of a lipid–DNA mixture involving "curvature-loving" helper lipid: the spontaneous curvature of the helper lipid is $c = -1/25\ Å^{-1}$. For the cationic lipid the spontaneous curvature taken is $c = 0\ Å^{-1}$. The bending rigidity for both lipids is $\kappa = 10\ k_BT$. The symbols S, H, B, I. and D denote, respectively, the L_α^c, H_{II}^c, L_α, H_{II}, and uncomplexed (naked) DNA phases. The broken line marks the single H_{II}^c phase. (From May, S., Harries, D., and Ben-Shaul, A., *Biophys. J.*, 2000, 79, 1747. Reprinted by permission from Biophysical Society.)

planar membranes. Results are presented for lipid membranes with a bending rigidity of $\kappa = 10\,k_BT$ per monolayer and spontaneous curvature $c = 0\ Å^{-1}$ (typical for many bilayer forming lipids [122]) for which only lamellar complexes are expected to form. As the overall lipid composition is enriched in CL (higher ϕ) the one phase persists over a wider range of ρ. This indicates that for higher CL content, the complex may be expected to be more stable toward addition of either DNA or lipid (hence moving away from the isoelectric point).

The Gibbs phase rule allows for up to three phases to coexist concomitantly for this three-component (DNA, HL, and CL) system. Figure 21.28 shows the theoretical prediction for the phase diagram for a system in which the HL has a strong negative spontaneous curvature ($\kappa = 10\,k_BT$ and $c = 1/25\ Å^{-1}$) [162]. For high ϕ values, the phase behavior resembles that of the previously discussed system. However, for lower values of ϕ, a multitude of regions of (up to three) different phases coexisting together can be found. In some regions, lamellar and hexagonal complexes appear coexisting side by side. A similarly complex diagram results when the membranes are soft (bending rigidity of $\approx k_BT$) as might be expected for membranes with added alcohols [162].

A more subtle demonstration of the underlying balance of forces can be found within the realm of the L_α^c complex. Thus far, the theoretical models considered for the lipid membranes in this lamellar phase assumed them to be perfectly planar slabs. However, this need not be so. When membranes are sufficiently soft (yet not soft enough to favor the H_{II}^c phase) or if one of the CL/HL has a propensity to form curved surfaces, the membrane may corrugate so as to optimize its contact with DNA (see Figure 21.22A). If the membrane is further softened, finally, a transition may occur to the H_{II}^c phase. In this respect, the membrane corrugation in the L_α^c complex may be regarded as a further stabilization of the lamellar complex, and a delay to the onset of the $L_\alpha^c \rightarrow H_{II}^c$ transition.

A possible consequence of membrane corrugation in the L_α^c phase is an induced locking between neighboring galleries. This follows the formation of "troughs" in a gallery, induced by the interaction of the membrane with DNA in adjacent galleries. This imposes "adsorption sites" for the DNA in the two neighboring galleries, which propagates the order on. The formation of these troughs, as well as a very weak electrostatic interaction between galleries, may thus correlate between the positions of DNA in different galleries [147,163,164]. Limited experimental evidence supports this notion. In cryo-transmission electron microscopy (cryo-TEM) studies of the L_α^c phase, spatial correlations were found between DNA strands in different galleries [165]. In another series of X-ray studies, the corrugation and charge density modulation in an L_α^c-like complex, in which the membranes are in the gel phase, were measured [166]. Further support for the possible formation of corrugations is gained from computer simulations of lipid–DNA complexes [147].

In order to assess the extent of membrane corrugation, a balance of forces between many degrees of freedom should be taken into account. The free energy minimum now depends on the local membrane composition—dictating membrane properties such as local charge density, spontaneous curvature, and bending elasticity—and the extent of local deformation around the DNA. Theoretical predictions show that for

a wide range of conditions, both stiff and soft membranes can show corrugations that are stable with respect to thermal undulations of the membranes [164]. The spacings between galleries and between DNA molecules are also predicted to change somewhat with respect to the case where no corrugations are allowed [163]. For the conditions in which the troughs are shallow, or absent altogether, one may anticipate the formation of phases where DNA in different galleries are positionally uncorrelated, while orientational order is preserved. These structures were predicted theoretically and termed "sliding phases" [119,120,165,167–169].

21.5.6 Lipoplex Structure and Transfection Efficiency

In recent years, a large number of CL–DNA formulations have been proposed as vectors. However, the fate of the CL–DNA complex once administered, its interaction with the cell membrane, and entry into the cell and subsequently into the cell nucleus, is likely complex and largely unresolved. The poorly understood [170–172] process of DNA release once in the cell interior must be important. For example, it has been shown from action in the nucleus that DNA expression is diminished when it is tightly complexed with lipids [175]. Hints to the mechanism of the intracellular release of lipoplexes come from experimental evidence in vitro showing that other added polyelectrolytes may compete with DNA and subsequently replace it in the complex [173]. This kind of replacement, by natural polyelectrolytes, may be one way in which DNA is released in cells [174]. Another possible mechanism is the fusion of complex lipids with lipid membranes in the cell [100,120].

Only a limited number of experiments have probed the relationship between the structure of CL–DNA complexes and the transfection efficiency. One emergent theme attributes an important role to complex frustration and destabilization in promoting transfection.

Experimental studies show that the two ordered complex structures, L_α^c and H_{II}^c, behave differently inside living cells. Furthermore, a correlation was found between the structure of the lipoplexes formed and the transfection efficiency. The structure formed depends in turn on the specific choice and relative amount of HL, CL, and DNA. The H_{II}^c complex was found (in the studied cases) to be a more potent vector than L_α^c [176,177]. Further information is gained from fluorescence studies of cell cultures with both complex types internalized in fibroblast L-cells. These indicate that the L_α^c complex is more stable inside the cells, while the H_{II}^c more readily disintegrates—its lipids fusing with the cell's own (endosomal or plasma) membranes—resulting in DNA release. This is in accord with the theoretical findings that the L_α^c complex structure is rather flexible toward changes in the system's compositional parameters due to its ability to tune both the membrane composition and the DNA–DNA spacing, while this tuning is more limited in the H_{II}^c phase.

The picture is further substantiated by a series of studies by Barenholtz and coworkers [101,171,172,178]. In general, it was shown that maximal transfection efficiency could be achieved in complexes that were formed in the excess lipid regime (with ρ in the range of 2–5). This correlated well with the point of maximal size heterogeneity of the complexes. These instabilities were shown to occur concomitantly with an increase in the amount of membrane defects that were in turn mainly attributed to the appearance of several coexisting structures in solution (e.g., H_{II}^c and L_α^c in DOTAP/DOPE lipoplexes, or micellar and lamellar phases in DOSPA/DOPE-based lipoplexes). This is in accordance with the theoretical prediction that the regions of most phase diversity and the largest number of coexisting phases occurs at high ρ (and low ϕ) values (see Figure 21.28 [101,132,159]).

Other evidence seems to agree with these notions. For example, some successful formulations, such as BIV, are also probably metastable [108,115,128]. This may suggest that it is in fact their instability, which helps them in releasing their DNA cargo once they are inside the cell. Attempts have also been made to destabilize lipoplexes more specifically once they are already internalized in the cells (rather than en route in the serum). Reduction-sensitive CLs were designed, and the subsequent lipoplexes that are formed were shown to undergo large structural changes when exposed to the cytoplasmic reductive systems. The lipoplexes are thus destabilized and the previously packaged DNA is released into the cytosol [103,179–181]. A decrease in the toxicity of the CL and increased transfection efficiency are thus achieved [182].

Recent experiments have shed additional light on the relation between complex structure and transfection efficiency. These studies concentrate on lamellar L_α^c complexes that are the ones most often encountered. It has been shown that the membrane charge density of the CL vector, rather than, say, the large valency of the CL is an important parameter that governs transfection efficiency. Specifically, the path for complex uptake is distinctly different for high versus low lipid charge density. While at both high and low charge densities, complexes are found to enter through endocytosis, at low lipid charge density, DNA was trapped in complexes, and those in turn were trapped inside endosomes, while at high density, endosomal entrapment does not seem to be a significant limiting factor. At very high lipid charge density, the transfection efficiency is again reduced. These findings have led to a new model of the intracellular release of DNA from lamellar complexes, through activated fusion with endosomal membranes. It has been suggested that complexes escape the endosome by fusion with the endosomal membrane. This fusion is favored by (attractive) electrostatic interaction energy that is higher for highly charged membranes [183–186].

In contrast, the transfection efficiency of the H_{II}^c complexes does not seem to depend on lipid charge density, perhaps because their structure leads to a distinctly different mechanism of cell entry. It seems that these complexes undergo rapid fusion with cellular membranes. The curvature-loving properties of the hexagonal complexes favor rapid fusion and escape of DNA from the endosome, and this process no longer limits the transfection rate.

Destabilizing lipoplexes is not the only barrier to transfection. For example, entry of DNA into the nucleus through the

nuclear pore complex is inefficient for large pieces of DNA. It has been shown that the cell's own nuclear import machinery may be utilized to increase transfection efficiency dramatically by attaching a peptide containing a nuclear localization signal (NLS) to the DNA [187,188]. Furthermore, the size of the complexes also seems to play a crucial role in determining transfection efficiencies [101,102,108,115]. Here, the repulsive interaction between like-surface charge of the complex due to over/under charging (excess lipid or DNA) can aid in stabilizing the complexes, once they are formed, from fusing further.

Another strategy to controlling the interaction between aggregates and the stability of the aggregate in vivo is to modify the composition of the outer wrapping sheath of the lipoplex. The caveat is that the lipoplexes are not stabilized to such a degree that they can no longer disintegrate once inside the cells. For example, short-chain lipids possessing a PEG headgroup (or a derivative thereof) have been used to increase the stability of the lipoplexes in the blood stream due to repulsive steric interactions, while not interfering with the endosomal unwrapping once the lipoplexes are internalized in cells. These "PEGylated" lipids can reduce the transfection efficiency, but also increase the stability of complexes en route to their targets [189–191]. The PEG chains that are attached to the lipids are present inside as well as at the surface of CL–DNA complexes. This gives rise to polymer-mediated forces, such as depletion attraction between DNA strands that arises because polymer disfavors confinement of its degrees of freedom when it is between DNA rods.

More generally, we can expect that understanding how to control and manipulate the formation of specific phases on the one hand, while better understanding the multistage transfection mechanism, and the parameters (conditions) affecting it on the other, should aid in the design of more potent lipid-based gene delivery vectors in the future. These, together with control over the coating and targeting of the complexes, may render these vectors as useful vehicles in gene therapy.

21.6 DNA–POLYCATION INTERACTIONS

Stiff polyelectrolytes like DNA are readily capable of spontaneously forming complexes with various oppositely charged macromolecules to form submicron-sized complexes [53]. It is primarily thought that the formation of these self-assemblies is driven by Coulombic electrostatic and polyelectrolyte bridging interactions as well as the entropic gains derived upon the release of bound water and counterions. These forces compensate for the entropic loss resulting from a close packing of the stiff polyelectrolyte chains. Due to their potential for protecting and delivering genetic information, condensation of DNA with polycations is of particular interest. The polycation–DNA complex, often called "polyplex" [99], forms spontaneously upon mixing positively charged polymers with negatively charged nucleic acids. The advantage of polymer formulations lies in their ability to be generated economically in large quantities while offering versatility of synthetic chemistry and allowing easy tailoring of various chemical structures, molecular weights, and topologies with low immunogenicity [192].

Similar to lipoplexes, the primary goal of polycation research is the condensation of DNA into particles of virus-like dimensions that can migrate through the blood stream and into target tissue, overcome the electrostatic repulsions of the cell membrane, yet protect the nucleic acid from degradation and undesired interactions [193]. A wide variety of natural and synthetic polycations have been investigated, most of them based on amine chemistry. Factors influencing DNA compaction include the number of charges per chain, the type of charge (e.g., primary, secondary), charge spacing along the chain, chain architecture (linear, branched, dendritic), and chain hydrophobicity. External conditions, such as solution ionic strength, concentration, positive-to-negative charge ratio of polycations to DNA, and mixing conditions also are observed to influence how polyplexes form. Observed differences in transfection efficiency to date are not easily correlated to polycation chemistry or structure. Large transfection differences are observed between various polycations as well as with the same polycation but of varied molecular weight or polymer chain architecture. Aggregation is generally diffusion limited upon mixing. Depending on the technical process of mixing one can form fibers; large micron-sized aggregates; or small rod, toroidal, or spherical aggregates [194–197]. Critical to increasing binding to the negatively charged cell membrane, polyplexes are usually overcharged by the polycation resulting in a net-positive colloidal aggregate.

In an ideal polyplex-mediated gene delivery, the polycations must not only compact DNA but also be able to overcome a wide variety of multibarrier processes to achieve successful transfection. Similar to a virus capsid, vector delivery would occur in a highly cell-specific manner, facilitate cellular uptake as well as endosomal release, and be able to maneuver through the cytoplasmic environment, disassociate, and then localize the desired nucleic acid vector into the cell nucleus ready for transcription. In addition, this ideal polycation would also be nontoxic, nonimmunogenic, and biodegradable. Obviously, this is a large list; in reality, no one polycation is likely to satisfy all these conditions. Consequently, a variety of additional functional elements have also been included in polyplex formulation to try to improve delivery, efficiency, targeting, and lower cytotoxicity. To date, no predictions of the correlation between polyplex structure and transfection efficiency can be made without extensive experiments. Clearly a balance of the molecular forces within and between the polyplexes is needed to create particles stable enough to carry the DNA to the nucleus yet sufficiently unstable to release the DNA when needed. In this chapter, we introduce our current understanding of the internal structure, phase behavior, and compressibility of polyplexes. We end with a brief discussion of recent advances in understanding of polyplex gene delivery.

21.6.1 Structure of Polyplexes

Early work investigating the internal packing and ordering of DNA–polycation complexes used small-angle X-ray scattering (SAXS) to look at pulled DNA fibers kept at constant

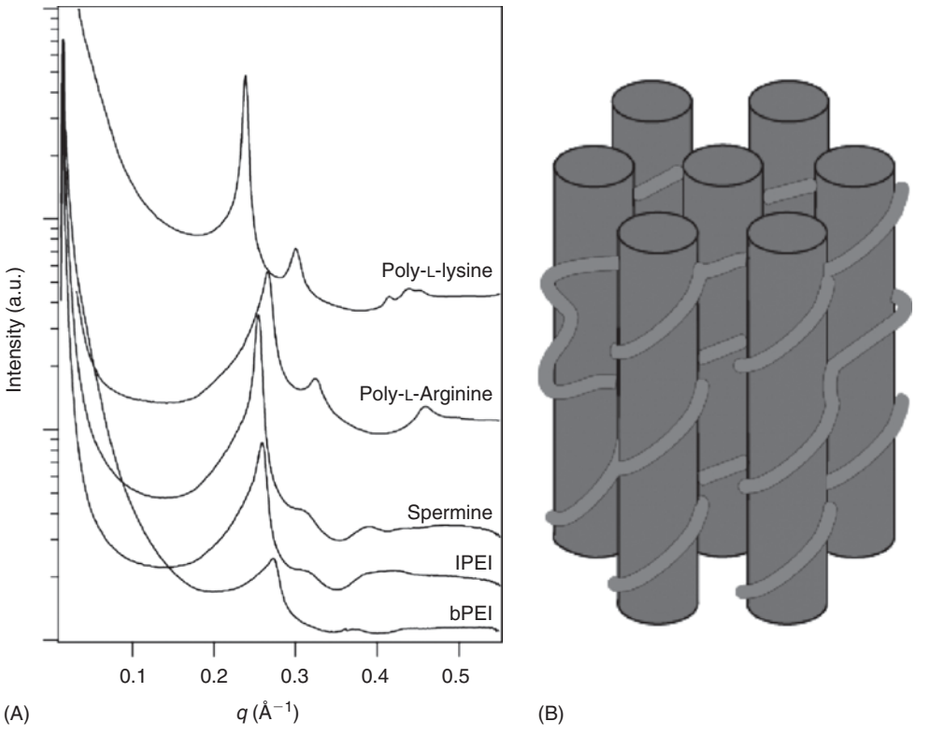

FIGURE 21.29 (A) Synchrotron small-angle X-ray intensity profiles for five different polycation–DNA complexes shifted in intensity for clarity. All samples were made with an excess of cationic charge to DNA phosphate and equilibrated in TE buffer without additional salt. (B) Schematic drawing of a close-packed hexagonal ordering of DNA rods held together by electrostatically bound polycations chains.

humidity levels [198–200]. More recent work has used SAXS to look at the internal packing and ordering of DNA–polycation complexes in buffered solutions [22,54]. Figure 21.29 shows a series of high-resolution synchrotron SAXS intensity profiles, shifted in intensity for clarity, for calf thymus DNA packaged with poly-L-lysine (PL), poly-L-arginine (PA), spermine (Sp), and linear and branched polyethylene imine (lPEI and bPEI, respectively) in TE buffer. Here, all samples are made with an excess of polycations and then washed to remove unreacted polycations.

All systems show a similar hexagonal close-packing of rods. A simple schematic view of this hexagonal ordering is shown in Figure 21.29. For simplicity, we represent DNA as a stiff rod to emphasize that on small length scales, such as those observable via SAXS, DNA behaves as a rigid polymer with a large persistence length ($L_p \sim 50$ nm) in stark contrast to the highly flexible polycation chains ($L_p \sim 1$ nm). Here, the flexible polycations act as a simple, electrostatically driven linker molecule, which can both wrap around a single DNA as well as bridge between DNA strands. The DNA packing dominates the scattering profiles here as DNA is significantly higher in electron density compared to the polycations. A dependence of the $d_{\text{DNA-DNA}}$ spacing, as well as small effects on the DNA pitch, is observed to depend on the chemical nature of the complexed polycation. Interhelical distances in buffer or low salt are typically of the order of 26–30 Å, equivalent to ~6–10 Å space between DNA rod surfaces. Due to the kinetic nature of polyplex formation, sample preparation is also observed to affect the polyplex internal structure. Typical conditions used to form gene therapy vectors (dilute solutions mixed under low salt conditions), were observed to give similar hexagonal packaging of the DNA as shown in Figure 21.29, but with significantly poorer long-range order in the DNA array. These particles were found to be kinetically trapped in nonequilibrium structures. Once formed, they equilibrate extremely slowly with significant, internal spacing rearrangements (~5%) observed on the timescale of several months as the chains try to rearrange themselves to reach their thermodynamic equilibrium spacing. Qualitatively, samples with natural amino acids, lysine and arginine, show a higher degree of long-range order compared to the short natural polyamine (spermine) and the synthetic PEI samples. This loss of long-range order may be due to the shortness of the chain for spermine and charge mismatching in the synthetic PEI polycations. Better ordering is observed for linear compared to branched PEI. This suggests that the chain architecture as well as the chemical nature of the polycations plays some role in determining the internal packing of the polyplexes. Only small effects in interaxial spacings (1–3%) are seen upon changing polycation molecular weight to significantly higher molecular weights, increased nitrogen to phosphate (N/P) charge ratio (above charge neutrality), or changing pH after polyplex formation. An exception is that d spacings were observed to change some 10% with increasing N/P ratio for

the PEI samples. However, as PEI is not a fully charged chain at neutral pH, the calculated N/P charge ratio does not reflect the true N/P ratio such that N/P significantly higher than one is necessary to achieve charge neutrality in the complex, consistent with known PEI behavior. Estimates for PEI place neutrality at N/P ~ 2.5 [201].

21.6.2 Polyplex Phase Behavior

The structure and phase behavior of lipoplexes have been investigated in some detail showing a wealth of possibilities tuned by varying intermolecular forces through changing lipid chemistry or chain shape. In contrast, polyplexes have not shown much variability and have not been explored in as much detail. To understand the phase behavior, polyplexes of calf thymus DNA condensed with spermine, polylysine, polyarginine, and linear and branched PEI were investigated as a function of external monovalent salt concentration [54]. The addition of monovalent salt can weaken the molecular interactions of the polycations with DNA through screening of the electrostatic and bridging interactions, displacement of bound multivalents, and/or chloride binding to multivalent ions (see Figure 21.30).

In this work, universal phase behavior was observed for all polyplexes with increasing salt concentration. Initially all samples are observed to form a "tight bundle" phase of hexagonally close-packed DNA rods as depicted in Figure 21.29. The Bragg reflection in the SAXS curves not only gives information about the interaxial spacing between the rods in the array but also the peak width indicates the long-range in-plane ordering of the array through a correlation length ξ. ξ is seen to depend on the polycations and sample preparation; at low salt concentrations, ξ is observed to be on the order of 15–30 DNA repeats for the various polyplexes studied. At low salt concentrations, this hexagonal packing shows simple linear swelling behavior with the observed scattering while maintaining the in-plane correlations. At a critical salt concentration, c_s^*, dependent on polycation, the onset of a coexistence regime is observed (shaded regions in Figure 21.30). The coexistence regime occurs over a relatively narrow range of salt concentrations and is characterized by an overlapping of the initial sharp Bragg reflection with a new broad peak at lower q spacings in the SAXS measurements. In this phase, a significant fraction of the polycations has been displaced from the DNA, and a salt-induced melting transition is observed. Here, the polycations are more loosely associated with the DNA. This results in a phase with a wider distribution of interaxial spacings and a poor in-plane packing of the DNA and identified as a "loose bundle" phase. A high local concentration of the DNA is maintained through the bridging interactions of the polycations.

Due to the intrinsic stiffness or persistence length of DNA, it maintains some order similar in nature to the liquid crystalline phases observed in pure DNA phases at high concentration [8]. For an intuition on the strength of these interactions, c_s^* ranged from ~300 mM for spermine to as much as 1.6 M NaCl for polyarginine. With still more added salt, this broad peak of the loose bundle phase is observed simultaneously to shift to smaller q, or larger d spacings, and to broaden significantly, corresponding to decreasing in-plane correlations of the DNA arrays. Interestingly, if all the polyplexes are normalized with respect to c_s^*, the swelling behavior in both regimes and ξ above c_s^* is observed to collapse to a single curve (see Figure 21.30). At c_s^*, ξ is observed to drop sharply to ~6–7 DNA repeats, independent of polycations; ξ continues to decrease to ~3 DNA repeats at the highest observed salt concentrations. At large polymer/DNA concentrations, a network phase is observed to form and to grow at the expense of the loose bundle phase. At still higher salt, or lower polymer–DNA concentrations, this network dissociates completely.

A simple model [54] was proposed using a free energy function balancing only the electrostatic attraction and entropic repulsion between the polymer chains for a hexagonal bundle and a network phase. In the bundle phase, condensation is driven by attractive electrostatic interactions. The entropic gains from releasing the bound counterions and water from the DNA compensate for the entropic loss from a close packing of the polymer chains parallel. The network phase, in contrast, is stabilized by highly localized bridge points between polymers and dominates at high salt concentration or low polymer densities. Building on established theory, the potentials for the electrostatic interactions and entropic repulsions can be used to estimate the free energy expressions for both the bundle and network phases [202,203]. This simple balance of electrostatic attraction and entropic repulsion quantitatively and qualitatively describes the transition from a hexagonal loose bundle to a network phase at high salt concentrations on the order of 1 M NaCl, where the network phase grows at the expense of the bundle phase. To induce a phase separation between loose and tight bundles, additional nonelectrostatic attractive forces have to be invoked. Furthermore, this model does not include short-ranged specific interactions, which must arise from chemically distinct polycations as observed experimentally.

21.6.3 Equation of State for Polyplexes

Insight into the intermolecular forces within condensed DNA arrays can be obtained through osmotic stress experiments. Stressing solutions of PEG exert a known osmotic pressure that is balanced by the intermolecular repulsion between helices. Measurement of the interhelical spacing at each osmotic pressure furnishes the DNA equation of state. Very few data have been collected on polyplexes, but we expect many similarities with the more extensively studied short condensing agents. Various condensing agents, ranging from divalent Mn salt to longer polycations such as spermidine and protamine, show many common features [22,48]. Equilibrium spacings, at zero osmotic pressure, depend on the polycations inducing assembly and do not change significantly at low pressures. The equilibrium spacing is typically 8–12 Å between DNA surfaces, indicating a balance of attraction and repulsion between helices. These surfaces can be brought

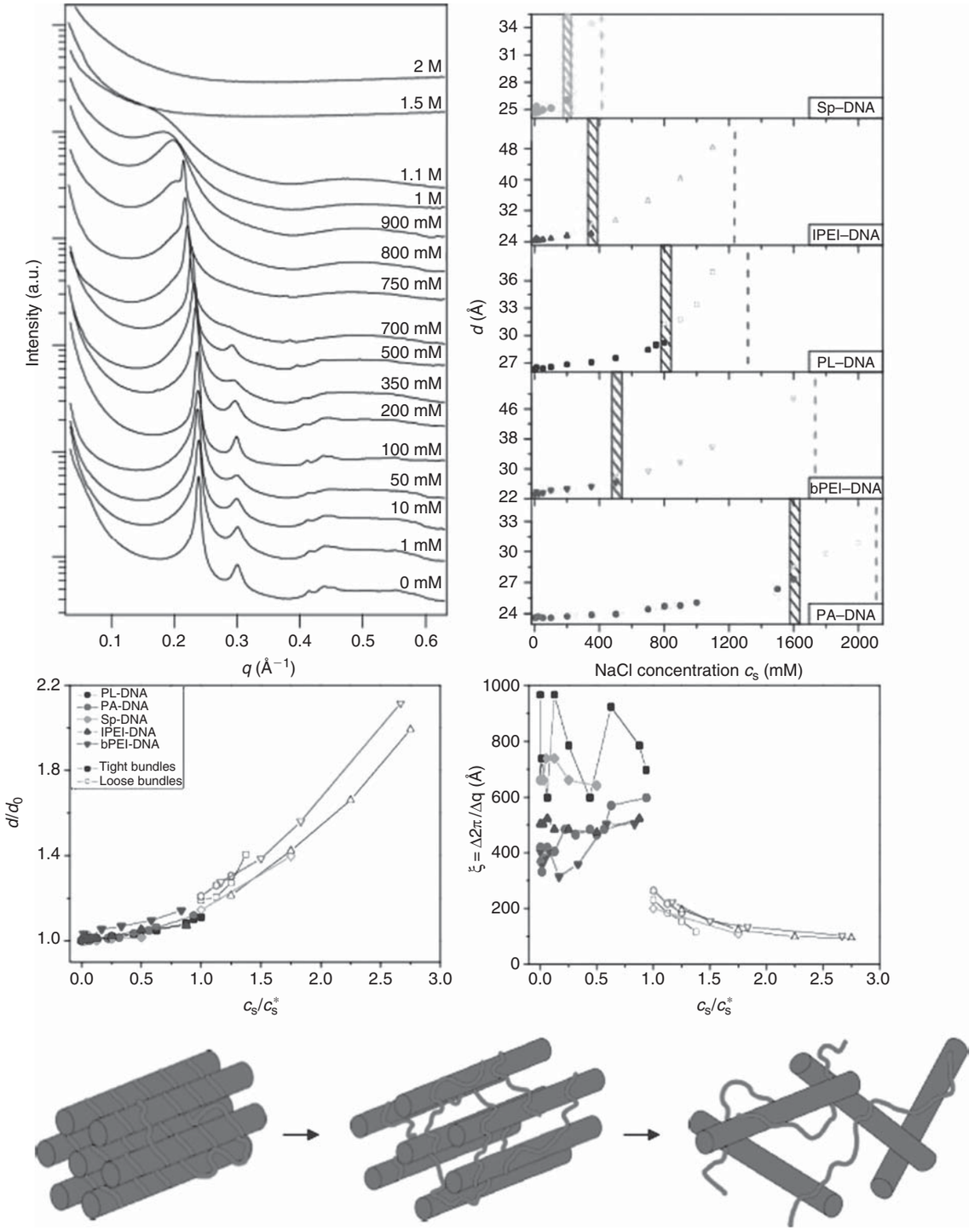

FIGURE 21.30 (See color insert following page xxx.) Phase behavior of polyplexes with increasing monovalent salt concentration. Universal phase behavior is observed for all systems with an initial swelling of a tightly packed hexagonal array of DNA rods. As a critical salt concentration, c_s^*, dependent on polycation, the onset of a coexistence regime is observed between tight and loose bundles. In-plane correlation lengths, ξ, representative of long-range order within the arrays show a sharp decrease upon crossing c_s^*. When scaled with respect to c_s^*, both swelling ratio (d/d_o) and ξ collapse onto universal behavior. With increasing salt, the loose bundles lose both positional and orientational order with an increase in a network structure at the expense of the loose bundle regime. At sufficiently high salt concentration, or dilute polymer concentration, all Coulombic interactions are screened and the samples disassociate completely into the dilute phase.

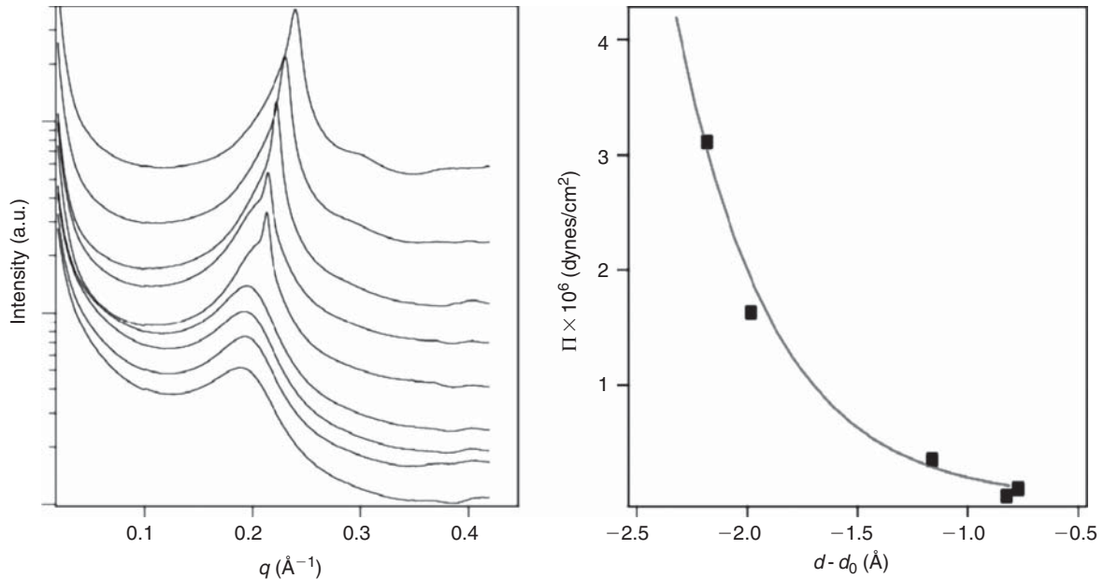

FIGURE 21.31 SAXS intensity curves of the osmotic stress induced reordering of PLL–DNA at 900 mM NaCl. With increasing pressure, the broad diffuse peak indicative of liquid crystalline–like "loose bundle" ordering is forced to reorder showing clear coexistence and then finally scattering from a purely tight-bundled phase is observed. Compression at low osmotic pressure in this loose bundle phase was predicted to scale as 1/*d* using a simple calculated energy balance of long-range electrostatic attraction against entropic repulsion. This 1/*d* scaling is shown in the inset and is found to agree well with the experimental results. (From DeRouchey, J., Netz, R.R., and Rädler, J.O., *Eur. Phys. J. E*, 2005, 16, 17.)

closer together with osmotic pressure and show net hydration repulsion modulated by the presence of the polycations. The force needed to push helices closer than the equilibrium spacing depends on the polyvalent ion identity. At high pressures, however, all samples show exponentially increasing forces with decay lengths of 1.5–2 Å independent of the counterion species. The decay lengths of these repulsive interactions are approximately half that for an overall net hydration repulsion observed in pure DNA arrays and are insensitive to external salt concentrations. While decay length is only weakly cation dependent, there are significant differences in the magnitudes of the forces. The exact nature of these forces is not completely understood. The data do set limits that show inconsistency with several proposed ionic fluctuating models such as direct ionic bridging, ionic fluctuation, and van der Waals attraction balanced against hydration/electrostatic repulsion.

Available data for polyplexes show similar osmotic stress force curves. Equilibrium spacings for polylysine or polyarginine polyplexes are similar to spacings of DNA condensed with small cations and curves appear to converge to similar exponential limits. Osmotic stress was used to investigate a complex phase diagram for PL–DNA involving two coexisting phases [54]. Using high salt concentrations, where at $\Pi = 0$, the samples are found to be in a pure loose bundle phase, osmotic stress was applied using a high molecular weight PEG. Initially, simple compression of the loose bundles is observed with the average interaxial spacing between DNA inside the array getting smaller. With increasing osmotic pressure, the system rearranges and the characteristic scattering for the coexistence regime is observed. Increasing the osmotic pressure further still results in the sample passing through the coexistence regime until scattering due solely to a tight bundle regime is observed. SAXS curves showing PLL–DNA at 900 mM NaCl, corresponding to loose bundles at $\Pi_{osm} = 0$, with increasing osmotic pressure are shown in Figure 21.31. Using osmotic pressure to stress from a loose bundle to a tight bundle phase showed that these two phases are in equilibrium.

21.6.4 Polyplex Transfection

Typical transfection formulations are mixed in low salt conditions with an excess of positive to negative charge ratio of polymer to DNA to limit aggregation, resulting in uniform nanometer-sized particles (hydrodynamic radii of the order of 20–50 nm). Unfortunately, free polycations, typically amines, are toxic because they destabilize cellular membranes. Optimal charge ratios for gene therapy are a balance between achieving small, stable aggregates while minimizing the toxic effects. Incorporation of uncharged hydrophilic polymers, such as PEG, has proven to be an effective method to shield polyplexes, lower particle surface charge, and reduce unspecific interactions with salt and blood components [204]. However, shielding typically results in reduced transfection efficiency. This reduction can, in part, be overcome by incorporation of targeting ligands or bioreversible shielding into the particles [205,206].

Cellular uptake and delivery is not well understood but is known to depend strongly on particle size. Polyplex nanoparticles are small enough to be brought into the cell through clathrin- and caveolae-dependent endocytosis [207,208]. However, clathrin- and caveolae-independent endocytosis has also been observed including macropinocytosis and phagocytosis [209,210]. Once inside the cell, single-particle tracking techniques suggest that polyplexes are actively transported to the perinuclear region by microtubule transport [211]. More recently, new single-particle tracking results suggest that polyplexes of poly(ethylene imine) (PEI/DNA) have many diffusive behaviors. Interestingly, in early stages, these polyplexes are seen to bind to the cell membrane and freely diffuse on the cell surface while inducing a progressive accumulation of syndecans, resulting in an actin cytoskeleton–mediated endocytosis. Once endocytosed, the active transport of polyplexes inside vesicles by molecular motors along microtubules filaments was observed [212].

One of the primary causes of poor gene delivery with synthetic formulations is believed to be inefficient endosomal release. PEI, one of the most frequently studied systems due to its low cost and excellent transfection efficiencies in vitro and significant transfections in vivo, shows significant improvement in endosomal release over other common polycations [213,214]. Endosomal escape is believed to proceed through the "proton sponge" effect where charges along the chain with a pK_a slightly below physiological pH gets activated upon acidification in the endosome, resulting in an influx of both protons and charge neutralizing Cl^- ions, inducing an osmotic stress that swells and destabilizes the endosome, releasing its contents into the cytoplasm [215,216]. These studies strongly suggest that the high transfection activity of PEI vectors is due to their unique ability to avoid acidic lysosomes. The subsequent steps, complex disassociation, and final nuclear transport of the plasmid are still not mechanistically well understood. While improved active transport across the nuclear membrane has been reported through the incorporation of NLS [217], clear evidence has also shown that passive DNA entry into the nucleus during cell division when the nuclear membrane is temporarily disrupted is important. Highest efficiencies are reported in dividing populations of cells [218]. While new techniques and studies are beginning to shed light on the complicated multiple barriers, both thermodynamic and kinetic, involved in successful gene delivery, clearly more work must be done to understand, balance, and use the molecular forces involved for improved delivery vectors.

21.7 RETROSPECT AND PROSPECT

Structural elucidation of the DNA–CL and DNA–polycation complexes and realization of the extent to which they share the structural features of pure-DNA or pure-lipid polymorphism have advanced notably in the past few years. Some old questions have been answered and new questions raised. It is these new questions that challenge our knowledge of the intricacies of interactions between macromolecules.

The DNA–lipid and DNA–polycation complexes found so far are only a sample of the much wider set of structures that will be seen on a full DNA–complex phase diagram. We argue that this larger set of possibilities be approached by firmly established methods to measure the energies of these structures at the same time that they are determined and located on a phase diagram. Built on principles of direct molecular interactions, recognizing the consequences of thermal agitation, this line of observation and analysis can lead to an understanding of the energetic "whys" and preparative "hows" of complex structures.

Forces so delineated are already knowledgeably applied in new preparations. Precisely how the structure of DNA–lipid and DNA–polycation aggregates will affect their efficacy in transfection remains to be seen. So far, the ideas we have are too general and have been learned from studying analytically tractable but technically inadequate preparations. General principles do not lead to specific results. Molecules are too interesting to allow easy success in clinical design. Still there is little doubt of a practical link between the energy and structure of these complexes and their viability in a technological application.

Even the present general understanding of forces, even the cartoon ideas of the directions in which forces act in macromolecular complexes can tutor the bench scientist on how to improve preparations. There is enough known for a healthy iteration between experimental attempt and theoretical reason. Experimental successes and failures become the data for molecular force analyses. Various DNA–lipid and DNA–polycation assemblies reflect the various actions of competing forces. Molecular theorists can define and delineate these forces as they act to create each form; they can provide a logic to design variations in preparation. Basic scientists and clinicians are already in a position to help each other to improve their ways.

ACKNOWLEDGMENT

We would like to thank Milan Hodoscek and Matjaz Licer for their help with molecular graphics in preparing some of the figures, and John Nagle and Stephanie Tristram-Nagle for their comments on an earlier version of this chapter. We would like to thank Don Rau for instructive discussions. R.P. and D.H. thank the support of the Israeli and Slovenian ministries of science and technology through a joint Slovenian–Israeli research grant. This research was supported by the Intramural Research Program of the NICHD, NIH.

REFERENCES

1. Bloomfield VA, Crothers DM, and Tinoco I. *Nucleic Acids: Structures, Properties and Functions*. Mill Valley: University Science Books, 1998.
2. Vologotskii AV. *Topology and Physics of Circular DNA* (*Physical Approaches to DNA*). Boca Raton, FL: CRC Press, 1992.
3. Strey HH, Podgornik R, Rau DC, and Parsegian VA. Colloidal DNA. *Curr Opin Coll Interf Sci* 1998; 3: 534–539.

4. Podgornik R, Strey HH, and Parsegian VA. DNA–DNA interactions. *Curr Opin Struc Biol* 1998; 8: 309–313.
5. Kabanov VA, Flegner P, and Seymour LW. *Self-Assembling Complexes for Gene Delivery*. New York: Wiley, 1998.
6. Lasic DD. *Liposomes in Gene Delivery*. Boca Raton, FL: CRC Press, 1997.
7. Podgornik R, Rau DC, and Parsegian VA. Parametrization of direct and soft steric-undulatory forces between DNA double helical polyelectrolytes in solutions of several different anions and cations. *Biophys J* 1994; 66: 962–971.
8. Livolant F and Leforestier A. DNA mesophases. A structural analysis in polarizing and electron microscopy. *Mol Cryst Liq Cryst* 1992; 215: 47–56.
9. Derjaguin BV, Churaev NV, and Muller VM. *Surface Forces*. New York: Plenum, 1987.
10. Bloomfield VA. DNA condensation. *Curr Opin Struc Biol* 1996; 6: 334–341.
11. Leikin S, Parsegian VA, Rau DC, and Rand RP. Hydration forces. *Annu Rev Phys Chem* 1993; 44: 369–395.
12. Darnell J, Lodish H, and Baltimore D. *Molecular Cell Biology*, 2nd ed. New York: Scientific American Books, 1990.
13. Cerritelli ME, Cheng N, Rosenberg AH, McPherson CE, Booy FP, and Steven AC. Encapsidated conformation of bacteriophage T7 DNA. *Cell* 1997; 91: 271–280.
14. Safinya CR, Koltover I, and Rädler J. DNA at membrane surfaces: An experimental overview. *Curr Opin Colloid Interf Sci* 1998; 1: 69–77.
15. Mahanty J and Ninham BW. *Dispersion Forces*. London: Academic Press, 1976.
16. Safran SA. *Statistical Thermodynamics of Surfaces, Interfaces and Membranes*. New York: Addison Wesley, 1994.
17. Eisenberg D and Kauzmann W. *The Structure and Properties of Water*. Oxford: Clarendon Press, 1969.
18. Parsegian VA, Rand RP, Fuller NL, and Rau DC. Osmotic stress for the direct measurement of intermolecular forces. *Methods Enzymol* 1986; 127: 400–416.
19. Marãelja S and Radiç N. Repulsion of interfaces due to boundary water. *Chem Phys Lett* 1976; 42: 129–130.
20. Rand RP and Parsegian VA. Hydration forces between phospholipid bilayers. *Biochim Biophys Acta* 1989; 988: 351–376.
21. Kornyshev AA and Leikin S. Fluctuation theory of hydration forces: the dramatic effects of inhomogeneous boundary conditions. *Phys Rev A* 1998; 40: 6431–6437.
22. Rau DC and Parsegian VA. Direct measurement of the intermolecular forces between counterion-condensed DNA double helices. Evidence for long range attractive hydration forces. *Biophys J* 1992; 61: 246–259.
23. Parsegian VA. Long-range physical forces in the biological milieu. *Annu Rev Biophys Bioeng* 1973; 2: 221–255.
24. Bernal JD and Fankuchen I. X-ray and crystallographic studies of plant virus preparations. *J General Physiol* 1942; 25: 111–165.
25. Verwey EJW and Overbeek JTG. *Theory of the Stability of Lyophobic Colloids*. New York: Elsevier, 1948.
26. Hill TL. *Statistical Mechanics: Principles and Selected Applications*. New York: Dover, 1956.
27. Andelman D. Electrostatic properties of membranes: the Poisson-Boltzmann theory. In: Lipowsky R and Sackmann E, eds. *Structure and Dynamics of Membranes*. Vol. 1B. Amsterdam: Elsevier, 1995, pp. 603–642.
28. Landau LD and Lifshitz EM. *The Classical Theory of Fields*, 4th ed. Butterworth-Heinemann, 1986.
29. McLaughlin S. Electrostatic potential at membrane solution interfaces. *Curr Top Membrane Transp* 1985; 4: 71–144.
30. Brenner SL and McQuarrie DA. Force balances in systems of cylindrical polyelectrolytes. *Biophys J* 1973; 13: 301–331.
31. Parsegian VA, Rand RP, and Fuller NL. Direct osmotic stress measurements of hydration and electrostatic double-layer forces between bilayers of double-chained ammonium acetate surfactants. *J Phys Chem* 1991; 95: 4777–4782.
32. Kjellander R. Ion–ion correlations and effective charges in electrolyte and macroion systems. *Ber Bunsenges Phys Chem* 1996; 100: 894–904.
33. Hunter RJ. *Foundations of Colloid Science*. New York: Oxford University Press, 1987.
34. Parsegian VA, Van der Waals Forces: A Handbook for Biologists, Chemists, Engineers, and Physicists. Cambridge, MA: Cambridge University Press, 2005.
35. Parsegian VA. Long range van der Waals forces. In: van Olphen H. and Mysels KL, eds. Physical chemistry: enriching topics from colloid and interface science. 1975: 27–72.
36. Landau LD and Lifshitz EM. Statistical Physics Part 2: Butterworth-Heinemann, 1986.
37. Parsegian VA and Rand RP. Interaction in membrane assemblies. In: Lipowsky R and Sackmann E, eds. *Structure and Dynamics of Membranes*, Vol. 1B. Amsterdam: Elsevier, 1995, pp. 643–690.
38. Parsegian VA. Non-retarded van der Waals between anisotropic long thin rods at all angles. *J Chem Phys* 1972; 56: 4393–4397.
39. Brenner SL and Parsegian VA. A physical method for deriving the electrostatic interaction between rod-like polyions at all mutual angles. *Biophys J* 1974; 14: 327–334.
40. Parsegian VA, Fuller N, and Rand RP. Measured work of deformation and repulsion of lecithin bilayers. *Proc Natl Acad Sci USA* 1979; 76: 2750–2754.
41. Lipowsky R. Generic Interactions of flexible membranes. In: Lipowsky R and Sackmann E, eds. *Structure and Dynamics of Membranes*, Vol. 1B. Amsterdam: Elsevier, 1995, pp. 521–596.
42. Helfrich W. Steric interactions of fluid membranes in multilayer systems. *Z Naturforsch* 1978; 33a: 305–315.
43. Strey HH, Parsegian VA, and Podgornik R. Equation of state for polymer liquid crystals: theory and experiment. *Phys Rev E* 1998; 59: 999–1008.
44. Seifert U and Lipowsky R. Morphology of vesicles. In: Lipowsky R and Sackmann E, eds. *Structure and Dynamics of Membranes*, Vol. 1A. Amsterdam: Elsevier, 1995, p. 403.
45. Podgornik R and Parsegian VA. Thermal–mechanical fluctuations of fluid membranes in confined geometries: the case of soft confinement. *Langmuir* 1992; 8: 557–562.
46. Podgornik R and Parsegian VA. Charge-fluctuation forces between rodlike polyelectrolytes: Pairwise summability reexamined. *Phys Rev Lett* 1998; 80: 1560–1563.
47. Ha BJ and Liu AJ. Counterion-mediated attraction between two like charged rods. *Phys Rev Lett* 1997; 79: 1289–1292.
48. Trizac E and Tellez G. Onsager-Manning-Oosawa condensation phenomenon and the effect of salt. *Phys Rev Lett* 2006; 96: 038302. AQ9
49. Rau DC and Parsegian VA. Direct measurement of temperature-dependent solvation forces between DNA double helices. *Biophys J* 1992; 61:260–271.
50. Hill TL. *An Introduction to Statistical Thermodynamics*. New York: Dover Publications, 1986.
51. Naji A, Jungblut S, Moreira AG, et al. Electrostatic interactions in strongly coupled soft matter. *Physica A* 2005; 352: 131–170.

52. Grosberg AY, Nguyen TT, and Shklovskii BI. Colloquium: The physics of charge inversion in chemical and biological systems. *Rev Mod Phys* 2002; 74: 329–345.
53. Oosawa F. *Polyelectrolytes*. New York: Marcel Dekker, 1971.
54. DeRouchey, J, Netz RR, and Rädler JO. Structural investigations of DNA–polycation complexes. *Eur Phys J E* 2005; 16: 17–28.
55. Podgornik R. Polyelectrolyte-mediated bridging interactions. *J Polym Sci, Polym Phys* 2004; 42: 3539–3556.
56. Podgornik R. Two-body polyelectrolyte mediated bridging interactions. *J Chem Phys* 2003; 118: 11286–11296.
57. Podgornik R and Saslow WM. Long-range many-body polyelectrolyte bridging interactions. *J Chem Phys* 2005; 122: 204902.
58. Saenger W. *Principles of Nucleic Acid Structure*. New York: Springer Verlag, 1984.
59. Rhodes D and Klug A. Helical periodicity of DNA determined by enzyme digestion. *Nature* 1980; 286: 573–578.
60. Rill RL. Liquid crystalline phases in concentrated DNA solutions. In: Pifa-Mrzljak G. ed. *Supramolecular Structure and Function*. New York: Springer, 1988, pp. 166–167.
61. De Gennes PG and Prost J. *The Physics of Liquid Crystals*, 2nd ed. Oxford: Oxford University Press, 1993.
62. Hagerman PJ. Flexibility of DNA. *Annu Rev Biophys Biophys Chem* 1988; 17: 265–286.
63. Pruss GJ and Drlica K. DNA supercoiling and prokaryotic transcription. *Cell* 1989; 56: 521–523.
64. Grosberg AY and Khokhlov AR. *Statistical Physics of Macromolecules* (AIP Series in Polymers and Complex Materials). Washington, DC: American Institute of Physics, 1994.
65. Rau DC, Lee BK, and Parsegian VA. Measurement of the repulsive force between polyelectrolyte molecules in ionic solution: hydration forces between parallel DNA double helices, *Proc Natl Acad Sci USA* 1984; 81: 2621–2625.
66. Strey HH, Parsegian VA, and Podgornik R. Equation of state for DNA liquid crystals: Fluctuation enhanced electrostatic double layer repulsion. *Phys Rev Lett* 1997; 78: 895–898.
67. Reich Z, Wachtel EJ, and Minsky A. In vivo quantitative characterization of intermolecular interaction. *J Biol Chem* 1995; 270: 7045–7046.
68. Barrat JL and Joanny JF. Theory of polyelectrolyte solutions. In: Prigogine I, Rice SA, eds. *Advances in Chemical Physics*. New York: Wiley, 1995, pp. 1–66.
69. Lyubartsev AP and Nordenskiold L. Monte Carlo simulation study of ion distribution and osmotic pressure in hexagonally oriented DNA. *J Phys Chem* 1995; 99: 10373–10382.
70. Oosawa F. *Polyelectrolytes*. New York: Marcel Dekker, 1971.
71. Rouzina I and Bloomfield VA. Macro-ion attraction due to electrostatic correlation between screening counterions. *J Phys Chem* 1996; 100: 9977–9989.
72. Podgornik R, Strey HH, Rau DC, and Parsegian VA. Watching molecules crowd: DNA double helices under osmotic stress. *Biophys Chem* 1995; 26: 111–121.
73. Lindsay SM, Lee SA, Powell JW, Weidlich T, Demarco C, Lewen GD, Tao NJ, and Rupprecht A. The origin of the A to B transition in DNA fibers and films. *Biopolymers* 1988; 17: 1015–1043.
74. Podgornik R, Strey HH, Gawrisch K, Rau DC, Rupprecht A, and Parsegian VA. Bond orientational order, molecular motion, and free energy of high-density DNA mesophases. *Proc Natl Acad Sci USA* 1996; 93: 4261–4266.
75. Strandberg D. *Bond-Orientational Order in Condensed Matter Systems*. New York: Springer, 1992.
76. Durand D, Doucet J, and Livolant F. A study of the structure of highly concentrated phases of DNA by X-ray diffraction. *J Phys II France* 1992; 2: 1769–1783.
77. Kamien RD. Liquids with chiral bond order. *J Phys II France* 1996; 6: 461–475.
78. Chaikin PM and Lubensky TC. *Principles of Condensed Matter Physics*. Cambridge, MA: Cambridge University Press. 1995.
79. Leforestier A and Livolant F. DNA liquid-crystalline blue phases—electron-microscopy evidence and biological implications. *Mol Cryst Liquid Cryst* 1994; 17: 651–658.
80. Wang L and Bloomfield VA. Small-angle X-ray scattering of semidilute rodlike DNA solutions: Polyelectrolyte behavior. *Macromolecules* 1991; 24: 5791–5795.
81. Podgornik R, Rau DC, and Parsegian VA. The action of interhelical forces on the organization of DNA double helices: Fluctuation enhanced decay of electrostatic double layer and hydration forces. *Macromolecules* 1989; 22: 1780–1786.
82. Frank-Kamenetskii MD, Anshelevich VV, and Lukashin AV. Polyelectrolyte model of DNA. *Sov Phys Usp* 1987; 4: 317–330.
83. Tanford C. *The Hydrophobic Effect. Formation of Micelles and Biological Membranes*. New York: Wiley, 1980.
84. Cevc G and Marsh D. *Phospholipid Bilayers: Physical Principles and Models* (Cell Biology: A Series of Monographs, Vol 5). AQ10
85. Parsegian VA and Evans EA. Long and short range intermolecular and intercolloidal forces. *Curr Opin Coll Interf Sci* 1996; 1: 53–60.
86. Duzgunes N, Willshut L, Hong K, Fraley R, Perry C, Friends DS, James TL, and Papahadjopoulos D. Physicochemical characterization of large unilamellar phospholipid vesicles prepared by reverse-phase evaporation. *Biophys Biochim Acta* 1983; 732: 289–299.
87. Seifert U. Configurations of fluid membranes and vesicles. *Adv Phys* 1997; 46: 13–137. AQ11
88. Small DM. *The Physical Chemistry of Lipids*: *From Alkanes to Phospholipids*. New York: Plenum Press, 1986.
89. Gruner SM, Parsegian VA, and Rand RP. Directly measured deformation energy of phospholipid H2 hexagonal phases. *Faraday Disc* 1986; 81: 213–221.
90. Daoud M and Williams CE. *Soft Matter Physics*. New York: Springer, 1999.
91. Lasic DD. *Liposomes: from Physics to Applications*. Amsterdam: Elsevier, 1993.
92. Parsegian VA and Podgornik R. Surface-tension suppression of lamellar swelling on solid substrates. *Colloids Surf A Physicochem Eng Asp* 1997; 129–130, 345–364.
93. Roux D and Safinya CR. A synchrotron X-ray study of competing undulation and electrostatic interlayer interactions in fluid multimembrane lyotropic phases. *J Phys—Paris* 1988; 49: 307–318.
94. Leneveu DM, Rand RP, Gingell D, and Parsegian VA. Apparent modification of forces between lecithin bilayers. *Science* 1976; 191: 399–400.
95. Parsegian VA. Reconciliation of van der Waals force measurements between phosphatidylcholine bilayers in water and between bilayer coated mica surfaces. *Langmuir* 1993; 9: 3625–3628.
96. Gouliaev N and Nagle JF. Simulations of interacting membranes in soft confinement regime. *Phys Rev Lett* 1998; 81: 2610–2613.
97. Rand RP and Parsegian, VA. Hydration forces between phospholipid bilayers. *Biochim Biophys Acta* 1989; 988: 351–376.

98. Petrache HI, Gouliaev N, Tristram-Nagle S, Zhang R, Suter RM, and Nagle JF. Interbilayer interactions from high-resolution X-ray scattering. *Phys Rev E* 1998; 57: 7014–7024.
99. Felgner PL, Barenholz Y, Behr JP, et al. Nomenclature for synthetic gene delivery systems. *Hum Gene Ther* 1997; 8: 511–512.
100. Safinya CR. Structure of lipid–DNA complexes: Supermolecular assembly and gene delivery. *Curr Opin Struc Biol* 2001; 11: 440–448.
101. Barenholz Y. Liposome application: Problems and prospects. *Curr Opin Coll Inter Sci* 2001; 6: 66–77.
102. Rädler JO. Structure and phase behavior of cationic-lipid DNA complexes. In: Holm C, Kékicheff P, and Podgornik R, eds. *Electrostatic Effects in Soft Matter and Biophysics.* Dordrecht: Kluwer, 2001, pp. 441–458.
103. Ilies MA and Balaban AT. Recent developments in cationic lipid-mediated gene delivery and gene therapy. *Expert Opin Ther Patents* 2001; 11: 1729–1751.
104. Ilies MA, William AS, and Balaban AT. Cationic lipids in gene delivery: principles, vector design and therapeutical applications. *Curr Pharm Des* 2002; 8: 125–133.
105. Audouy S and Hoekstra D. Cationic-mediated transfection in vitro and in vivo. *Mol Membr Biol* 2001; 18: 129–143.
106. Felgner PL, Gadeck T, Holen M et al. Lipofectin: a highly efficient lipid-mediated DNA transfection procedure. *Proc Acad Sci USA* 1987; 84: 7413–7417.
107. Felgner PL and Ringold GM. Cationic liposome-mediated transfection, *Nature* 1989; 337: 387–388.
108. Tempelton NS. Developments in liposomal gene delivery systems. *Expert Opin Biol Ther* 2001; 1: 1–4.
109. Fraley R, Subramani S, Berg P, and Papahadjopoulos D. Introduction of liposome-encapsulated SV40 DNA into cells. *J Biol Chem* 1980; 255: 10431–10435.
110. Fillion P, Desjardins A, Sayasith K, and Lagace J. Encapsulation of DNA in negatively charged liposomes and inhibition of bacterial gene expression with fluid liposome-encapsulated antisense oligonucleotides. *Biochim Biophys Acta Biomembr* 2001; 1515: 44–54.
111. Lakkaraju A, Dubinsky JM, Low WC, and Rahman YE. Neurons are protected from excitotoxic death by p53 antisense oligonucleotides delivered in anionic liposomes. *J Biol Chem* 2001; 276: 32000–32007.
112. Patil SD and Rhodes DG. Conformation of oligodeoxynucleotides associated with anionic liposomes. *Nucleic Acids Res* 2000; 28: 4125–4129.
113. Liang H, Harries D, and Wong GCL. Polymorphism of DNA-anionic liposome complexes reveals hierarchy of ion-mediated interactions. *Proc Natl Acad Sci USA* 2005; 102: 11173–11178.
114. Pisani M, Bruni P, Caracciolo G, et al. Structure and phase behavior of self-assembled DPPC–DNA–metal cation complexes *J Phys Chem B* 2006; 110: 13203–13211.
115. Lasic DD and Templeton NS. Liposomes in gene therapy. *Adv Drug Deliv Rev* 1996; 20: 221–266.
116. Lasic DD, Strey H, Stuart MCA, Podgornik R, and Frederik PM. The structure of DNA–liposome complexes. *J Am Chem Soc* 1997; 119: 832–833.
117. Rädler JO, Koltover I, Salditt T, et al. Structure of DNA–cationic liposome complexes: DNA intercalation in multilamellar membranes in distinct interhelical packing regimes. *Science* 1997; 275: 810–814.
118. Koltover I, Salditt T, Rädler JO, et al. An inverted hexagonal phase of cationic liposome–DNA complexes related to DNA release and delivery. *Science* 1998; 281: 78–81.
119. Salditt T, Koltover I, Rädler O, et al. Self-assembled DNA-cationic-lipid complexes: Two-dimensional smectic ordering, correlations, and interactions. *Phys Rev E* 1998; 58: 889–904.
120. Salditt T, Koltover I, Rädler J, and Safinya CR. Two dimensional smectic ordering of linear DNA chains in self-assembled DNA–cationic liposome mixtures. *Phys Rev Lett* 1997; 79: 2582–258. AQ11
121. Rädler JO, Koltover I, Jamieson A, Salditt T, and Safinya CR. Structure and interfacial aspects of self-assembled cationic lipid–DNA gene carrier complexes. *Langmuir* 1998; 14: 4272–4283.
122. Sackmann E. Physical basis of self-organization and function of membranes: physics of vesicles. In: Lipowsky R and Sackmann E, eds. *Structure and Dynamics of Membranes.* Amsterdam: Elsevier, 1995, pp. 213–304.
123. Tarahovsky YS, Khusainova RS, Gorelov AV, et al. DNA initiates polymorphic structural transitions lecithin. *FEBS Lett* 1996; 390: 133–136.
124. Ghirlando R, Wachtel EJ, Arad T, and Minsky A. DNA packaging induced by micellar aggregates: a novel in vitro DNA condensation system. *Biochemistry* 1992; 31: 7110–7119.
125. Gershon H, Ghirlando R, Guttman SB, and Minsky A. Mode of formation and structural features of DNA–cationic liposome complexes Used for transfection. *Biochemistry* 1993; 32: 7143–7151.
126. Ewert KK, Evans HM, Zidovska A, et al. A columnar phase of dendritic lipid-based cationic liposome–DNA complexes for gene delivery: Hexagonally ordered cylindrical micelles embedded in a DNA honeycomb lattice. *J Am Chem Soc* 2006; 128: 3998–4006.
127. Koynova R, Rosenzweig HS, Wang L, et al. Novel fluorescent cationic phospholipid, O-4-napthylimido-1-butyl-DOPC, exhibits unusual foam morphology, forms hexagonal and cubic phases in mixtures, and transfects DNA. *Chem Phys Lipids* 2004; 129: 183–194.
128. May S and Ben-Shaul S. DNA–lipid complexes: Stability of honeycomb-like and spaghetti-like structures. *Biophys J* 1997; 73: 2427–2440.
129. Dan N. The structure of DNA complexes with cationic liposomes—cylindrical or lamellar? *Biophys Biochim Acta* 1998; 1369: 34–38.
130. Sternberg B, Sorgi FL, and Huang L. New structures in complex-formation between DNA and cationic liposomes visualized by freeze-fracture electron-microscopy. *FEBS Lett* 1994; 356: 361–366.
131. Sternberg B. New structures in complex formation between DNA and cationic liposomes visualized by freeze-fracture electron microscopy. *FEBS Lett* 1994; 356: 361–366.
132. Simberg D, Danino D, Talmon Y, Minsky A, Ferrari ME, Wheeler CJ, and Barenholz Y. Phase behavior, DNA ordering, and size instability of cationic lipoplexes. *J Biol Chem* 2001; 276: 47453–47459.
133. Pitard B, Aguerre O, Airiau M, Lachages AM, et al. Virus-sized self-assembling lamellar complexes between plasmid DNA and cationic micelles promote gene transfer. *Proc Natl Acad Sci USA* 1997; 94: 14412–14417.
134. Boukhnikashvili T, Aguerre-Chariol O, Airiau M, Lesieur S, Ollivon M, and Vacus J. Structure of in-serum transfecting DNA-cationic lipid complexes. *FEBS Lett* 1997; 409: 188–194.
135. Templeton NS, Lasic DD, Frederik PM, Strey HH, Roberts DD, and Pavlakis GN. Improved DNA: Liposome complexes for increased systemic delivery and gene expression. *Nature Biotech* 1997; 15: 647–652.

136. Record TM Jr, Anderson CF, and Lohman TM. Thermodynamic analysis of ion effects on the binding and conformational equilibria of proteins and nucleic acids: the roles of ion association or release, screening, and ion effects on water activity. *Quart Rev Biophys* 1978; 11: 103–178.
137. Bruinsma R. Electrostatics of DNA–cationic lipid complexes: Isoelectric instability. *Eur Phys J B* 1998; 4: 75–88.
138. Wagner K, Harries D, May S, et al. Counterion release upon cationic lipid–DNA complexation. *Langmuir* 2000; 16: 303–306.
139. Bordi F, Cametti C, Sennato S, et al. Counterion release in overcharging of polyion-liposome complexes. *Phys Rev E* 2006; 74: Art. No. 030402.
140. Barreleiro PCA, Olofsson G, and Alexandridis P. Interaction of DNA with cationic vesicles: A calorimetric study. *J Phys Chem B* 2000; 104: 7795–7802.
141. Kennedy MT, Pozharski EV, Rakhmanova VA, and MacDonald RC. Factors governing the assembly of cationic phospholipid–DNA complexes. *Biophys J* 2000; 78: 1620–1633.
142. Huebner S, Battersby BJ, Grimm R, and Cevc G. Lipid mediated complex formation: Reorganization and rupture of lipid vesicles in the presence of DNA as observed by cryoelectron microscopy. *Biophys J* 199; 76: 3158–3166.
143. Dan N. Multilamellar structures of DNA complexes with cationic liposomes. *Biophys J* 1997; 73: 1842–1846.
144. Harries D, May S, Gelbart WM, and Ben-Shaul A. Structure, stability and thermodynamics of lamellar DNA–lipid complexes. *Biophys J* 1998; 75: 159–173.
145. Parsegian VA and Gingell D. On the electrostatic interaction across a salt solution between two bodies bearing unequal charges. *Biophys J* 1972; 12: 1192–1204.
146. Mitrakos P and Macdonald PM. DNA-induced lateral segregation of cationic amphiphiles in lipid bilayer membranes as detected via ^{2}H NMR. *Biochemistry* 1996; 35: 16714–16722.
147. Bandyopadhyay S, Tarek M, and Klein ML. Molecular dynamics study of a lipid–DNA complex. *J Phys Chem B* 1999; 103: 1007–1008.
148. Garidel P, Johann C, and Blume A. Thermodynamics of lipid organization and domain formation in phospholipid bilayers. *J Liposome Res* 2000; 10: 131–158.
149. Koltover I, Wagner K, and Safinya CR. DNA condensation in two dimensions. *Proc Natl Aca Sci USA* 2000; 97: 14046–14051.
150. Dubois M, Zemb Th, Fuller N, Rand RP, and Parsegian VA. Equation of state of a charged bilayer system: measure of the entropy of the lamellar–lamellar transition in DDABr. *J Chem Phys* 1998; 18: 7855–7869.
151. Bostrom M, Williams DRM, and Ninham B. Specific ion effects: why DLVO theory fails. *Phys Rev Lett* 2001; 87: Art No. 168103.
152. Fang Y and Yang J. Two-dimensional condensation of DNA molecules on cationic lipid membranes. *J Phys Chem B* 1997; 101: 441–449.
153. Mou J, Czajkowsky DM, Zhang Y, and Shao Z. High-resolution atomic force microscopy of DNA: The pitch of the double helix. *FEBS Lett* 1995; 371: 279–282.
154. May S, Harries D, and Ben-Shaul A. Lipid demixing and protein–protein interactions in the adsorption of charged proteins on mixed membranes. *Biophys J* 2000; 79: 1747–1760.
AQ11 155. Dan N. Formation of ordered domains in membrane-bound DNA. *Biophys J* 1996; 71: 1267–127.
156. Fang Y and Yang J. Effect of cationic strength and species on 2-D condensation of DNA. *J Phys Chem B* 1997; 101: 3453–3456.
157. Safinya CR, Sirota EB, Roux D, and Smith GS. Universality in interacting membranes: The effect of cosurfactants on the interfacial rigidity. *Phys Rev Lett* 1989; 62: 1134–1137.
158. Szleifer I, Kramer D, Ben-Shaul A, Roux D, and Gelbart MW. Curvature elasticity of pure and mixed surfactant films. *Phys Rev Lett* 1998; 60: 1966–1969.
159. Gawrisch K, Parsegian VA, Hajduk DA, Tate MW, Gruner SM, Fuller NL, and RP. Energetics of a hexagonal-lamellar-hexagonal-phase transition sequence in dioleoylphosphatidylethanolamine membranes. *Biochemistry* 1992; 31: 2856–2864. AQ12
160. Kozlov MM, Leikin S, and Rand RP. Bending, hydration, and intersticial energies quantitatively account for the hexagonal-lamellar-hexagonal reentrant phase transition in dioleoylphosphatidylethanolamine. *Biophys J* 1994; 67: 1603–1611.
161. Chen Z and Rand RP. Comparative study of the effects of several *n*-alkanes on phospholipid hexagonal phases. *Biophys J* 1998; 74: 944–952.
162. May S, Harries D, and Ben-Shaul A. The phase behavior of cationic lipid–DNA complexes. *Biophys J* 2000; 78: 1681–1697.
163. Schiessel H and Aranda-Espinoza H. Electrostatically induced undulations of lamellar DNA–lipid complexes. *Eur Phys J E* 2001; 5: 499–506.
164. Harries D. Electrostatic interaction between macromolecules and mixed lipid membranes. PhD dissertation. The Hebrew University, Jerusalem, Israel, 2001. Available from www.fh.huji.ac.il/~daniel/.
165. Battersby BJ, Grimm R, Huebner S, and Cevc G. Evidence for three-dimensional interlayer correlations in cationic lipid–DNA complexes as observed by cryo-electron microscopy. *Biochim Biophys Acta* 1998; 1372: 379–383.
166. Artzner F, Zantl R, Rapp G, and Rädler JO. Observation of a rectangular columnar phase in condensed lamellar cationic lipid–DNA complexes. *Phys Rev Lett* 1998; 81: 5015–5018.
167. O'Hern CS and Lubensky TC. Sliding columnar phase of DNA lipid complexes. *Phys Rev Lett* 1998; 80: 4345–4348.
168. Golubovic L and Golubovic M. Fluctuations of quasi-two-dimensional smectics intercalated between membranes in multilamellar phases of DNA cationic lipid complexes. *Phys Rev Lett* 1998; 80: 4341–4344.
169. Podgornik R and Žekž B. Coupling between smectic and twist modes in polymer intercalated smectics. *Phys Rev Lett* 1998; 80: 305–308.
170. Hui SW, Langner M, Zhao Y-L, Patrick R, Hurley E, and Chan K. The role of helper lipids in cationic liposome–mediated gene transfer. *Biophys J* 1996; 71: 590–59. AQ11
171. Zuidam NJ, Lerner DH, Margulies S, and Barenholz Y. Lamellarity of cationic liposomes and mode of preparation of lipoplexes affect transfection efficiency. *Biophys Biochim Acta* 1999; 1419: 207–220.
172. Meidan VM, Cohen JS, Amariglio N, Hirsch-Lerner D, and Barenholz Y. Interaction of oligonucleotides with cationic lipids: the relationship between electrostatics, hydration and state of aggregation. *Biochem Biophys Acta* 2000; 1464; 251–261.
173. Artzner F, Zantl R, and Rädler JO. Lipid–DNA and lipid–polyelectrolyte mesophases: Structure and exchange kinetics. *Cell Molec Biol* 2000; 46: 967–978.
174. Wiethoff CM, Smith JG, Koe GS, and Middaugh CR. The potential role of proteoglycans in cationic lipid-mediated gene delivery—Studies of the interaction of cationic lipid–DNA complexes with model glycosaminoglycans. *J Biol Chem* 2001; 276: 32806–32813.

175. Zabner J, Fasbender AJ, Moninger T, Poellinger KA, and Welsh MJ. Cellular and molecular barriers to gene transfer by a cationic lipid. *J Biol Chem* 1995; 270: 18997–19007.
176. Lin AJ, Slack NL, Ahmad A, Koltover I George CX, Samuel CE, and Safinya CR. Structure and structure–function studies of lipid/plasmid DNA complexes. *J Drug Targeting* 2000; 8: 13–27.
177. Zuhorn IS, Bakowsky U, Polushkin E, Visser WH, Stuart MC, Engberts JB, and Hoekstra D. Nonbilayer phase of lipoplex–membrane mixture determines endosomal escape of genetic cargo and transfection efficiency. *Mol Ther* 2005; 11:801–10.
178. Hirsch-Lerner D and Barenholz Y. Probing DNA–cationic lipid interactions with the fluorophore trimethylammonium diphenyl-hexatrien (TMADPH). *Biochim Biophys Acta* 1998; 1370: 17–30.
179. Tang F and Hughes JA. Use of dithiodilycolic acid as a tether for cationic lipids decreases the cytotoxicity and increases transgene expression of plasmid DNA in vitro. *Bioconjug Chem* 1999; 10: 791–796.
180. Byk G, Wetzer B, Frederic M, et al. Reduction sensitive lipopolyamines as a novel nonviral gene delivery system for modulated release of DNA with improved transgene expression. *J Med Chem* 2000; 43: 4377–4387.
181. Balasubramaniam RP, Bennett MJ, Aberle AM, Malone JG, Nantz MH, and Malone RW. Structural and functional analysis of cationic transfection lipids: the hydrophobic domain. *Gene Ther* 1996; 3: 163–172.
182. Weltzer B, Byk G, Frederic M, et al. Reducible cationic lipids for gene transfer. *Biochem J* 2001; 356: 747–756.
183. Lin AJ, Slack NL, Ahmad A, George CX, Samuel CE, and Safinya CR. Three-dimensional imaging of lipid gene-carriers: Membrane charge density controls universal transfection behavior in lamellar cationic liposome–DNA complexes. *Biophys J* 2003; 84: 3307–3316.
184. Ewert KK, Ahmad A, Evans HM, Ahmad A, Slack NL, Lin AJ, Martin-Herranz A, and Safinya CR. Cationic lipid–DNA complexes for non-viral gene therapy: Relating supramolecular structures to cellular pathways. *Expert Opin Biol Therapy* 2005; 5: 33–53.
185. Lin AJ, Slack NL, Ahmad A, et al. Three-dimensional imaging of lipid gene-carriers: Membrane charge density controls universal transfection behavior in lamellar cationic liposome–DNA complexes. *Biophys J* 2003; 84: 3307–3316.
186. Ewert K, Slack NL, Ahmad A, Evans HM, Lin AJ, Samuel CE, and Safinya CR. Cationic lipid–DNA complexes for gene therapy: Understanding the relationship between complex structure and gene delivery pathways at the molecular level. *Curr Med Chem* 2004; 11: 133–149.
187. Zanta MA, Belguise-Valladier P, and Behr JP. Gene delivery: A single nuclear localization signal peptide is sufficient to carry DNA to the cell nucleus. *Proc Natl Acad Sci USA* 1999; 96: 91–96.
188. Cartier R and Reszka R. Utilization of synthetic peptides containing nuclear localization signal for nonviral gene transfer systems. *Gene Ther* 2002; 9: 157–167.
189. Wheeler JJ, Palmer L, Ossanlou M, et al. Stabilized plasmid–lipid particles: construction and characterization. *Gene Ther* 1999; 6: 271–281.
190. Martin-Herranz A, Ahmad A, Evans HM, Ewert K, Schulze U, and Safinya CR. Surface functionalized cationic lipid–DNA complexes for gene delivery: PEGylatedlamellar complexes exhibit distinct DNA–DNA interaction regimes. *Biophys J* 2004; 86: 1160–1168.
191. Schulze, U, Schmidt, H-W, and Safinya, CR. Synthesis of novel cationic poly(ethylene glycol) containing lipids. *Bioconjugate Chem* 1999; 10: 548–552.
192. Duncan R. The dawning era of polymer therapeutics. *Nat Rev Drug Discovery* 2003; 2: 347–360.
193. Wagner E and Kloeckner J. Gene delivery using polymer therapeutics. *Adv Polymer Sci* 2006; 192: 135–173.
194. Maurstad G, Danielsen S, and Stokke BT. Analysis of compacted semiflexible polyanions visualized by atomic force microscopy: Influence of chain stiffness on the morphologies of polyelectrolyte complexes. *J Phys Chem B* 2003; 107: 8172–8180.
195. Dunlap DD, Maggi A, Soria MR, et al. Nanoscopic structure of DNA condensed for gene delivery. *Nucleic Acids Res* 1997; 25: 3095–3101.
196. Golan R, Pietrasanta LI, Hsieh W, et al. DNA toroids: Stages in condensation. *Biochemistry* 1999; 38: 14069–14076.
197. Liu D, Wang C, Lin Z, et al. Visualization of the intermediates in a uniform DNA condensation system by tapping mode atomic force microscopy. *Surface Interface Anal* 2001; 32: 15–19.
198. Suwalsky M. Comparative X-ray study of a nucleoprotamine and DNA complexes with polylysine and polyarginine. *Biopolymers* 1972; 11: 2223–2231.
199. Suwalsky M. An X-ray study of interaction of DNA with spermine. *J Mol Biol* 1969; 42: 363–373.
200. Azorin F. Interaction of DNA with lysine-rich polypeptides and proteins—The influence of polypeptide composition and secondary structure. *J Mol Biol* 1985; 185: 371–387.
201. Boeckle S, von Gersdorff K, van der Piepen S, et al. Purification of polyethylenimine polyplexes highlights the role of free polycations in gene transfer. *J Gene Med* 2004; 6: 1102–1111.
202. Netz RR. Variational charge renormalization in charged systems. *Eur Phys J E* 2003; 11: 301–311.
203. Odijk T. Undulation-enhanced electrostatic forces in hexagonal polyelectrolyte gels. *Biophys Chem* 1993; 46: 69–75.
204. Ogris M, Brunner S, Schuller S, Kircheis R, and Wagner E. PEGylated DNA/transferrin–PEI complexes: reduced interaction with blood components, extended circulation in blood and potential for systemic gene delivery. *Gene Ther* 1999; 6: 595–605.
205. Walker GF, Fella C, Pelisek J, Fahrmeir J, Boeckle S, Ogris M, and Wagner E. Toward synthetic viruses: Endosomal pH-triggered deshielding of targeted polyplexes greatly enhances gene transfer in vitro and in vivo. *Mol Ther* 2005; 11: 418–425.
206. Schatzlein AG. Targeting of synthetic gene delivery systems. *J Biomed Biotechnol* 2003; 2: 149–158.
207. von Gersdorff K, Sanders NN, Vandenbroucke R, et al. The internalization route resulting in successful gene expression depends on polyethylenimine both cell line and polyplex type. *Molec Ther* 2006; 14: 745–753.
208. Rejman J, Oberle V, Zuhorn IS, et al. Size-dependent internalization of particles via the pathways of clathrin- and caveolae-mediated endocytosis. *Biochem J* 2004; 377: 159–169.
209. Kopatz I, Remy JS, and Behr JP. A model for non-viral gene delivery: through syndecan adhesion molecules and powered by actin. *J Gene Med* 2004; 6: 769–776.
210. Goncalves C, Mennesson E, Fuchs R, et al. Macropinocytosis of polyplexes and recycling of plasmid via the clathrin-dependent pathway impair the transfection efficiency of human hepatocarcinoma cells. *Molec Ther* 2004; 10: 373–385.

211. Suh J, Wirtz D, and Hanes J. Efficient active transport of gene nanocarriers to the cell nucleus. *Proc Natl Acad Sci USA* 2003; 100: 3878–3882.
212. Bausinger R, von Gersdorff K, Braeckmans K, et al. The transport of nanosized gene carriers unraveled by live-cell imaging. *Ang Chem Int Ed* 2006; 45: 1568–1572.
213. Furgeson DY and Kim SW. Recent advances in poly(ethylene imine) gene carrier design. *ACS Symp Ser* 2006; 923: 182–197.
214. Neu M, Fischer D, and Kissel T. Recent advances in rational gene transfer vector design based on poly(ethylene imine) and its derivatives. *J Gene Med* 2005; 7: 992–1009.
215. Boussif O, Lezoualch F, Zanta MA, et al. A versatile vector for gene and oligonucleotide transfer into cells in culture and in-vivo - polyethyleneimine. *Proc Natl Acad Sci USA* 1995; 92: 7297–7301.
216. Akinc A, Thomas M, Klibanov AM, et al. Exploring polyethylenimine-mediated DNA transfection and the proton sponge hypothesis. *J Gene Med* 2005; 7: 657–663.
217. Wilson GL, Dean BS, Wang G, et al. Nuclear import of plasmid DNA in digitonin-permeabilized cells requires both cytoplasmic factors and specific DNA sequences. *J Biol Chem* 1999; 274: 22025–22032.
218. Dean DA, Strong DD, and Zimmer WE. Nuclear entry of nonviral vectors. *Gene Ther* 2005; 12: 881–890.
219. Peterlin A. Light scattering by very stiff chain molecules, *Nature* 1953; 171: 259–260.

AUTHOR QUERIES

[AQ1] Please specify the section.
[AQ2] Would you consider revising the sentence "Through the dielectric constant…network of water molecules" to "In case of water, a network is built: its dielectric constant or dielectric permittivity facilitates electrostatic interactions, neutral pH enables its interaction in charging equilibria, and its fundamental molecular geometry creates the hydrogen bond network topoloyg around simple solutes" for clarity?
[AQ3] Would it be appropriate to say "equivalently in pressures of hundreds of atmospheres."
[AQ4] Should E be replaced by the symbol =?
[AQ5] Please expand s.c.
[AQ6] Please expand DMPC.
[AQ7] Please check the figure has SD, S and SB symbols.
[AQ8] Please check change Okay?
[AQ9] Please confirm if this is an online reference. Please insert (online) if it is the case.
[AQ10] Please provide publisher and location.
[AQ11] Please check page range for this Reference.
[AQ12] Please provide the author name.